CONFIDENTIAL

Copy 135
RM L56A19

THIS DOCUMENT AND EACH AND EVERY
PAGE HEREIN IS HEREBY RECLASSIFIED
FROM Conf TO Unclass
AS PER LETTER DATED NACA Res
notice #116

NACA

RESEARCH MEMORANDUM

EXPERIMENTAL DETERMINATION OF THE EFFECTS OF FREQUENCY AND AMPLITUDE ON THE LATERAL STABILITY DERIVATIVES FOR A DELTA, A SWEPT, AND AN UNSWEPT WING OSCILLATING IN YAW

By Lewis R. Fisher

Langley Aeronautical Laboratory
Langley Field, Va.

CLASSIFIED DOCUMENT

This material contains information affecting the National Defense of the United States within the meaning of the espionage laws, Title 18, U.S.C., Sections 793 and 794, the transmission or revelation of which in any manner to an unauthorized person is prohibited by law.

NATIONAL ADVISORY COMMITTEE
FOR AERONAUTICS

WASHINGTON
April 4, 1956

CONFIDENTIAL

NATIONAL ADVISORY COMMITTEE FOR AERONAUTICS

RESEARCH MEMORANDUM

EXPERIMENTAL DETERMINATION OF THE EFFECTS OF FREQUENCY AND AMPLITUDE ON THE LATERAL STABILITY DERIVATIVES FOR A DELTA, A SWEPT, AND AN UNSWEPT WING OSCILLATING IN YAW

By Lewis R. Fisher

SUMMARY

Three wing models were oscillated in yaw about their vertical axes to determine the effects of systematic variations of frequency and amplitude of oscillation on the in-phase and out-of-phase combination lateral stability derivatives resulting from this motion. The tests were made at low speeds for a 60° delta wing, a 45° swept wing, and an unswept wing; the latter two had an aspect ratio of 4.

The results indicate that large changes in the magnitude of the stability derivatives due to the variation of frequency occur at high angles of attack, particularly for the delta wing. The greatest variations of the derivatives with frequency take place for the lowest frequencies of oscillation; at the higher frequencies, the effects of frequency are smaller and the derivatives become more linear with angle of attack.

Effects of amplitude of oscillation on the stability derivatives for the delta wing were evident for certain high angles of attack and for the lowest frequencies of oscillation. As the frequency became high, the amplitude effects tended to disappear.

The algebraic addition of the component derivatives determined in separate investigations were generally in good agreement with the combination derivatives obtained herein. The major contributions to the out-of-phase derivatives are made by the sideslipping acceleration derivatives, whereas the in-phase derivatives are determined chiefly by the sideslipping velocity derivatives.

INTRODUCTION

Recent investigations have shown that large-magnitude stability derivatives exist at high angles of attack for wings undergoing rotary accelerations in yaw or transverse accelerations in sideslip. The results of one such investigation are presented in reference 1 for which wing models were forced to oscillate in a pure yawing motion (zero sideslip) at a constant frequency of oscillation. The stability derivatives resulting from this investigation include the yawing and rolling moments due to yawing velocity $C_{n_{r,\omega}}$ and $C_{l_{r,\omega}}$ and the yawing and rolling moments due to yawing acceleration $C_{n_{\dot{r},\omega}}$ and $C_{l_{\dot{r},\omega}}$. These derivatives were measured for a 60° delta wing, a 45° sweptback wing, and an unswept wing; the latter two had an aspect ratio of 4.

The same wing models were oscillated in a pure sideslipping motion for the investigation of reference 2. The measured stability derivatives resulting from this type of motion included the yawing and rolling moments due to sideslipping velocity $C_{n_{\beta,\omega}}$ and $C_{l_{\beta,\omega}}$ and the yawing and rolling moments due to sideslipping acceleration $C_{n_{\dot{\beta},\omega}}$ and $C_{l_{\dot{\beta},\omega}}$. These derivatives were measured primarily at one frequency of oscillation; however, some limited data involving a variation of oscillation frequency in this reference indicated that the sideslipping derivatives at high angles of attack were dependent upon frequency. The results of reference 3 substantiated these effects of frequency at high angles of attack on the lateral stability derivatives for a similar set of wings. Reference 3 also includes a comprehensive discussion of the probable origin of the large-magnitude acceleration derivatives, and reference 4 points out the importance of including these derivatives in dynamic stability calculations, particularly at high angles of attack where the derivatives assume large magnitudes.

A reasonably simple oscillation test technique for extracting the lateral stability derivatives for a model is the method of oscillating the model in yaw about its vertical wind axis. Since the motion of the model is then a combination of yawing and sideslipping, the stability derivatives measured by this technique are the combination derivatives $C_{n_{r,\omega}} - C_{n_{\dot{\beta},\omega}}$, $C_{l_{r,\omega}} - C_{l_{\dot{\beta},\omega}}$, $C_{n_{\beta,\omega}} + k^2 C_{n_{\dot{r},\omega}}$, and $C_{l_{\beta,\omega}} + k^2 C_{l_{\dot{r},\omega}}$, where k is the reduced frequency parameter $\omega b/2V$.

The present investigation employed this technique for the purpose of determining the effects of a systematic variation of frequency and amplitude of oscillation on the resulting combination stability derivatives. Furthermore, in order to establish the relative importance of the individual derivatives which form the combination derivatives, the results

of reference 1 and of additional tests similar to those of reference 2 are compared individually and as an algebraic sum with the results of the present investigation. These comparisons provide an indication of the degree to which the results of the individual sideslipping and yawing tests are additive and attest to the linearity of the aerodynamic phenomena responsible for the large magnitude derivatives.

COEFFICIENTS AND SYMBOLS

The data are referred to the system of stability axes and are presented in the form of standard coefficients of forces and moments about the quarter-chord point of the mean aerodynamic chord of each wing tested. (See fig. 1.) The coefficients and symbols used herein are defined as follows:

C_L lift coefficient, Lift/qS

C_D drag coefficient, Drag/qS

C_m pitching-moment coefficient, Pitching moment/$qS\bar{c}$

C_l rolling-moment coefficient, Rolling moment/qSb

C_n yawing-moment coefficient, Yawing moment/qSb

α angle of attack, deg

b span, ft

β angle of sideslip, radians or deg

$\dot{\beta} = \frac{\partial \beta}{\partial t}$

β_o amplitude of sideslip, deg

$\bar{c}$ mean aerodynamic chord, ft

k reduced frequency parameter, $\omega b/2V$

ω circular frequency of oscillation, radians/sec

ψ angle of yaw, radians or deg

$\dot{\psi} = \frac{\partial \psi}{\partial t}$

ψ_o amplitude of yaw, deg

q dynamic pressure, $\frac{1}{2}\rho V^2$, lb/sq ft

ρ mass density of air, slugs/cu ft

$r = \dot{\psi}$

$\dot{r} = \frac{\partial^2 \psi}{\partial t^2}$

S wing area, sq ft

t time, sec

V free-stream velocity, ft/sec

$C_{n_\beta} = \frac{\partial C_n}{\partial \beta}$ $\qquad$ $C_{n_r} = \frac{\partial C_n}{\partial\left(\frac{rb}{2V}\right)}$

$C_{n_{\dot{\beta}}} = \frac{\partial C_n}{\partial\left(\frac{\dot{\beta}b}{2V}\right)}$ $\qquad$ $C_{n_{\dot{r}}} = \frac{\partial C_n}{\partial\left(\frac{\dot{r}b^2}{4V^2}\right)}$

$C_{l_\beta} = \frac{\partial C_l}{\partial \beta}$ $\qquad$ $C_{l_r} = \frac{\partial C_l}{\partial\left(\frac{rb}{2V}\right)}$

$C_{l_{\dot{\beta}}} = \frac{\partial C_l}{\partial\left(\frac{\dot{\beta}b}{2V}\right)}$ $\qquad$ $C_{l_{\dot{r}}} = \frac{\partial C_l}{\partial\left(\frac{\dot{r}b^2}{4V^2}\right)}$

All the above derivatives are nondimensionalized in this paper (1/radians).

The symbol ω following the subscript of a derivative denotes the oscillatory derivative.

APPARATUS AND MODELS

Oscillation Apparatus

The equipment used to oscillate the models consisted of the motor-driven flywheel, connecting rod, crank arm, and model-support strut shown schematically in figure 2 and photographically in figures 3 and 4. The connecting rod was pinned to an eccentric center on the flywheel and transmitted a sinusoidal yawing motion to the support strut by means of the crank arm. Because the models were mounted to the support strut at their assumed centers of gravity, the oscillation therefore was forced about the vertical wind, or stability, axes of the models. The apparatus was driven by a 1-horsepower direct-current motor through a geared speed reducer. The frequency of oscillation was varied by changing the voltage supplied to the motor, and the amplitude of oscillation was varied by adjusting the throw of the eccentric on the flywheel.

Because the reduced frequency of the tests of reference 2 differed from that of reference 1, some additional tests similar to those of reference 2 were made for this investigation at a reduced frequency which corresponded to that of reference 1. The results in reference 2 were obtained from freely damped sideslipping oscillation tests in which the motion was forced by a set of coil springs. For these additional tests, however, the coil springs were replaced by a flywheel and crank mechanism similar to that used for the yawing-oscillation tests described above. The resulting motion, therefore, was a continuous sideslipping oscillation of constant amplitude. Check tests for comparable frequencies indicated that the derivatives measured by either technique were about the same.

Models

The models tested were the three wings used for the investigations of references 1 and 2 and shown in the photographs of figure 4. These consisted of a 60° delta, a 45° sweptback, and an unswept wing. The latter two wings had an aspect ratio of 4, taper ratios of 0.6, and rounded tips. Each of the wings was constructed from 3/4-inch plywood having essentially a flat-plate airfoil section with a circular leading edge and a beveled trailing edge. The trailing edges of all wings were beveled to provide a trailing-edge angle of 10° that was constant across the span. Sketches of the three wings and their geometric characteristics are presented as figure 5.

Recording of Data

The recording of data was accomplished by means of the equipment described completely in the appendix of reference 1. Briefly, the rolling

and yawing moments acting on the model during oscillation were measured by means of resistance-type strain gages, mounted on the oscillating strut, to which the model was attached. The moments were modified by a sine-cosine resolver driven by the oscillating mechanism so that the output signals of the strain gages were proportional to the in-phase and out-of-phase components of the strain-gage signals. These signals were read visually on a highly damped direct-current meter and the aerodynamic coefficients were obtained by multiplying the meter readings by the appropriate constants, one of which was the system calibration constant.

Although the data measured for the freely damped oscillation tests of reference 2 were recorded graphically by a recording oscillograph, the additional sideslipping oscillation tests required for the present investigation made use of the newer equipment described above.

TESTS

All tests were conducted in the 6- by 6-foot test section of the Langley stability tunnel at a dynamic pressure of 24.9 pounds per square foot which corresponds to a Mach number of 0.13. The Reynolds number based on the mean aerodynamic chord was approximately 1.6×10^6 for the 60° delta wing and 0.71×10^6 for the swept and unswept wings.

The oscillation tests with the delta wing were conducted for a range of frequencies of oscillation which included 0.5, 1.0, 2.0, 3.0, and 3.3 cycles per second. These frequencies correspond to values of the reduced frequency parameter $\omega b/2V$ of 0.033, 0.065, 0.130, 0.195, and 0.215. The amplitudes of oscillation $\pm\psi_o$ for each of these frequencies was 2°, 4°, 6°, 8°, and 10° for the delta wing. For the swept and unswept wings, the reduced frequency 0.195 and the amplitude 8° were omitted from the tests.

The in-phase and out-of-phase yawing and rolling moments were measured for the delta wing in angle-of-attack increments of 4° from $\alpha = 0^\circ$ to $\alpha = 16^\circ$ and thereafter in 2° increments up to $\alpha = 32^\circ$; for the swept wing, in increments of 4° from $\alpha = 0^\circ$ to $\alpha = 20^\circ$ plus the angles 10°, 18°, and 22°; and for the unswept wing, in increments of 2° from $\alpha = 0^\circ$ to $\alpha = 16^\circ$.

For each amplitude, frequency, and angle-of-attack condition, both a wind-on and a wind-off run were made. The effects of the inertia of the model were eliminated from the data by subtracting the wind-off from the wind-on results.

The reduced frequency $\omega b/2V = 0.215$ (or 3.3 cps) was selected because it corresponded to the reduced frequency of the tests of reference 1.

The tests of reference 2 were made at lower values of the reduced frequency. In order to arrive at a better frequency basis of comparison, the additional tests made by the method similar to that of reference 2 were for $\omega b/2V = 0.22$ and $\beta_o = \pm 6^o$. These were forced-oscillation rather than the free-oscillation tests of reference 2, however.

RESULTS AND DISCUSSION

Presentation of Results

In figure 6 are shown the lift, drag, and pitching-moment data as functions of angle of attack for the three wings tested. These data are taken from reference 2 and are for a dynamic pressure of 39.8 pounds per square foot, which is somewhat higher than the dynamic pressure used for the present tests. The static variations of rolling moment and yawing moment with sideslip angles up to $\pm 10^o$ are presented in figure 7 for given angles of attack. These data exhibit no extreme nonlinearities in the range of sideslip angles being considered.

The data measured during these oscillation tests are presented for the delta wing in figure 8, for the swept wing in figure 9, and for the unswept wing in figure 10. These data are comprised of four combination lateral stability derivatives resulting from the combined oscillatory yawing and sideslipping motion employed for the tests. The derivatives are shown for five frequencies of oscillation of the delta wing and four frequencies of oscillation for the swept and unswept wings as functions of angle of attack. Each lettered part of figures 8, 9, and 10 presents the data for a different amplitude of oscillation from $\psi_o = 2^o$ to $\psi_o = 10^o$ in 2° increments. The amplitude of $\psi_o = 8^o$ is omitted for the swept and unswept wings, however. In these figures the static derivatives C_{n_β} and C_{l_β} are also shown for comparison with the oscillatory derivatives $C_{n_{\beta,\omega}} + k^2 C_{n_{\dot{r},\omega}}$ and $C_{l_{\beta,\omega}} + k^2 C_{l_{\dot{r},\omega}}$, respectively. The static derivatives were taken from reference 2 and were measured at Reynolds numbers slightly higher than those for the present tests.

The effects of frequency on the measured stability derivatives are shown directly for the three wings tested in figures 11 to 14 wherein each figure is for a different stability derivative. These cross-plotted data are given for four angles of attack for each wing.

The measured stability derivatives are also cross plotted directly as functions of amplitude of oscillation for the three wings in figures 15 to 18 for the same angles of attack shown in the preceding figures.

In figure 19, the values of the derivative $C_{n_{r,\omega}}$ measured during the tests of reference 1 are added algebraically to the values of the derivative $C_{n_{\dot{\beta},\omega}}$ measured by means of tests similar to those of reference 2. The sums of these derivatives are compared with experimental values of $C_{n_{r,\omega}} - C_{n_{\dot{\beta},\omega}}$ for a corresponding frequency and amplitude of oscillation. Figures 20, 21, and 22 are similar comparison figures for the derivatives $C_{l_{r,\omega}} - C_{l_{\dot{\beta},\omega}}$, $C_{n_{\beta,\omega}} + k^2 C_{n_{\dot{r},\omega}}$, and $C_{l_{\beta,\omega}} + k^2 C_{l_{\dot{r},\omega}}$, respectively.

Although the following discussion has been divided into sections on the effects of angle of attack, of frequency, and of amplitude, it should be pointed out that, because of the apparent interrelationship among all three quantities, it is not possible to isolate the discussion concerning these parameters without discussing the related quantities as well. However, each of the following sections concerns itself primarily with the effect of the parameter being considered.

Effect of Angle of Attack

In discussing angle-of-attack effects on the measured stability derivatives, it will be convenient to refer to a low range of angle of attack and a high range of angle of attack. For the delta wing, this division takes place at approximately $\alpha = 18^{\circ}$; for the swept wing, at approximately $\alpha = 10^{\circ}$; and for the unswept wing, at approximately $\alpha = 8^{\circ}$. These are the angles, for the respective wings, below which frequency effects appear to be relatively small, and above which frequency effects are relatively large. It may be noted, from figure 6, that these angles of attack correspond to the angles where initial changes take place in the lift-curve slopes for each wing, indicating that these are also the angles of attack where flow separation has begun. Reference 3 shows that the magnitude of these stability derivatives depends substantially upon the degree of separation present on the wing.

The largest effects of frequency on the stability derivatives take place in the high-angle-of-attack range for each wing. At low angles of attack, a variation of reduced frequency had a slight effect on the magnitude of the derivatives, but at high angles of attack, frequency had a determining effect on the magnitude and, in some instances, on the sign of the derivatives. These results are, generally, in agreement with the effects of angle of attack and frequency presented in reference 3 for a set of wings of similar plan form to those tested for this investigation.

The data shown in figures 8, 9, and 10 are presented as functions of the nominal values of the uncorrected angle of attack. The same angles of attack corrected for jet-boundary effects are shown in figure 6.

Damping in yaw.- The damping-in-yaw derivative $C_{n_{r,\omega}} - C_{n_{\dot{\beta},\omega}}$ has small negative values at low angles of attack for each of the three wings tested (figs. 8, 9, and 10). At high angles of attack, the derivative becomes large and negative for the delta and swept wings with the largest negative values resulting for the lowest frequencies of oscillation. The derivative becomes positive at high angles of attack for the unswept wing with the largest positive values resulting for the lowest frequencies of oscillation. Those derivatives obtained for the swept wing at its highest angle of attack are substantially smaller than those measured for the delta wing at its highest angle of attack. The absolute magnitudes of $C_{n_{r,\omega}} - C_{n_{\dot{\beta},\omega}}$ for the unswept wing are likewise much smaller than for the swept wing at the highest angle for each wing.

Rolling moment due to yawing.- The rolling moment due to yawing parameter $C_{l_{r,\omega}} - C_{l_{\dot{\beta},\omega}}$ is small and generally positive at low angles of attack for the delta and swept wings. As the angle of attack is increased, the derivative becomes more positive for these wings with the largest values being realized for the lowest frequencies of oscillation. With an increase in frequency, the derivative tends to become more linear with angle of attack. The magnitudes of the derivative reached for the swept wing are not as large as those for the delta wing at the highest angle of attack for each wing.

In the case of the unswept wing, $C_{l_{r,\omega}} - C_{l_{\dot{\beta},\omega}}$ is generally small and positive at low angles of attack, except for perhaps the lowest frequency of oscillation for which some small negative values were measured. At high angles of attack, $C_{l_{r,\omega}} - C_{l_{\dot{\beta},\omega}}$ for the unswept wing becomes large and negative with the magnitude of the derivative again depending upon frequency. At $\alpha = 14^{\circ}$ for this wing, the variation of the derivative with angle of attack tends to reverse itself. This is the angle of attack where figure 6 indicates this wing to be completely stalled.

Directional stability.- The directional stability parameter $C_{n_{\beta,\omega}} + k^2 C_{n_{\dot{r},\omega}}$ for the delta and the swept wings is positive and increases with angle of attack at low angles of attack. At the high angles of attack, and for the lowest frequencies of oscillation, the derivative decreases and, for certain conditions, reverses sign and becomes negative. The higher frequencies reduce this trend toward the negative direction and make the variation of the derivative become more linear with angle of attack. The derivative for the unswept wing is a small positive value at low angles of attack and becomes increasingly positive as the angle of attack is increased through the high range. Frequency has only a small effect for this wing at high angles of attack but, again, the lower test frequencies produce the largest values of the derivative.

The static values of C_{n_β} are also shown in figures 8, 9, and 10 together with the oscillatory values of $C_{n_{\beta,\omega}} + k^2 C_{n_{\dot{r},\omega}}$. These static derivatives were measured for the investigation of reference 2 at slightly higher Reynolds numbers than those for the present tests. The static values of C_{n_β} exhibit the same trend with angle of attack as is shown by the oscillatory derivative at the lowest frequencies.

Effective dihedral.- The effective dihedral parameter $C_{l_{\beta,\omega}} + k^2 C_{l_{\dot{r},\omega}}$ is negative at zero angle of attack and increases negatively as the angle of attack is increased in the low angle-of-attack range for all three wings. For the delta and swept wings, the variation with angle of attack tends to reverse itself at high angles and, for the lowest frequencies of oscillation, the reversal causes a definite reduction in the derivative and a change of sign under certain conditions. As the frequency is increased, the derivative tends to become more linear with angle of attack at least for the delta wing. In the case of the swept wing, the derivative becomes positive at high angles of attack for all frequencies with the possible exception of the highest frequency for which the derivative approaches zero magnitude at $\alpha \approx 16^\circ$ and then increases in the negative direction at higher angles of attack. The derivative for the unswept wing continues increasing in the negative direction as the angle of attack is increased to its largest value. The largest negative values of the derivative were obtained for the lowest frequency of oscillation.

The static values of C_{l_β} from reference 2 are also shown in figures 8, 9, and 10 together with the oscillatory derivatives $C_{l_{\beta,\omega}} + k^2 C_{l_{\dot{r},\omega}}$. The static values of C_{l_β} had about the same variation with angle of attack as is shown by the oscillatory derivatives. The change of sign of C_{l_β} for the swept wing occurred at a somewhat higher angle of attack than it did for the oscillation derivatives. Check tests, however, indicated that the proper Reynolds number would shift this angle of attack to the lower value shown by the oscillation data.

Effect of Frequency

Damping in yaw.- The effect of frequency on the damping in yaw $C_{n_{r,\omega}} - C_{n_{\dot{\beta},\omega}}$ is shown more directly in figure 11 for the delta, swept, and unswept wings. These cross plots are presented for four angles of attack for each wing and for all amplitudes of oscillation. At $\alpha = 18^\circ$ for the delta wing, frequency has little or no effect on the damping (fig. 11(a)), but for each succeedingly higher angle, the effect of frequency is to make the overall variation of $C_{n_{r,\omega}} - C_{n_{\dot{\beta},\omega}}$ greater as

the angle of attack is increased. The largest values of the derivative result for the smallest values of the reduced frequency for each angle of attack. For the swept wing (fig. 11(b)) frequency has only a slight effect on the derivative at $\alpha = 18^{\circ}$ and a somewhat larger effect at $\alpha = 22^{\circ}$. These curves show trends with frequency similar to those for the delta wing with the difference that the frequency effects are much smaller. The results for the unswept wing in figure 11(c), in general, indicate no frequency effects on $C_{n_{r,\omega}} - C_{n_{\dot{\beta},\omega}}$ up to the highest angle of attack at which tests were made.

Rolling moment due to yawing.- The rolling moment due to yawing parameter $C_{l_{r,\omega}} - C_{l_{\dot{\beta},\omega}}$ is shown directly as a function of frequency in figure 12 for the three wings. There is little effect of frequency indicated for the delta wing at $\alpha = 18^{\circ}$ in figure 12(a), but as the angle of attack was increased thereafter, the variation due to frequency became greater for each successive angle of attack. The largest effects of frequency were found at the lower frequencies of oscillation for each angle of attack.

A small frequency effect on the derivative is indicated for the swept wing in figure 12(b) at $\alpha = 18^{\circ}$ and a somewhat larger effect at $\alpha = 22^{\circ}$. These changes due to frequency are similar to but are much smaller than those indicated for the delta wing in figure 12(a). The unswept wing in figure 12(c) exhibits values of $C_{l_{r,\omega}} - C_{l_{\dot{\beta},\omega}}$ which vary slightly with frequency at the two higher angles of attack in a manner opposite to the variations shown by the delta and swept wings. The derivative becomes more positive as the frequency is increased rather than more negative as for the delta and swept wings.

Directional stability.- The derivative $C_{n_{\beta,\omega}} + k^2 C_{n_{\dot{r},\omega}}$ is shown in figure 13 directly as a function of the reduced frequency for four angles of attack for each of the three wings. As the frequency parameter is increased from its lowest value at $\alpha = 18^{\circ}$ for the delta wing (fig. 13(a)), there takes place a slight positive increase in the derivative. This effect of frequency becomes larger at the higher angles of attack until, at $\alpha = 32^{\circ}$, $C_{n_{\beta,\omega}} + k^2 C_{n_{\dot{r},\omega}}$ may be either negative (at the lowest frequencies) or positive depending on the frequency. For the swept wing in figure 13(b) the directional stability varies with frequency at the higher angles of attack in the manner of, but not as much as for, the delta wing. No particular effects of frequency are indicated on this derivative for the unswept wing in figure 13(c) at any angle of attack.

The static values of C_{n_β} appear in figure 13 as the $\omega b/2V = 0$ value of $C_{n_{\beta,\omega}} + k^2 C_{n_{\dot{r},\omega}}$. In general, the variation of the oscillatory derivative with frequency parameter approaches the static C_{n_β} for each

angle of attack for all wings. This approach to zero frequency appears to be somewhat smoother for the larger amplitudes of oscillation than for the smaller amplitudes.

Effective dihedral.- The effect of the frequency parameter on $C_{l_{\beta,\omega}} + k^2 C_{l_{\dot{r},\omega}}$ is shown directly in figure 14. The frequency effect that is indicated at $\alpha = 18^\circ$ for the delta wing becomes larger for each angle as the angle of attack is increased. At high frequencies of oscillation, the derivative has about the same magnitudes regardless of the angle of attack, but at the low frequencies, the derivative becomes more positive as the angle of attack grows larger. For the two highest angles of attack, the derivative becomes positive at the lowest frequency of oscillation.

The results for the swept wing in figure 14(b) indicate that the effective dihedral derivative is generally more positive than it is for the delta wing, but that the effect of frequency is roughly the same. The unswept wing in figure 14(c) shows little effect of frequency except at $\alpha = 16^\circ$ where the frequency effect appears to be somewhat dependent upon amplitude of oscillation. For the largest amplitudes, the derivative becomes less negative as the frequency is increased; for the smallest amplitude, however, the derivative in general becomes more negative at higher frequencies of oscillation.

The extreme nonlinearities which occur particularly for low-frequency and small-amplitude oscillations such as are shown for the unswept wing in figure 14(c) may be at least partially the fault of the data-reduction process employed. Because the measured moments were divided by the frequency and the amplitude in order to evolve the derivative form, small errors of measurement tend to be exaggerated for low-frequency and small-amplitude conditions of oscillation.

The oscillatory values of $C_{l_{\beta,\omega}} + k^2 C_{l_{\dot{r},\omega}}$, in general, tend to approach the static values of C_{l_β} for all wings, especially for the higher amplitudes of oscillation. The static C_{l_β} is shown in figure 14 as the $\omega b/2V = 0$ value of the oscillation derivative.

Effect of Amplitude

The effect of the variation of amplitude on the oscillatory derivatives under consideration is not as clear cut or consistent as is the effect previously discussed of the variation of frequency. The amplitude effects that appear in the data are interdependent with both frequency and angle of attack in that certain trends with amplitude may appear at one angle or one range of amplitude variation whereas reverse trends may

appear at a slightly different angle of attack or another range of the amplitude variation.

Damping in yaw.- Where amplitude effects on the damping in yaw do occur, they appear to be most important at the lowest frequencies of oscillation. For those angles of attack where an amplitude effect is in evidence, this effect diminishes as the frequency is increased and generally disappears at the highest frequencies. For example, in figure 15(a) where $C_{n_{r,\omega}} - C_{n_{\dot{\beta},\omega}}$ is shown directly as a function of oscillation amplitude for the delta wing, certain effects of amplitude are indicated. For the lowest frequency, at $\alpha = 18^{\circ}$, a slight reduction in damping takes place as the amplitude is increased from $\psi_o = 2^{\circ}$ to $\psi_o = 6^{\circ}$, but as the amplitude is increased further the damping remains constant. At $\alpha = 24^{\circ}$ for the lowest frequency, the damping increases as the amplitude becomes larger than 4° whereas at $\alpha = 28^{\circ}$ and $\alpha = 32^{\circ}$ the damping generally increases at low amplitudes, but decreases and then levels off at the larger amplitudes. Higher frequencies of oscillation tend to diminish the amplitude effect until, at the highest frequency, the damping shows a variation with amplitude only at $\alpha = 32^{\circ}$ and this effect is small.

The swept wing in figure 15(b) exhibits an effect of amplitude on the damping only at $\alpha = 22^{\circ}$ for the lower frequencies of oscillation. The unswept wing in figure 15(c) shows some effects at low frequencies and small amplitudes of oscillation.

Rolling moment due to yawing.- The effects of amplitude on $C_{l_{r,\omega}} - C_{l_{\dot{\beta},\omega}}$, which are indicated in figure 16, are similar to those described for $C_{n_{r,\omega}} - C_{n_{\dot{\beta},\omega}}$. For the delta wing at $\alpha = 18^{\circ}$, the derivative becomes more positive with increased amplitude, although as the frequency is increased this effect is diminished. At $\alpha = 24^{\circ}$, the greatest change in the derivative takes place at the large amplitudes and the lowest frequency, whereas at $\alpha = 28^{\circ}$, the greatest change takes place at the small amplitudes and the lowest frequency.

Directional stability.- The derivative $C_{n_{\beta,\omega}} + k^2 C_{n_{\dot{r},\omega}}$ varies with amplitude in the manner shown in figure 17. The delta wing exhibits amplitude effects for all frequencies of oscillation at $\alpha = 28^{\circ}$ and $\alpha = 32^{\circ}$ which are about equal in magnitude but opposite in direction. At $\alpha = 28^{\circ}$, an increase in amplitude generally reduces the derivative, whereas at $\alpha = 32^{\circ}$, an increase in amplitude makes the derivative more positive.

For the swept wing at $\alpha = 22^{\circ}$ (fig. 17(b)), an increase of amplitude makes the derivative slightly more positive for the lowest frequency; for the highest frequency a reverse effect, although slight, is indicated.

Effective dihedral.- The effect of amplitude on $C_{l_{\beta,\omega}} + k^2 C_{l_{\dot{r},\omega}}$ is shown in figure 18. For the delta wing at $\alpha = 18^\circ$, and for the lowest frequency of oscillation, an increase in amplitude reduces the magnitude of the derivative at low amplitudes, whereas at the higher amplitudes, the magnitude of the derivative remains about constant with amplitude. At $\alpha = 24^\circ$, for the lowest frequency, increasing the amplitude reduces the derivative for all amplitudes. A reversal in the variation with amplitude is indicated at $\alpha = 28^\circ$ for this frequency; and at $\alpha = 32^\circ$ the derivative increases in magnitude throughout the amplitude range.

The data for the swept wing at $\alpha = 22^\circ$, in figure 18(b), shows a reversal in trend with amplitude between the lowest and highest frequencies of oscillation. The derivative for the unswept wing at the higher angles of attack (fig. 18(c)) exhibits large variations due to amplitude and reversals in trend between the low and high amplitudes of oscillation. These variations with amplitude are strongly dependent upon frequency.

Comparison of Experimental Derivatives and Addition of Component Derivatives

The derivatives $C_{n_{r,\omega}}$, $C_{n_{\dot{r},\omega}}$, $C_{l_{r,\omega}}$, and $C_{l_{\dot{r},\omega}}$ were measured at $\omega b/2V = 0.22$ and an amplitude corresponding to $\psi_o = 8^\circ$ for the investigation of reference 1. The derivatives $C_{n_{\beta,\omega}}$, $C_{n_{\dot{\beta},\omega}}$, $C_{l_{\beta,\omega}}$, and $C_{l_{\dot{\beta},\omega}}$ were determined by a series of tests similar to those of reference 2. The latter were forced-oscillation tests with $\omega b/2V = 0.22$ and an amplitude of sideslip of $\beta_o = 6^\circ$. These individual derivatives, and the appropriate algebraic additions thereof, are compared in figures 19 to 22 with the corresponding combination derivatives measured in the present investigation for $\omega b/2V = 0.22$ and $\psi_o = 6^\circ$. In general, the comparisons are good. In figure 19, the experimentally combined damping-in-yaw derivative for the delta wing is just a little larger than the sum of the individual derivatives through the angle-of-attack range. The comparisons for the swept and unswept wings are also generally in good agreement. Figure 19 indicates for these wings that the $C_{n_{\dot{\beta},\omega}}$ derivative is larger in absolute magnitude than the $C_{n_{r,\omega}}$ derivative at high angles of attack and therefore is the major contributor to the damping in yaw as determined in these tests.

The algebraic sum of the individual derivatives $C_{l_{r,\omega}}$ and $C_{l_{\dot{\beta},\omega}}$ appears to be somewhat more positive by an almost constant increment through the angle-of-attack range than the experimentally obtained combination derivative for the delta wing (fig. 20). The added derivatives

are also more positive than the experimental derivatives for the swept wing up to $\alpha = 16^{\circ}$, and for the unswept wing at all angles of attack greater than zero. Figure 20 indicates that, at least for the delta and swept wings, the $C_{l_{\dot{\beta},\omega}}$ contributes a greater portion to the combination derivative than does $C_{l_{r,\omega}}$.

The algebraically added derivatives $C_{n_{\beta,\omega}}$ and $k^2C_{n_{\dot{r},\omega}}$ are presented in figure 21 and compared with the experimental derivatives. Although $C_{n_{\dot{r},\omega}}$ can have large magnitudes of its own, as demonstrated by the investigation of reference 1, the multiplication of this derivative by k^2 would be expected to reduce the significance of this term in the determination of the directional stability parameter except for, perhaps, extremely large values of the reduced frequency or the derivative $C_{n_{\dot{r},\omega}}$. Figure 21 shows this $k^2C_{n_{\dot{r},\omega}}$ contribution to be small relative to the large $C_{n_{\beta,\omega}}$ contributions for the delta and the unswept wings at high angles of attack. The swept wing has relatively small values of $C_{n_{\beta,\omega}}$ which are of about the same magnitude as $k^2C_{n_{\dot{r},\omega}}$ for most of the high-angle-of-attack range.

The contribution of $k^2C_{l_{\dot{r},\omega}}$ to the effective dihedral derivative is also small relative to $C_{l_{\beta,\omega}}$ for the delta and the unswept wings (fig. 22). At lower frequencies of oscillation, the $k^2C_{l_{\dot{r},\omega}}$ contribution to the derivative would be of less significance still since the k^2 factor would overpower even $C_{l_{\dot{r},\omega}}$ derivatives of very large magnitude as k approached zero. The nonlinear variation with angle of attack shown by $C_{l_{\beta,\omega}} + k^2C_{l_{\dot{r},\omega}}$ for the swept wing can be attributed to the $C_{l_{\beta,\omega}}$ portion of the derivative.

The particular model yawing motion employed for these tests was such that the amplitude of the sideslipping motion was the negative of the amplitude of the yawing motion so that $\beta_o/\psi_o = -1$. Airplane lateral motions may be made up of any ratio of these amplitudes, although motions wherein $\beta_o/\psi_o \approx -1$ occur quite frequently. When this ratio is close to -1 and when the phase relationship between the separate motions is small, then the stability derivatives may be combined in the airplane lateral equations of motion in the forms used in this paper. The resulting agreement between the addition of the separately determined β and ψ derivatives and the combination derivatives measured herein, indicate that for $\beta_o/\psi_o = -1$, at least, and for $\omega b/2V = 0.22$, the aerodynamic phenomena responsible for the individual derivatives are linear to a large degree in that the individual derivatives are approximately

additive. For low values of the reduced frequency, however, it is possible that the individual derivatives may not add up quite as well as at the high reduced frequency because of the large effects of frequency and amplitude which exist at low frequencies and which indicate lessening linearity.

CONCLUSIONS

A delta wing, a swept wing, and an unswept wing were oscillated in yaw about their quarter-chord points in order to determine the separate effects of frequency and amplitude on the combination lateral stability derivatives resulting from this motion. The results of this investigation indicate the following conclusions:

1. The frequency of oscillation had a determining influence on the stability derivatives for the delta wing at high angles of attack. The largest changes in the variations of the derivatives with angle of attack took place for the lowest frequencies of oscillation; as the frequency increased, the effects of frequency became smaller and the derivatives became more linear with angle of attack. Similar effects of frequency, but to a smaller extent, were shown for the derivatives of the swept wing. Those for the unswept wing were apparently influenced only slightly by frequency.

2. The effect of amplitude of oscillation on the stability derivatives appears to depend substantially upon the angle of attack of the wing and upon the frequency of oscillation. Some large effects of amplitude were shown on the derivatives for the delta wing at high angles of attack and for the lowest frequency of oscillation. As the frequency was increased to its highest value, these effects of amplitude, in general, disappeared. Similar amplitude effects were indicated for the swept wing to a lesser degree, but, in general, did not appear for the unswept wing.

3. A comparison of the present results with the results of previous investigations for a corresponding frequency and amplitude indicated that the $\dot{\beta}$ derivatives are somewhat larger in absolute magnitude than the r derivatives with which they are generally combined. The $\dot{r}$ derivatives, while of large magnitude themselves, lose significance when combined with the β derivatives because of their multiplication by the square of the frequency parameter. Hence, in the range of frequencies being considered, the in-phase stability derivatives are determined primarily by the β derivatives. As the frequency of oscillation became smaller, the combination in-phase derivatives approached the static (zero frequency) β derivatives.

4. The algebraic addition of the component derivatives gave results which were generally in good agreement with the derivatives obtained in combination for the present investigation. These results indicate that the aerodynamic phenomena responsible for these derivatives are linear to a large degree.

Langley Aeronautical Laboratory,
National Advisory Committee for Aeronautics,
Langley Field, Va., January 6, 1956.

REFERENCES

1. Queijo, M. J., Fletcher, H. S., Marple, C. G., and Hughes, F. M.: Preliminary Measurements of the Aerodynamic Yawing Derivatives of a Triangular, a Swept, and an Unswept Wing Performing Pure Yawing Oscillation, With a Description of the Instrumentation Employed. NACA RM L55L14, 1956.

2. Riley, Donald R., Bird, John D., and Fisher, Lewis R.: Experimental Determination of the Aerodynamic Derivatives Arising From Acceleration in Sideslip for a Triangular, a Swept, and an Unswept Wing. NACA RM L55A07, 1955.

3. Campbell, John P., Johnson, Joseph L., Jr., and Hewes, Donald E.: Low-Speed Study of the Effect of Frequency on the Stability Derivatives of Wings Oscillating in Yaw With Particular Reference to High Angle-of-Attack Conditions. NACA RM L55H05, 1955.

4. Campbell, John P., and Woodling, Carroll H.: Calculated Effects of the Lateral Acceleration Derivatives on the Dynamic Lateral Stability of a Delta-Wing Airplane. NACA RM L54K26, 1955.

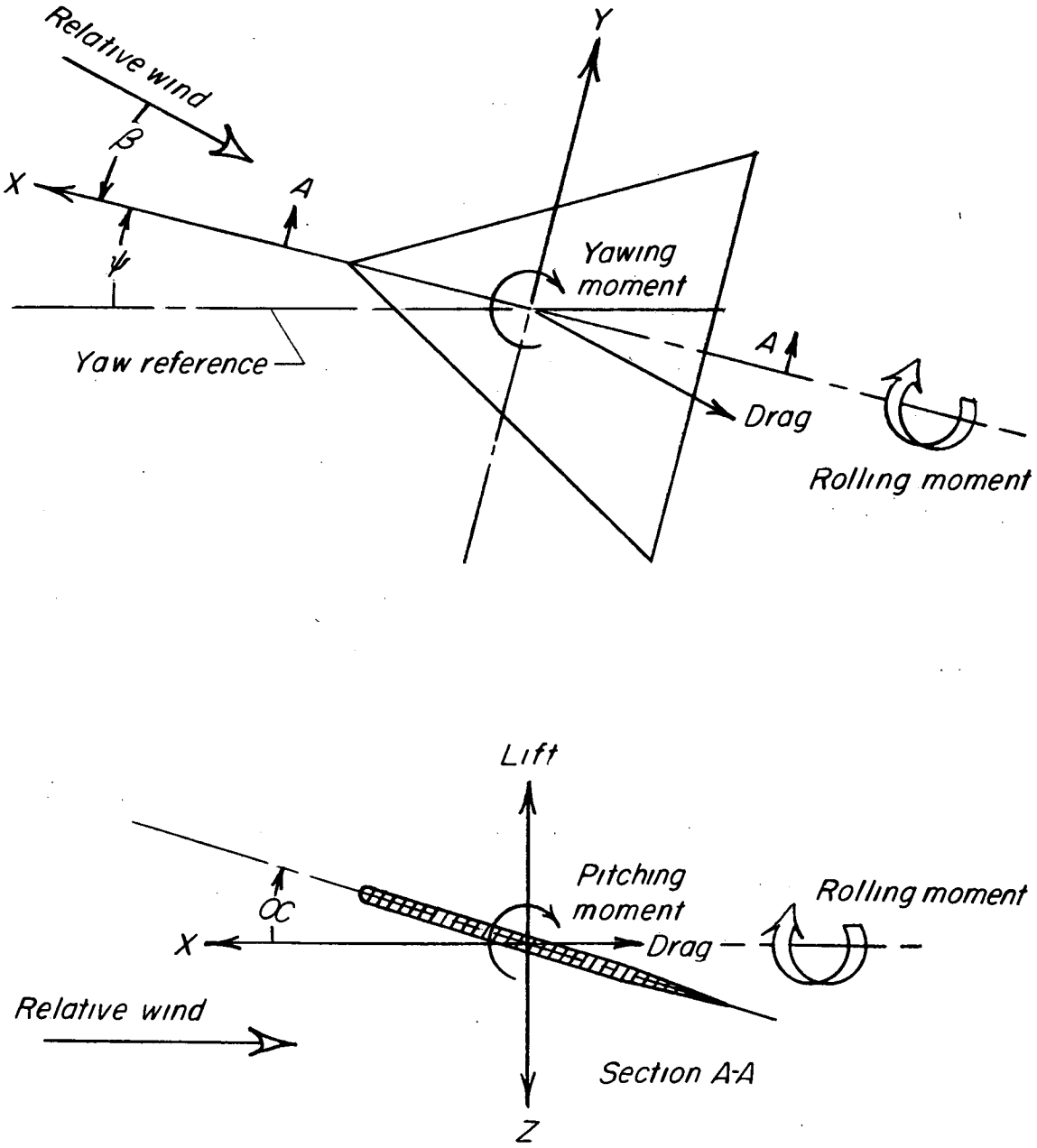

Figure 1.- System of stability axes. Arrows indicate positive forces, moments, and angular displacements. Yaw reference is generally chosen to coincide with initial relative wind.

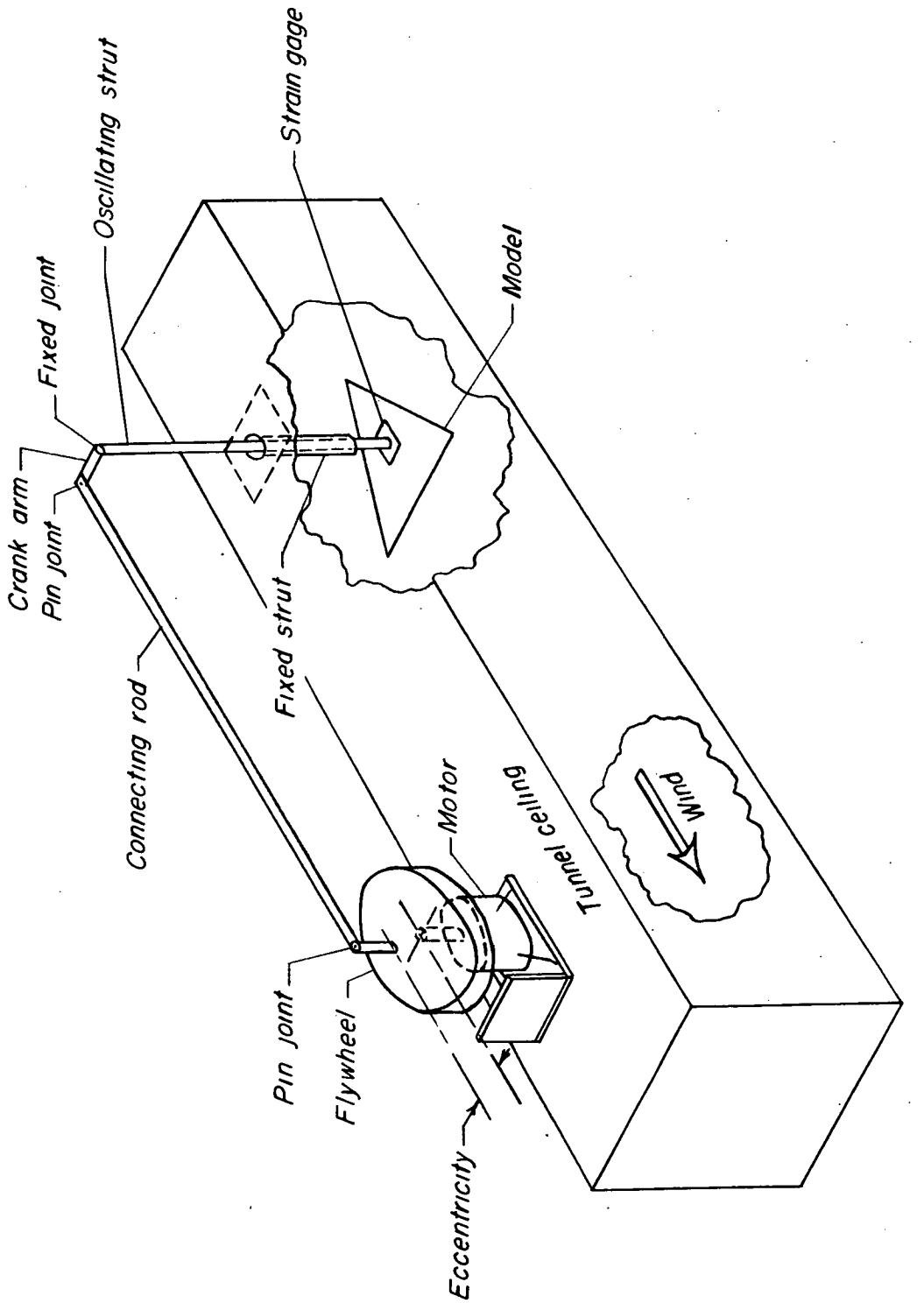

Figure 2.- Sketch of oscillation-in-yaw equipment.

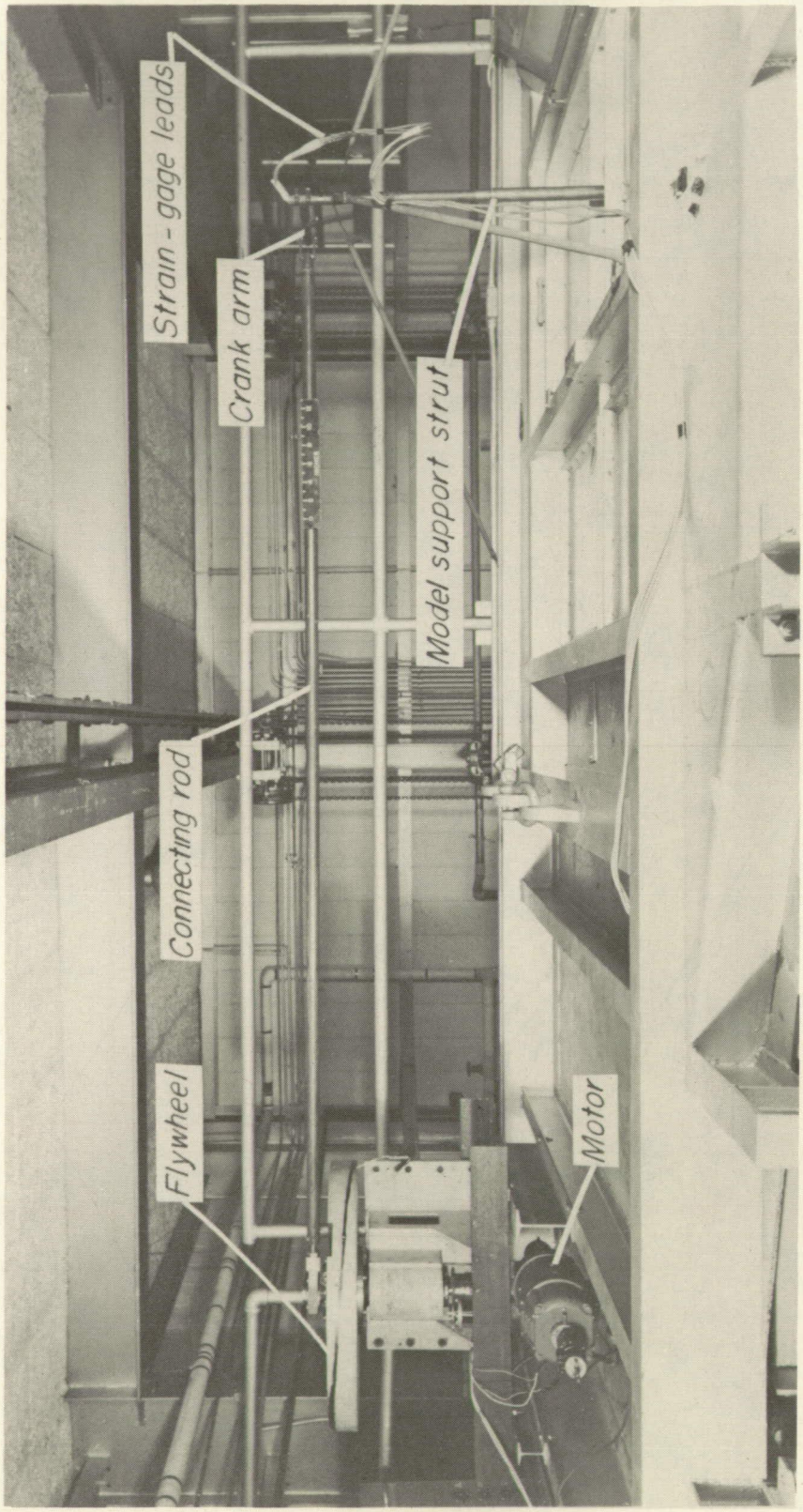

L-90944.1

Figure 3.- Photograph of oscillation-in-yaw equipment on top of tunnel test section.

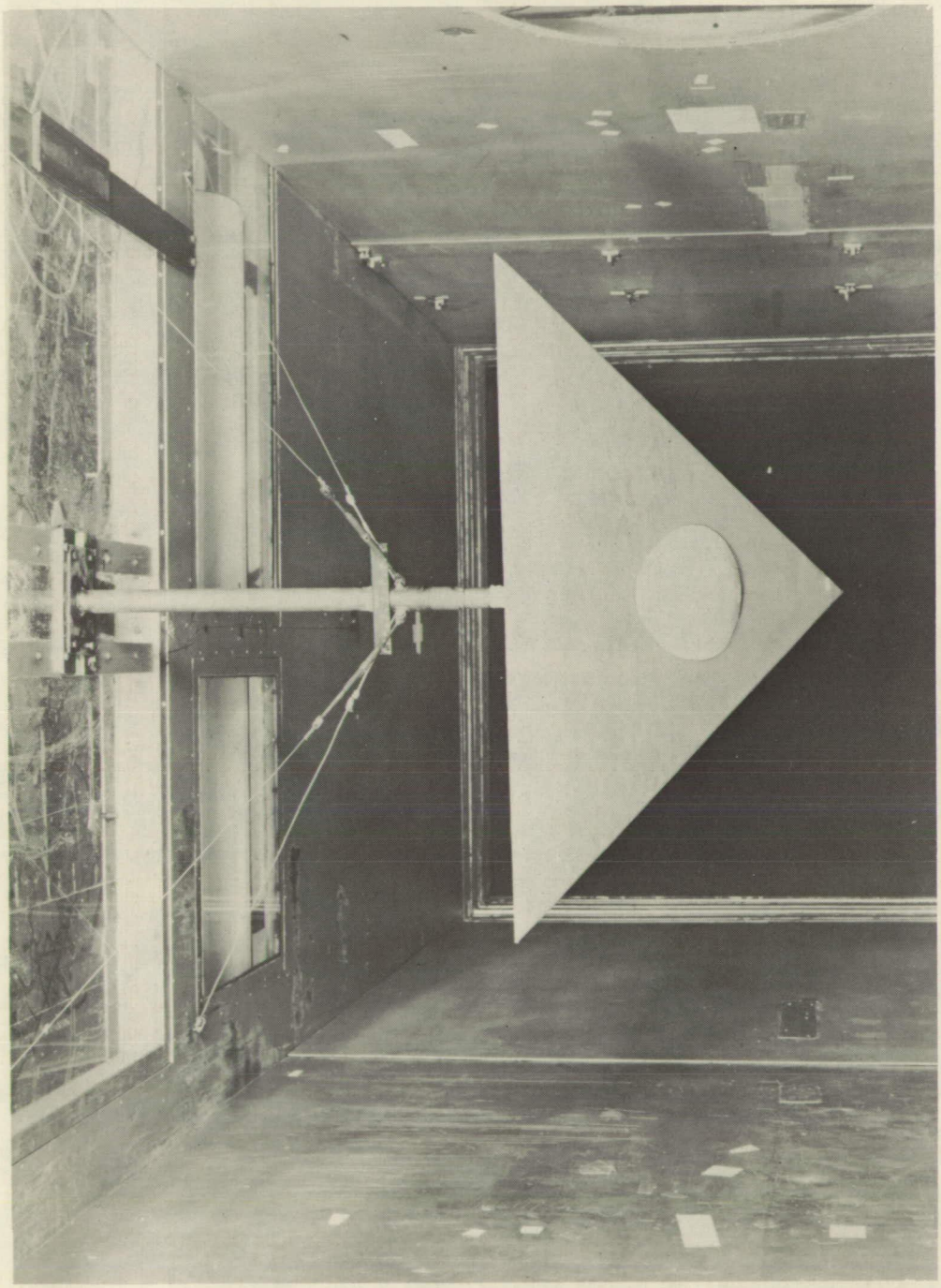

L-90948

(a) 60° delta wing.

Figure 4.- Photographs of models in tunnel test section.

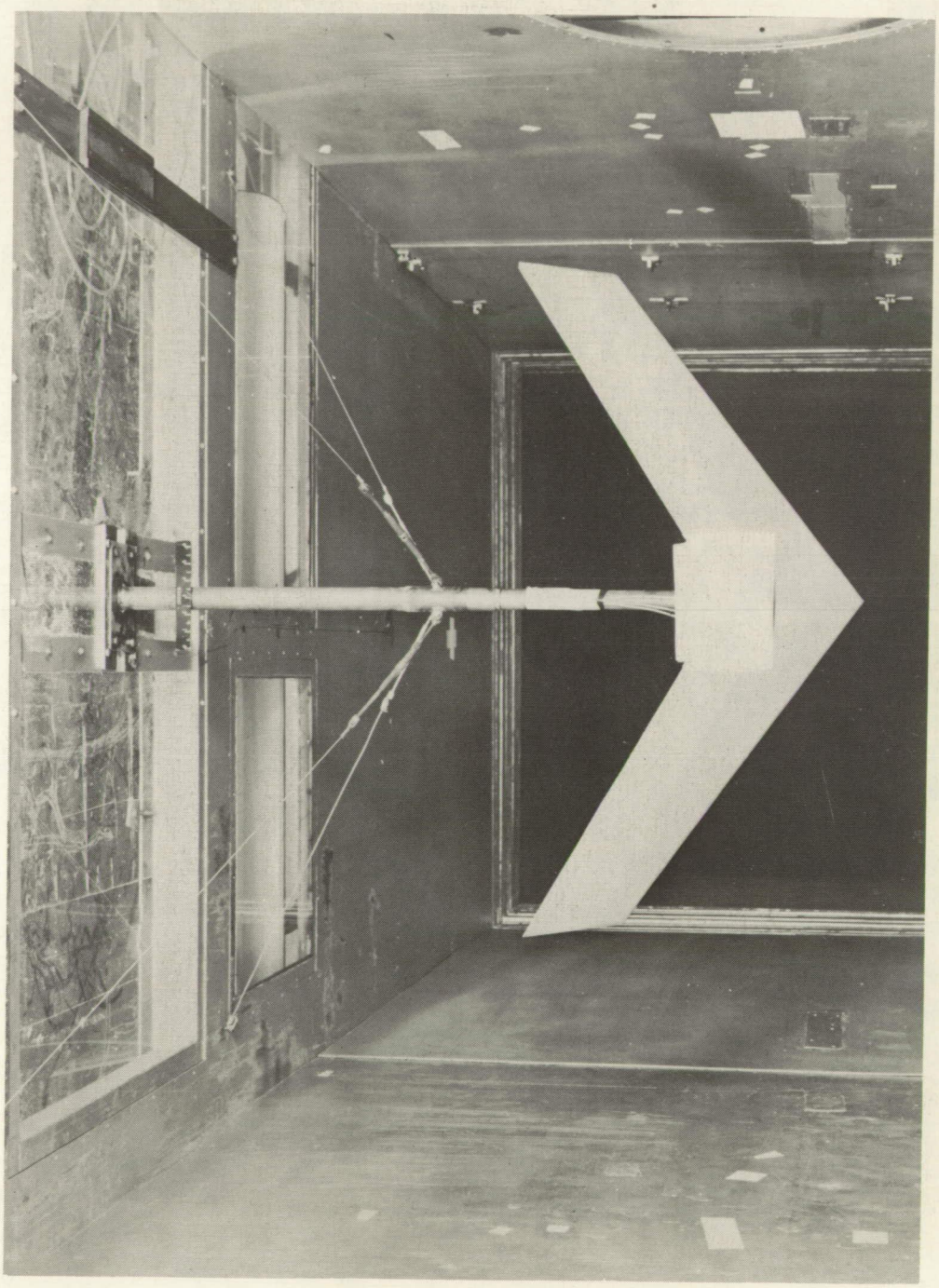

L-90946

(b) 45° swept wing.

Figure 4.- Continued.

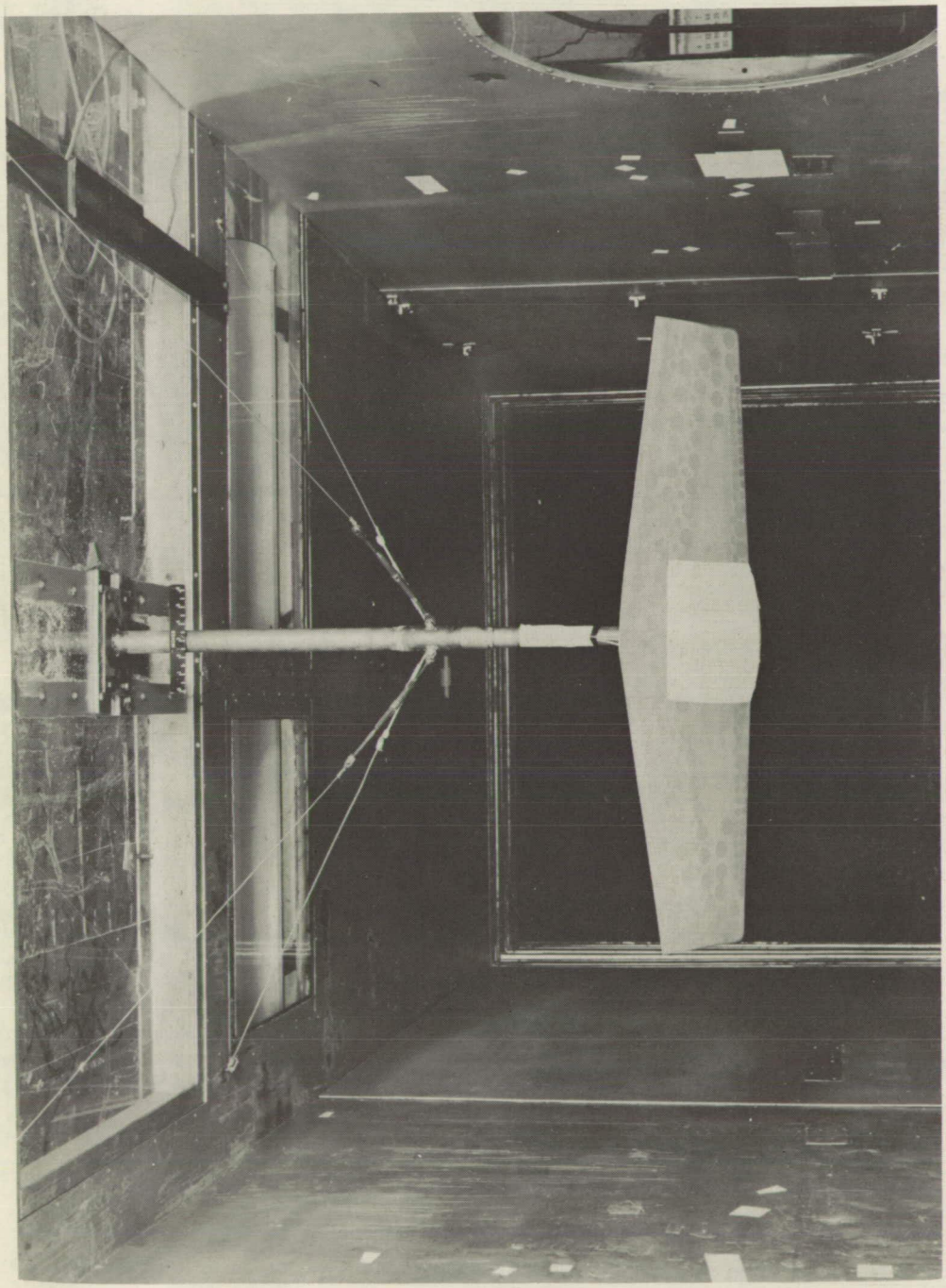

L-90947

(c) Unswept wing.

Figure 4.- Concluded.

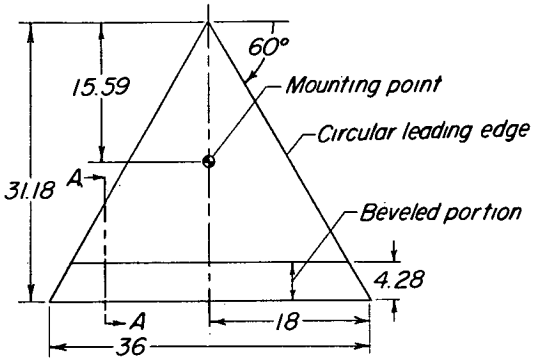

Delta wing

Aspect ratio	2.31
Leading-edge sweep angle, deg.	60
Dihedral angle, deg.	0
Twist, deg.	0
Airfoil section	Flat plate
Area, sq. in.	561.20
Span, in.	36.00
Mean aerodynamic chord, in.	20.79

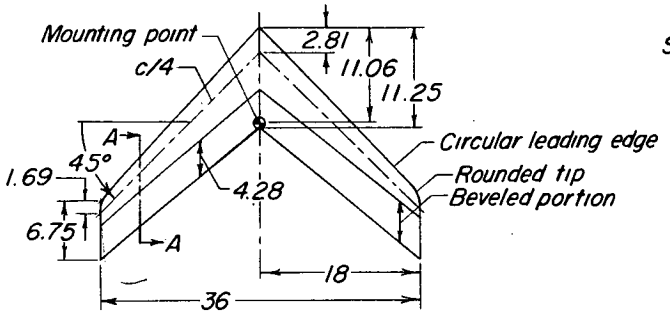

Swept wing

Aspect ratio	4.0
Taper ratio	0.6
Quarter chord sweep angle, deg.	45
Dihedral angle, deg.	0
Twist, deg.	0
Airfoil section	Flat plate
Area, sq. in.	324
Span, in.	36
Mean aerodynamic chord, in.	9.19

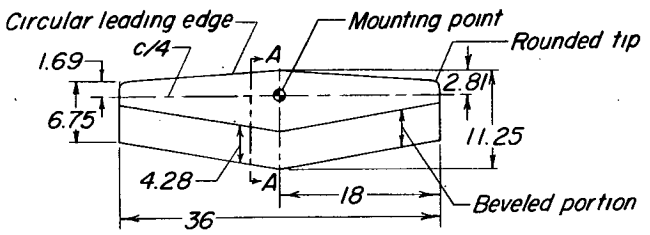

Unswept wing

Aspect ratio	4.0
Taper ratio	0.6
Quarter chord sweep angle, deg.	0
Dihedral angle, deg.	0
Twist, deg.	0
Airfoil section	Flat plate
Area, sq. in.	324
Span, in.	36
Mean aerodynamic chord, in.	9.19

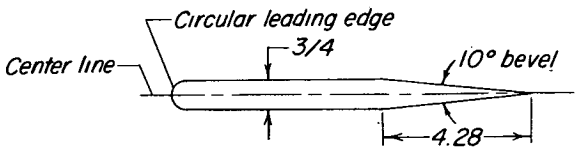

Section A-A

Figure 5.- Sketches and geometric characteristics of the three wing models investigated. All dimensions are in inches.

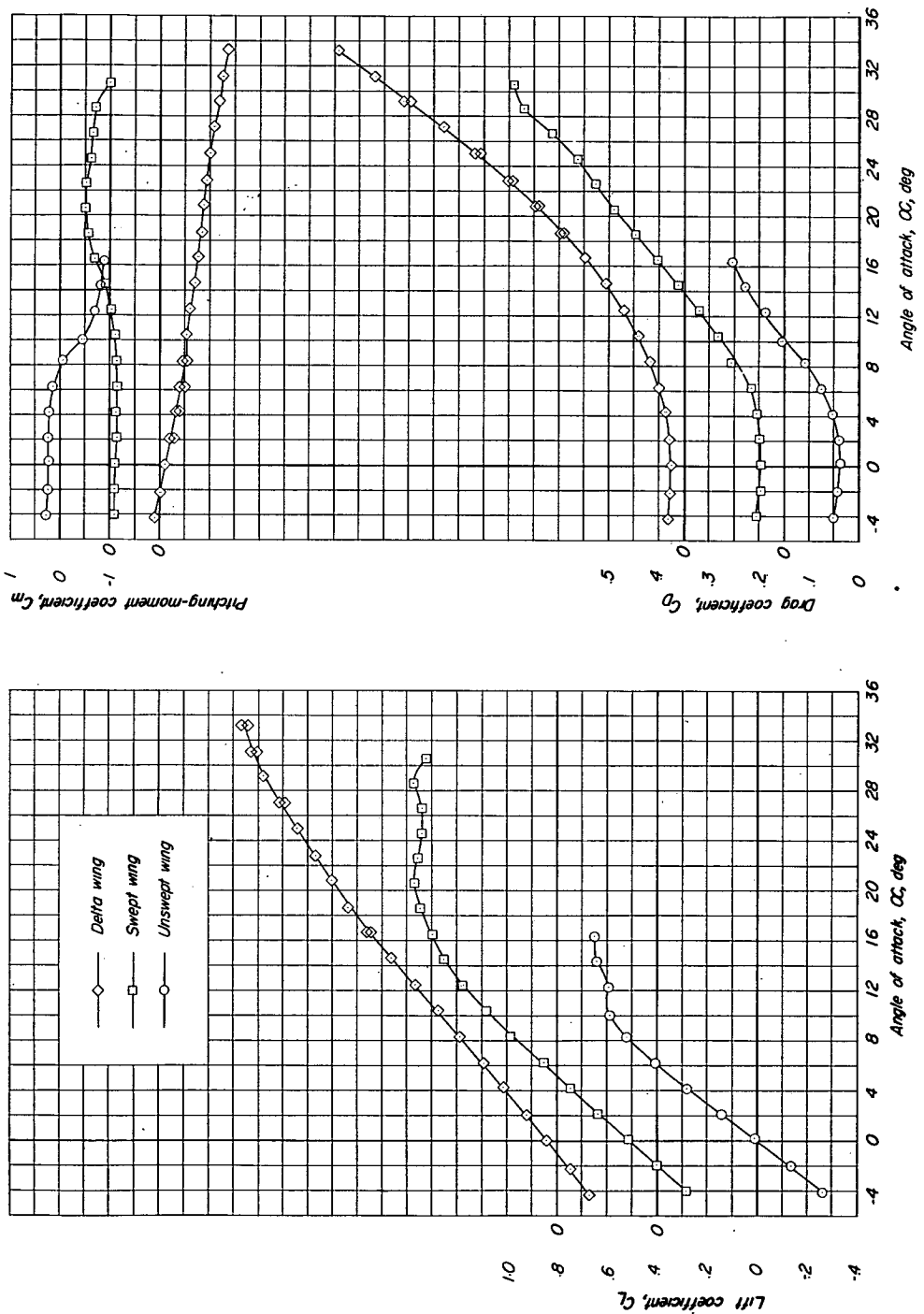

Figure 6.- Lift, drag, and pitching-moment characteristics as a function of angle of attack for the unswept, the 45° swept, and the 60° delta wings. q = 40 lb/sq ft.

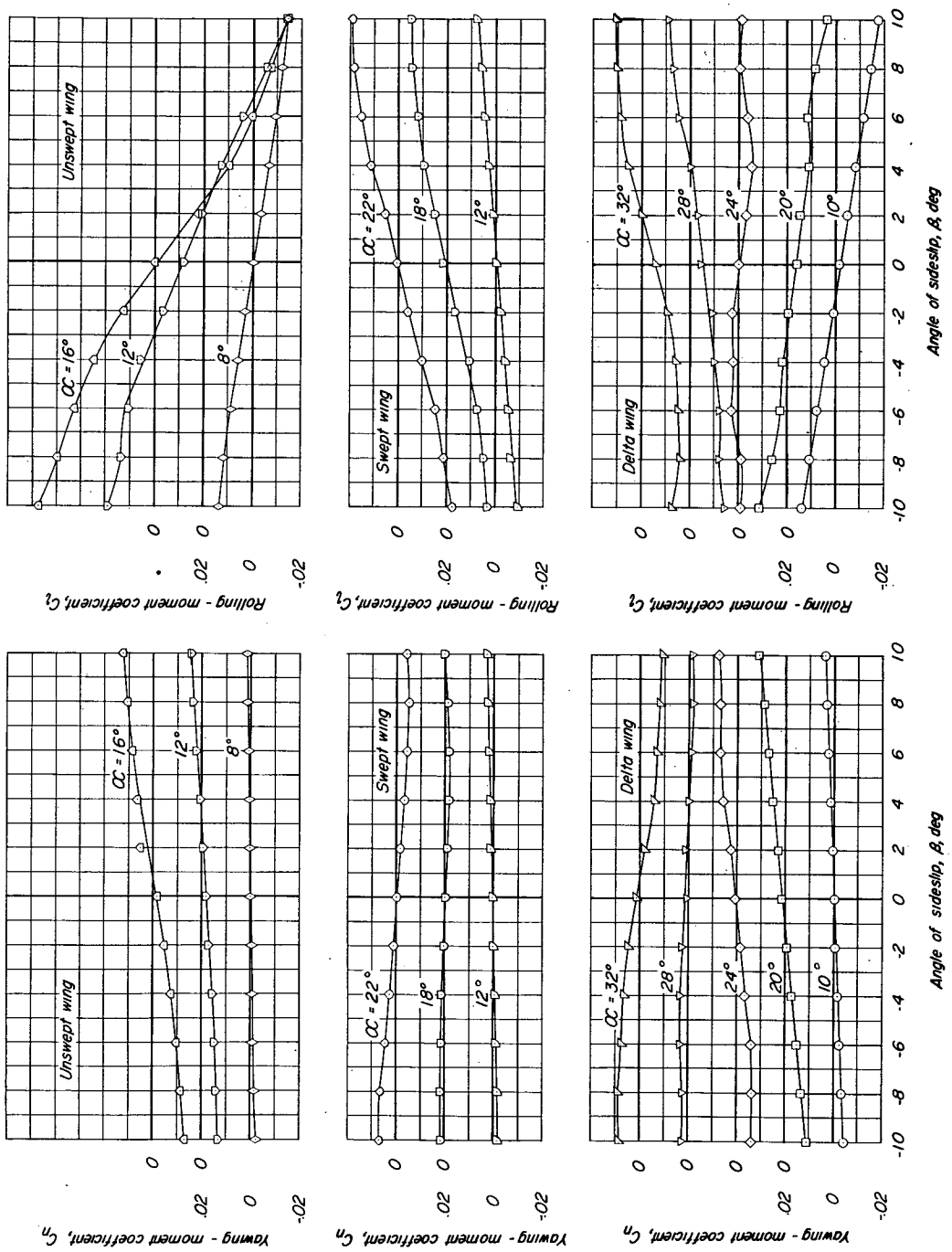

Figure 7.- The variation of yawing-moment and rolling-moment coefficients with angle of sideslip for q = 25 lb/sq ft.

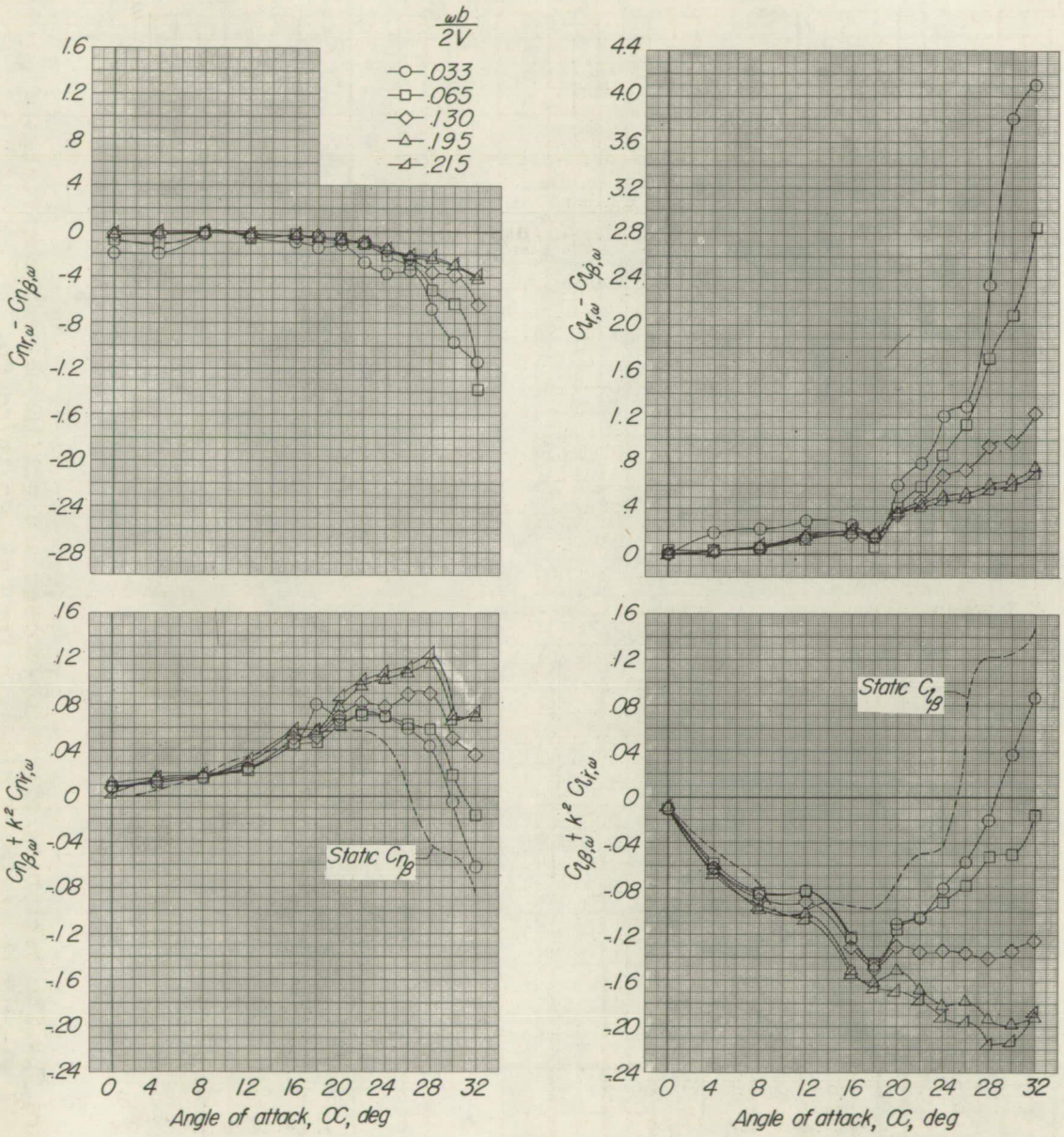

(a) $\psi_o = 2^o$.

Figure 8.- The stability derivatives measured during oscillation for the delta wing.

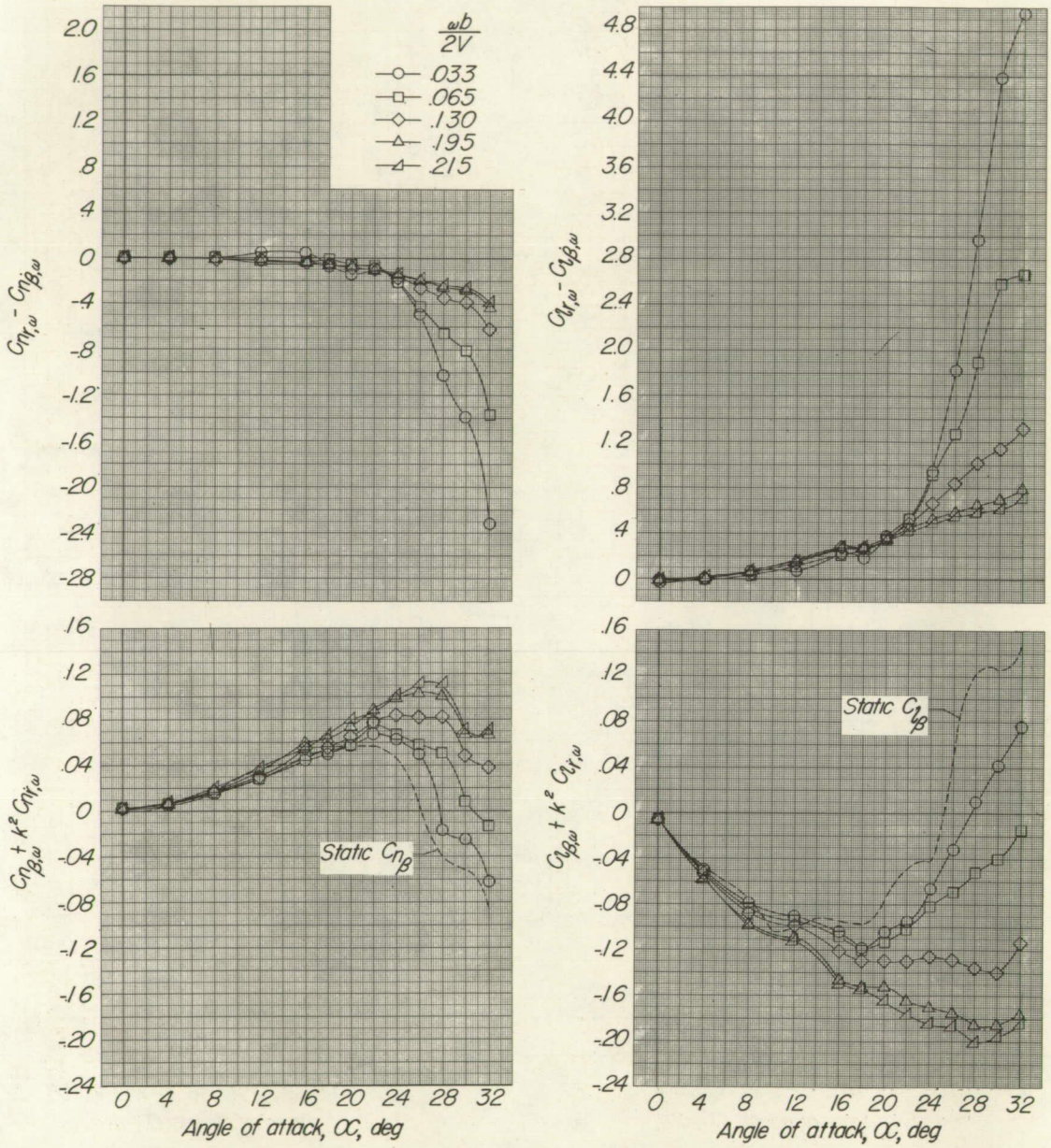

(b) $\psi_o = 4^o$.

Figure 8.- Continued.

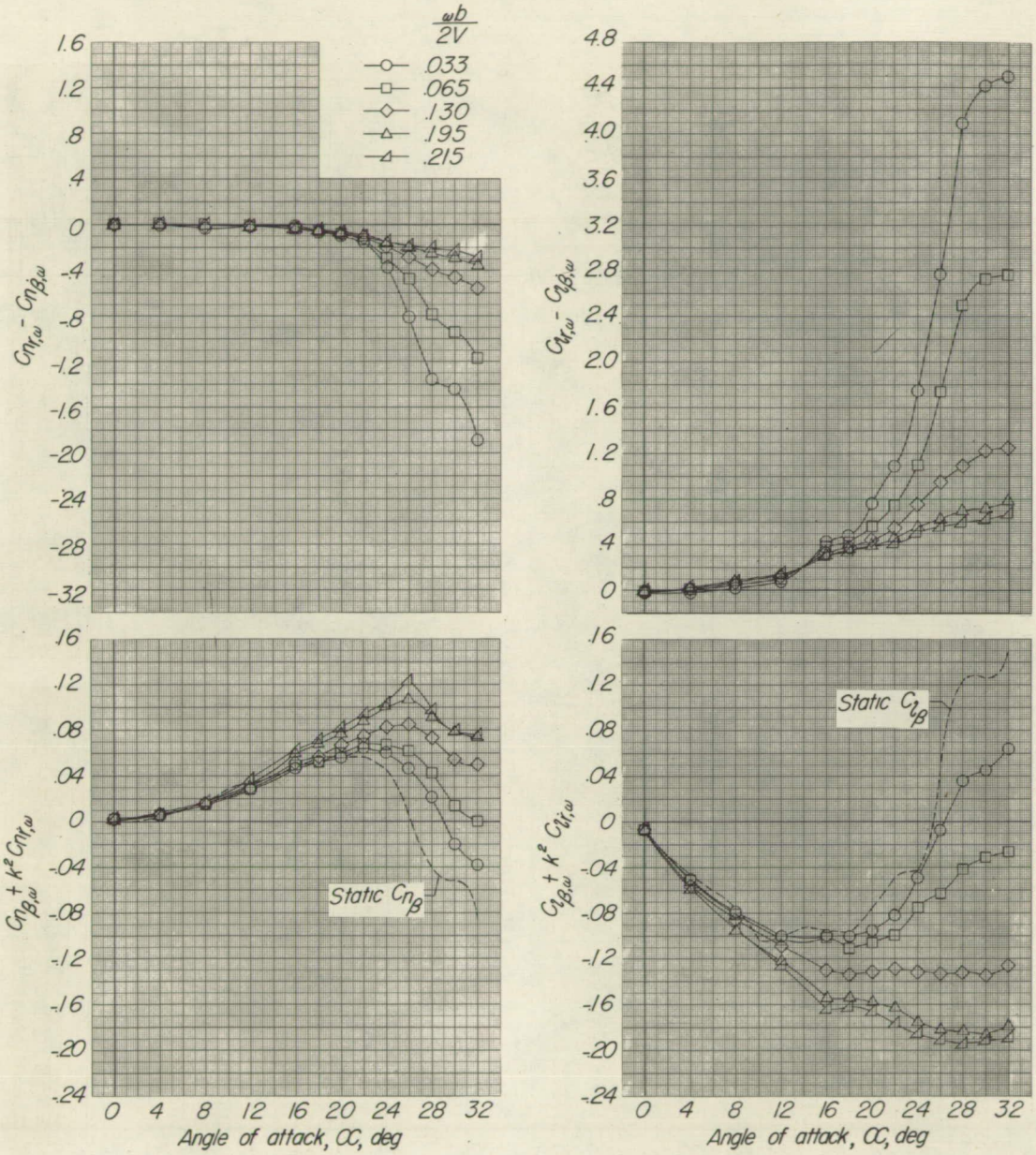

(c) $\psi_o = 6^\circ$.

Figure 8.- Continued.

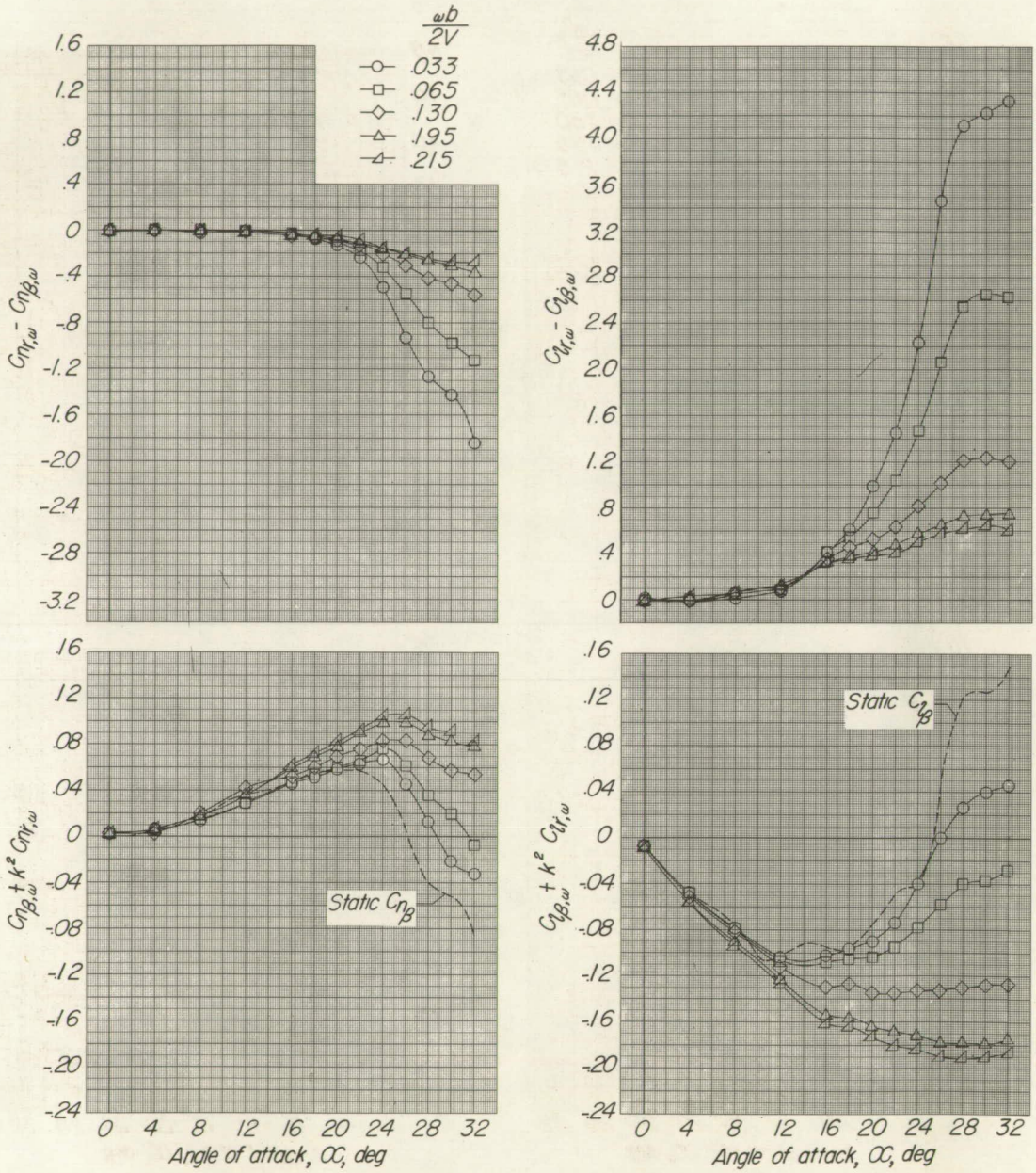

(d) $\psi_o = 8^o$.

Figure 8.- Continued.

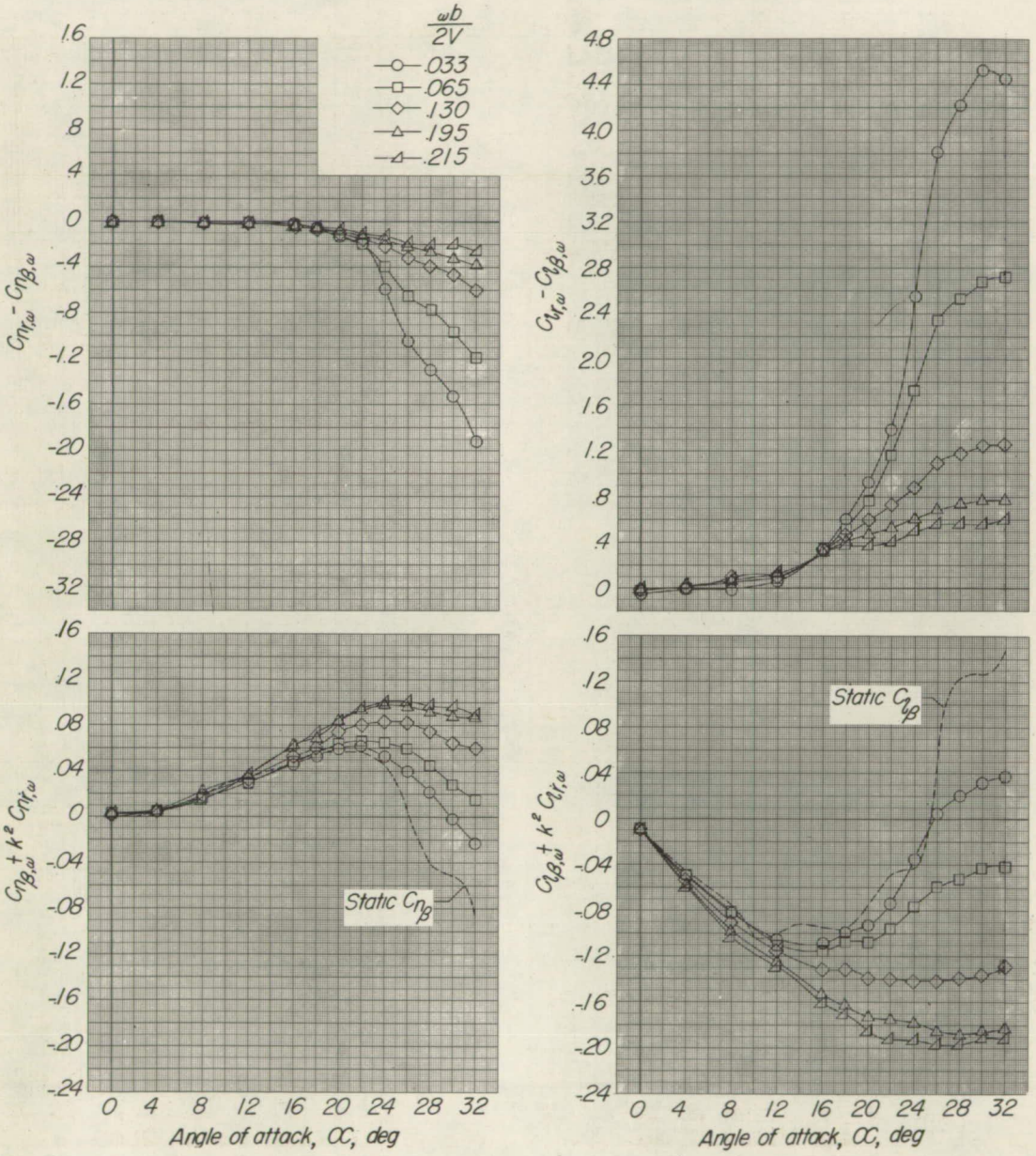

(e) $\psi_o = 10^o$.

Figure 8.- Concluded.

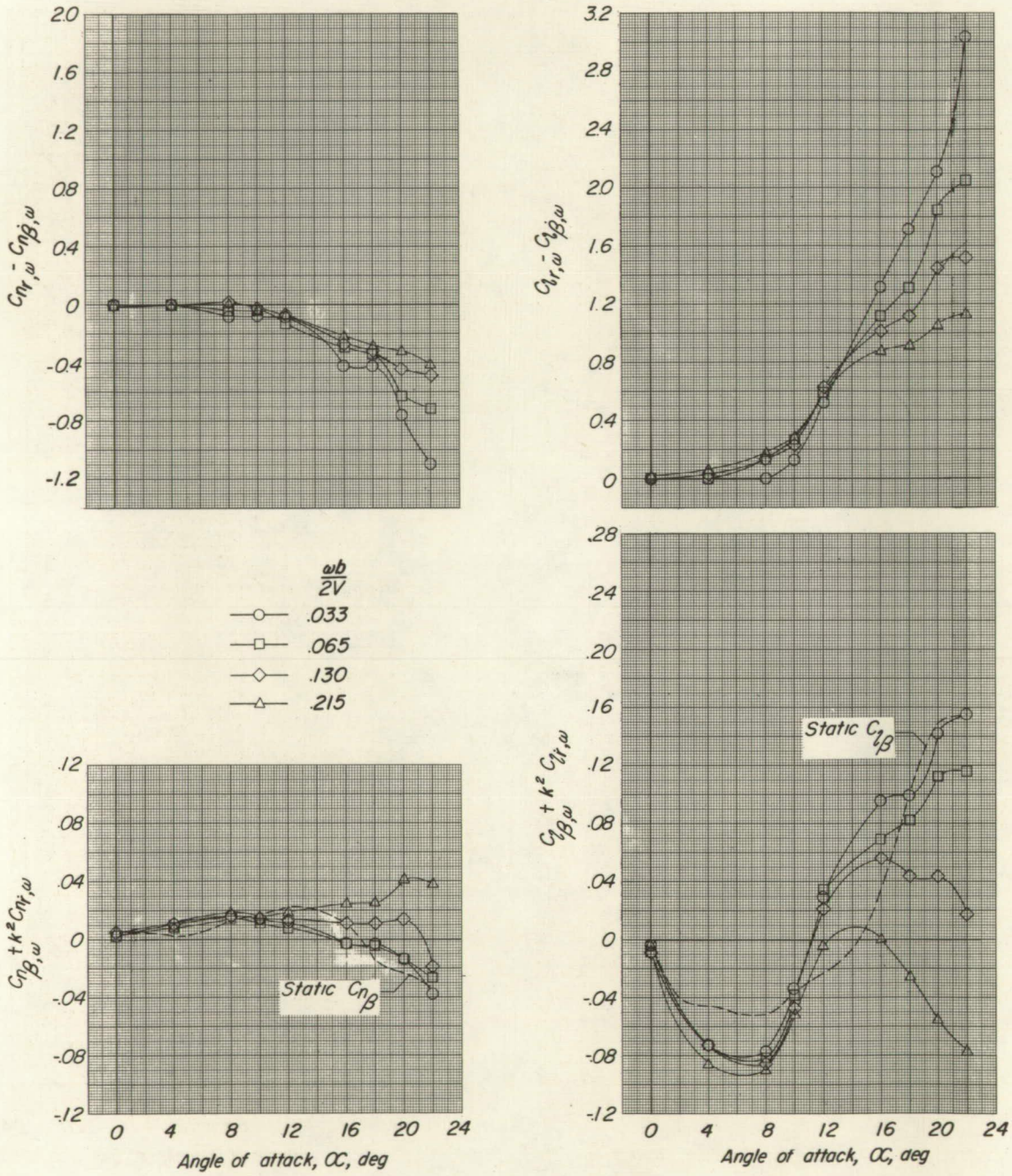

(a) $\psi_o = 2^o$.

Figure 9.- The stability derivatives measured during oscillation for the swept wing.

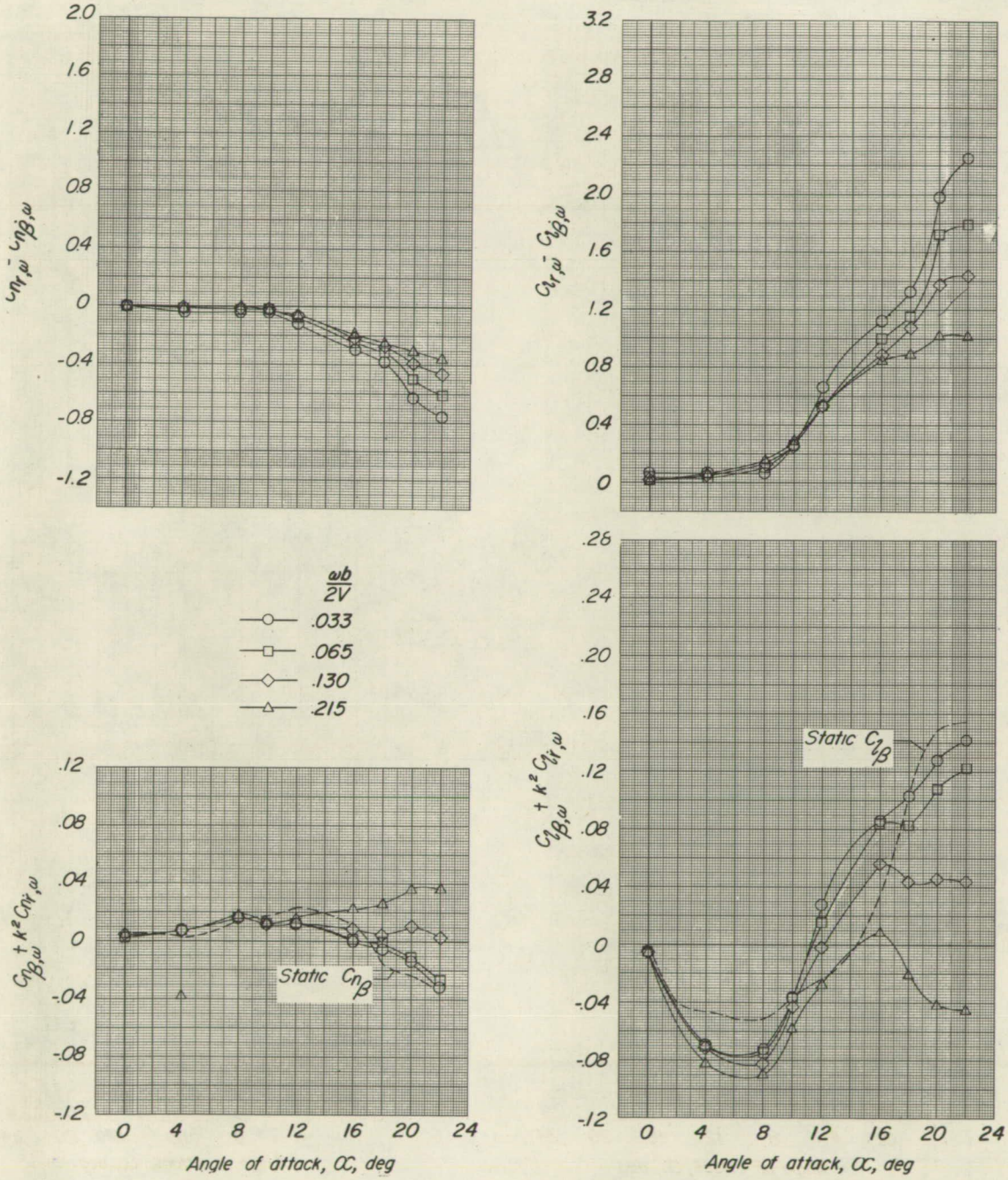

(b) $\psi_o = 4^o$.

Figure 9.- Continued.

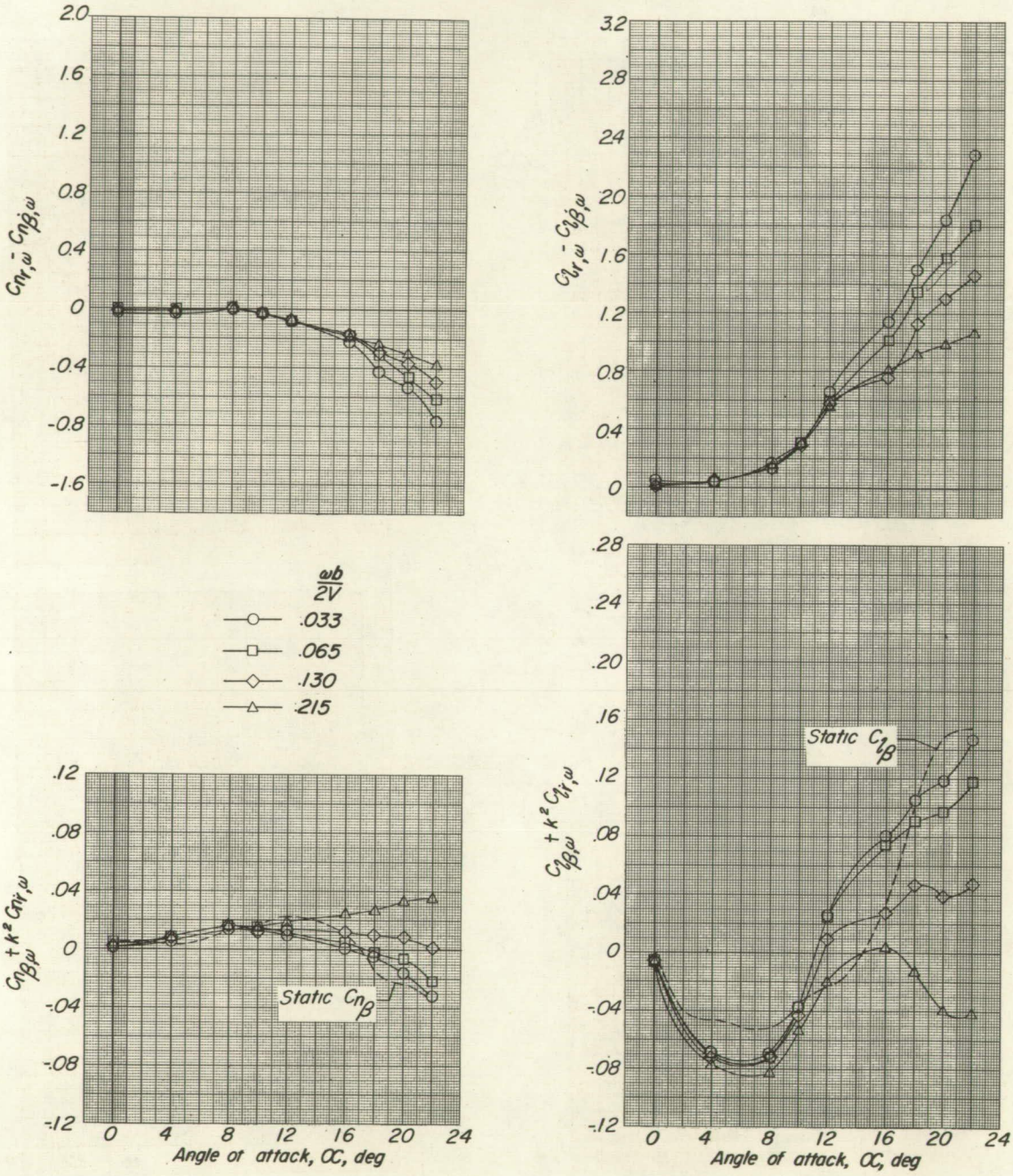

(c) $\psi_o = 6^o$.

Figure 9.- Continued.

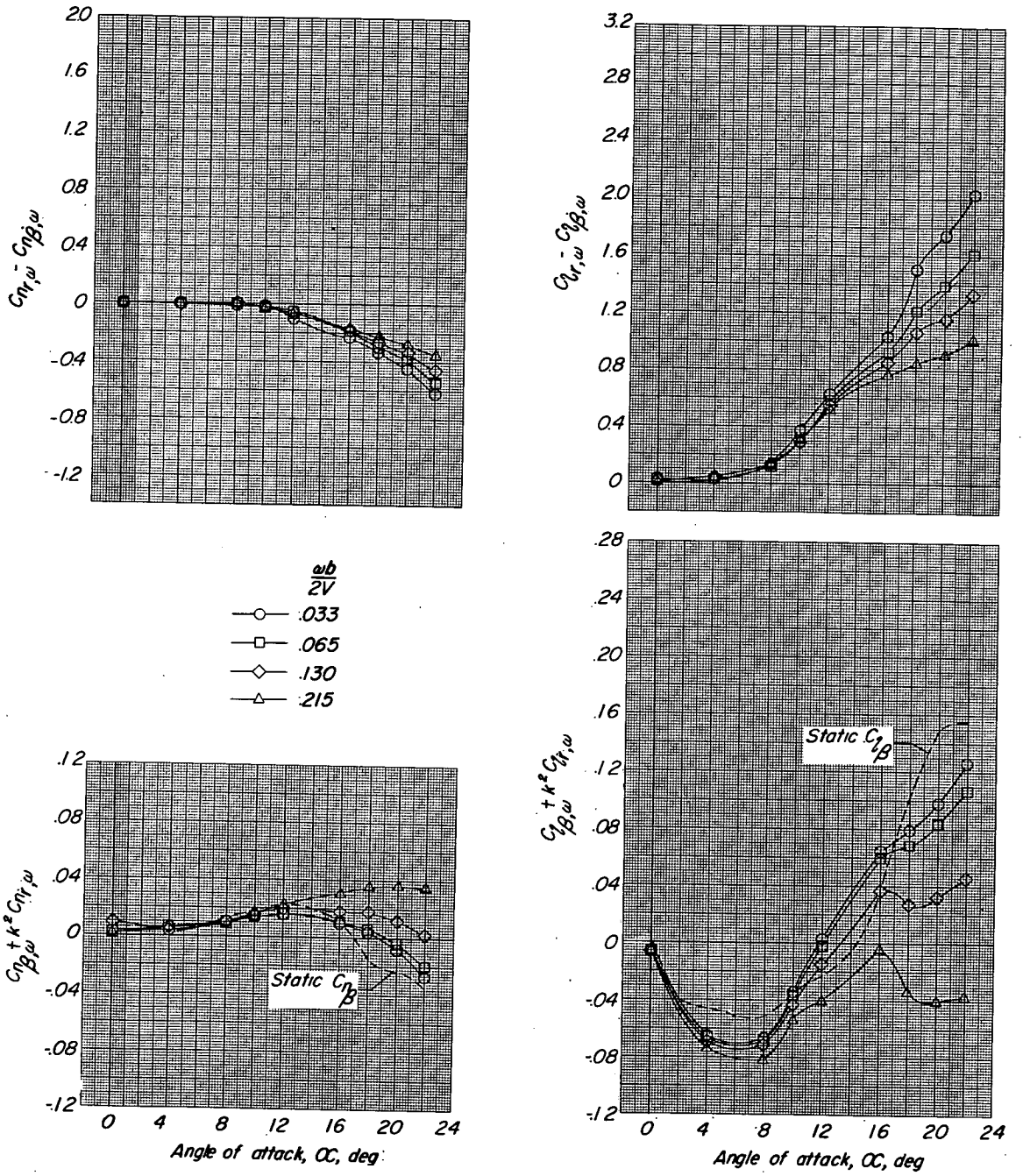

(d) $\psi_o = 10^o$.

Figure 9.- Concluded.

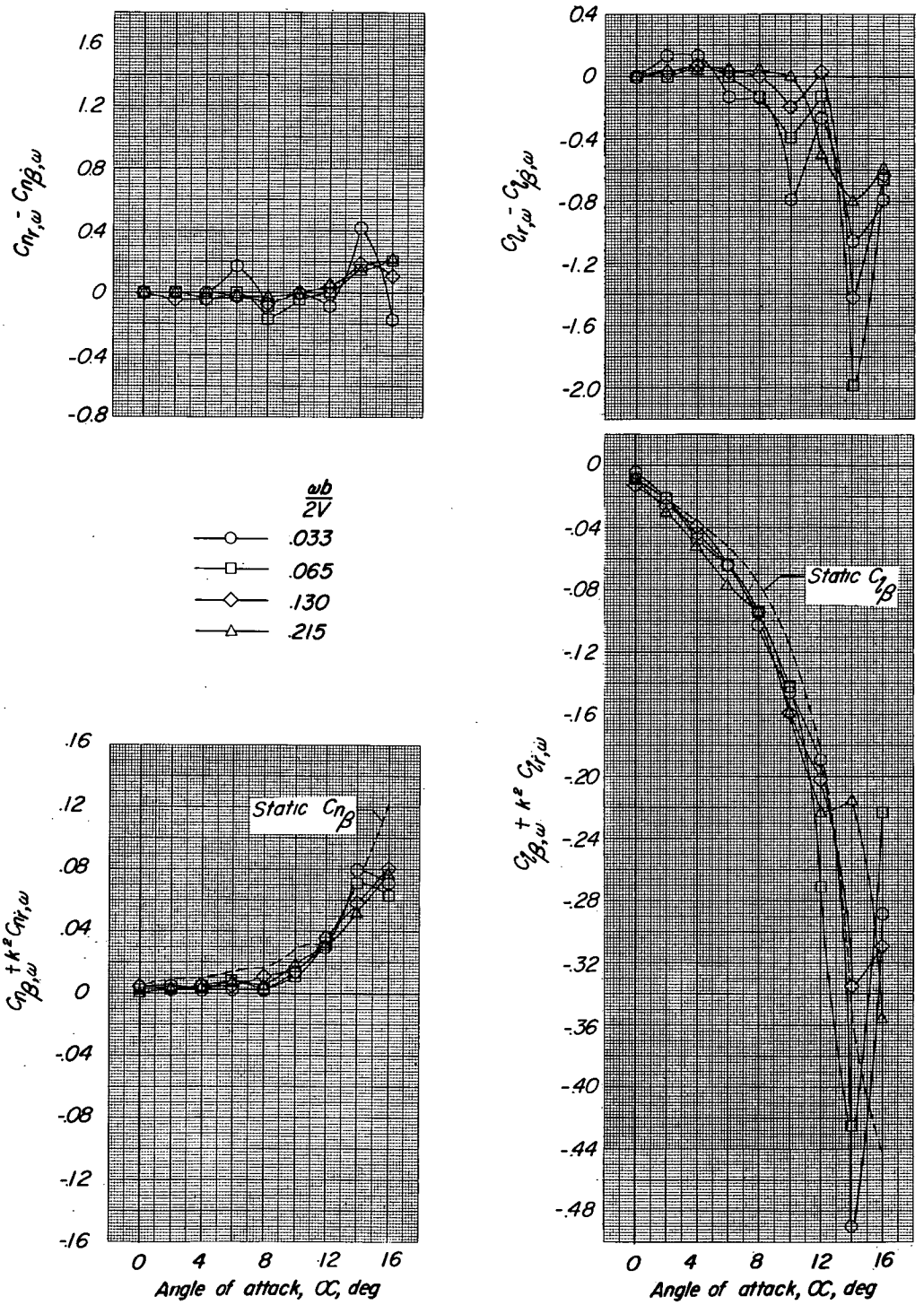

(a) $\psi_o = 2^o$.

Figure 10.- The stability derivatives measured during oscillation for the unswept wing.

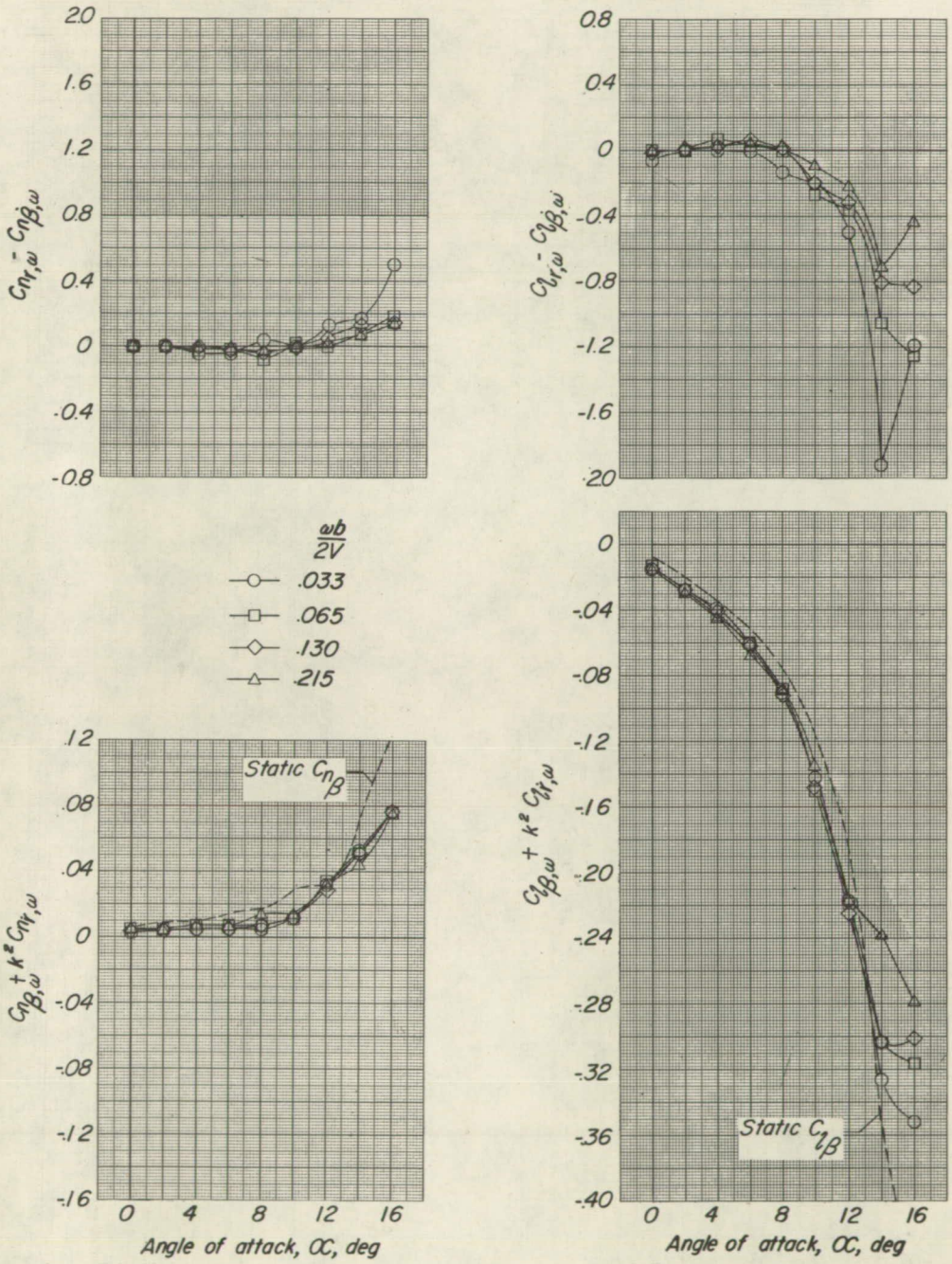

(b) $\psi_o = 4^\circ$.

Figure 10.- Continued.

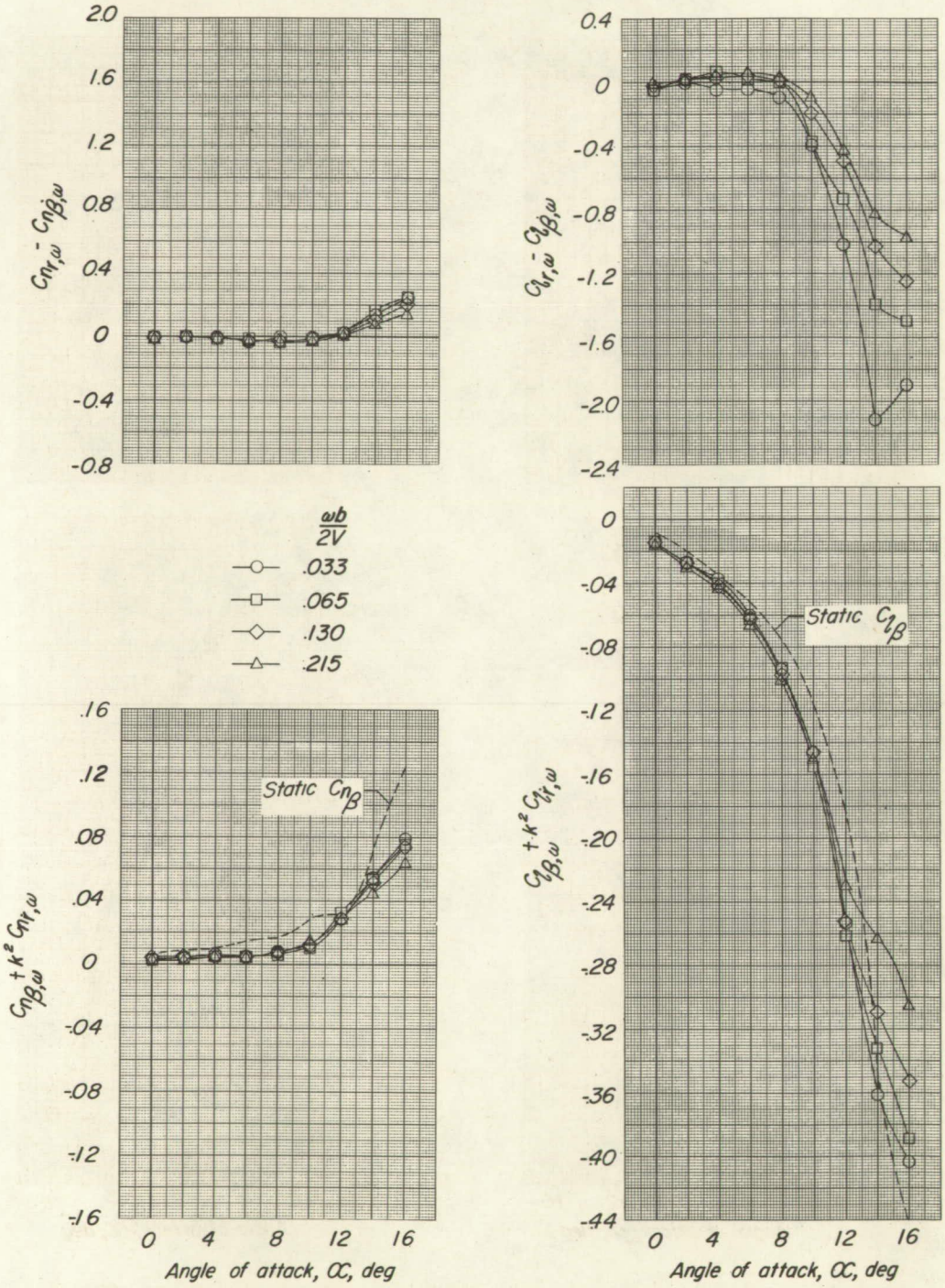

(c) $\psi_o = 6^o$.

Figure 10.- Continued.

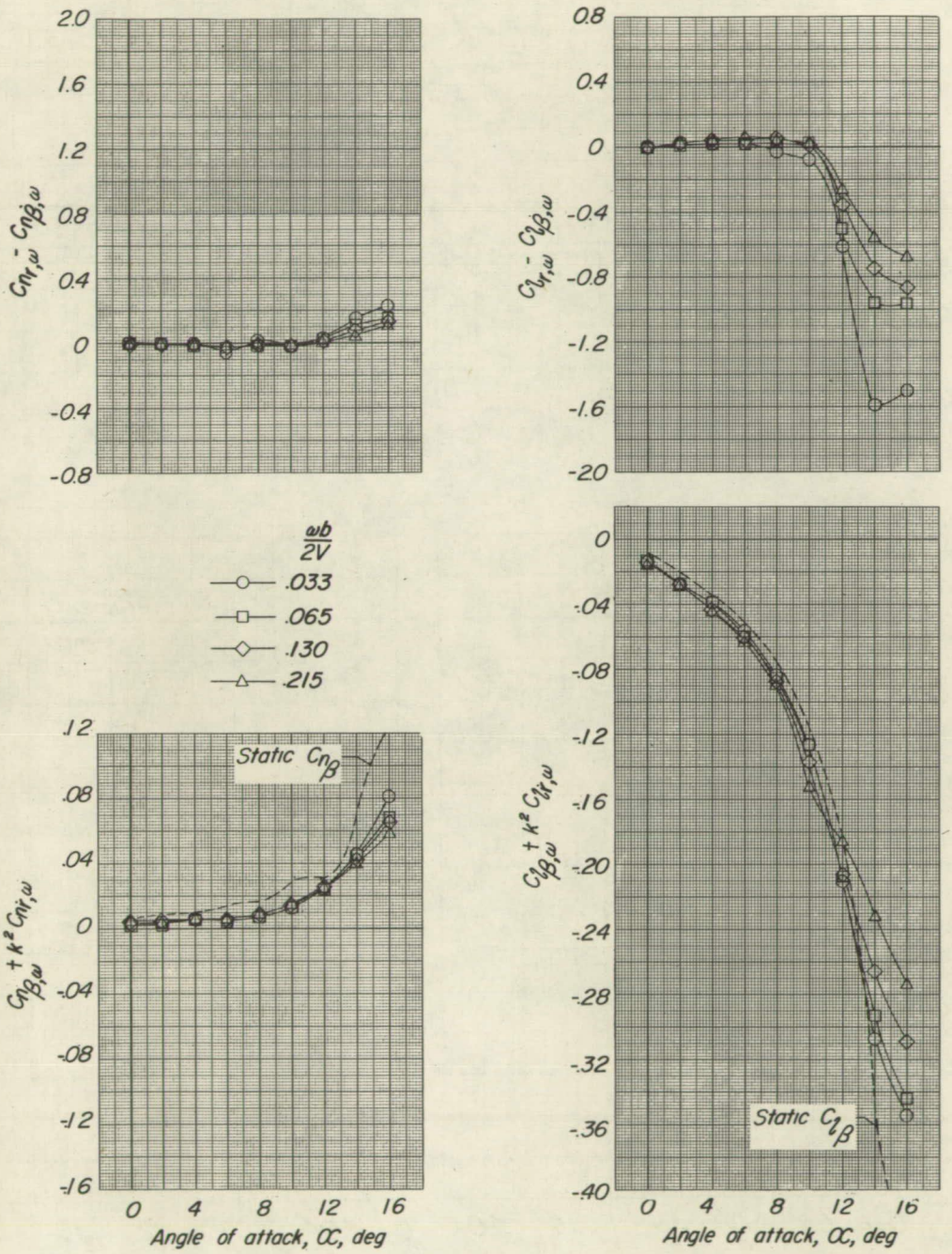

(d) $\psi_o = 10^o$.

Figure 10.- Concluded.

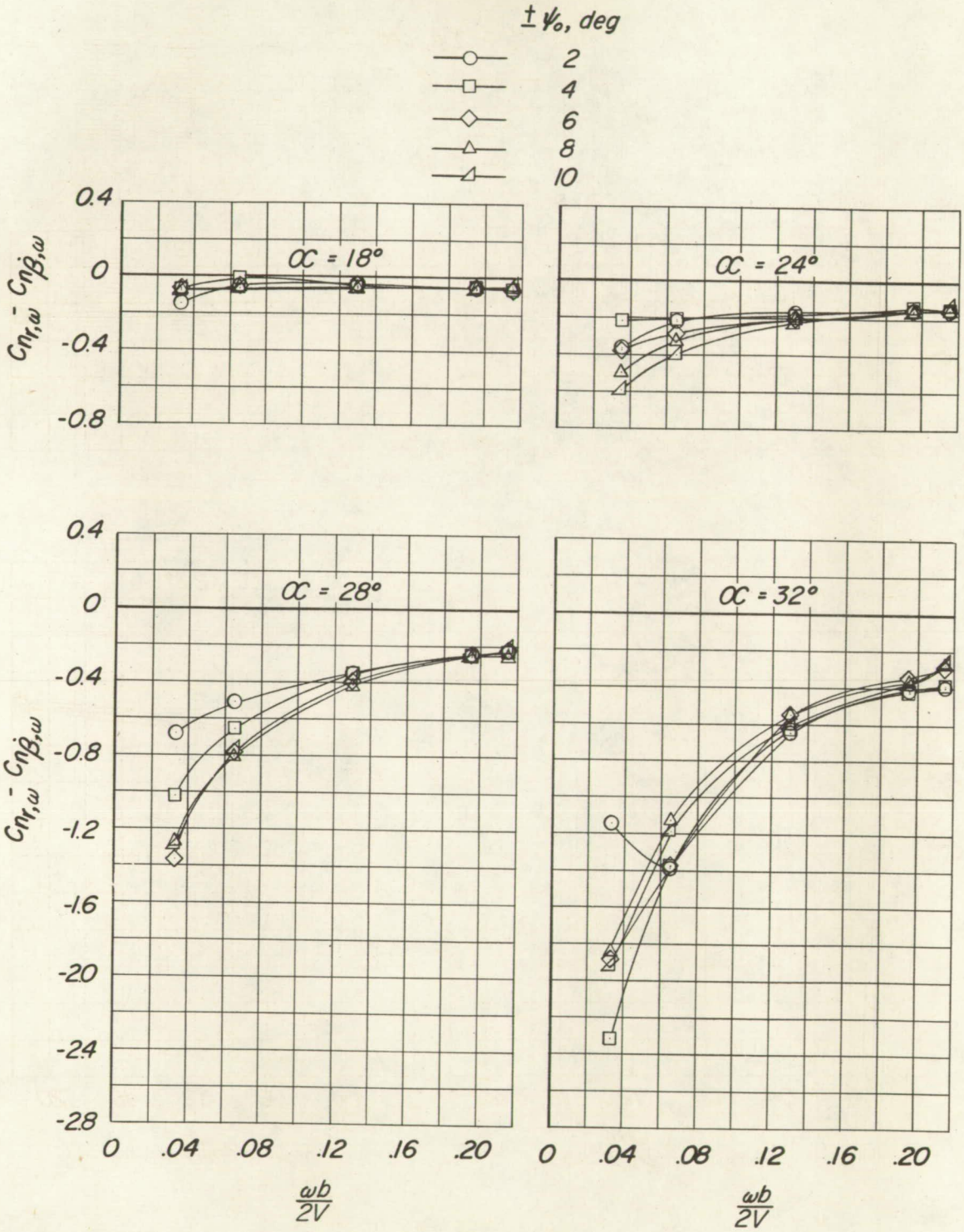

(a) Delta wing.

Figure 11.- The effect of frequency parameter on the damping in yaw.

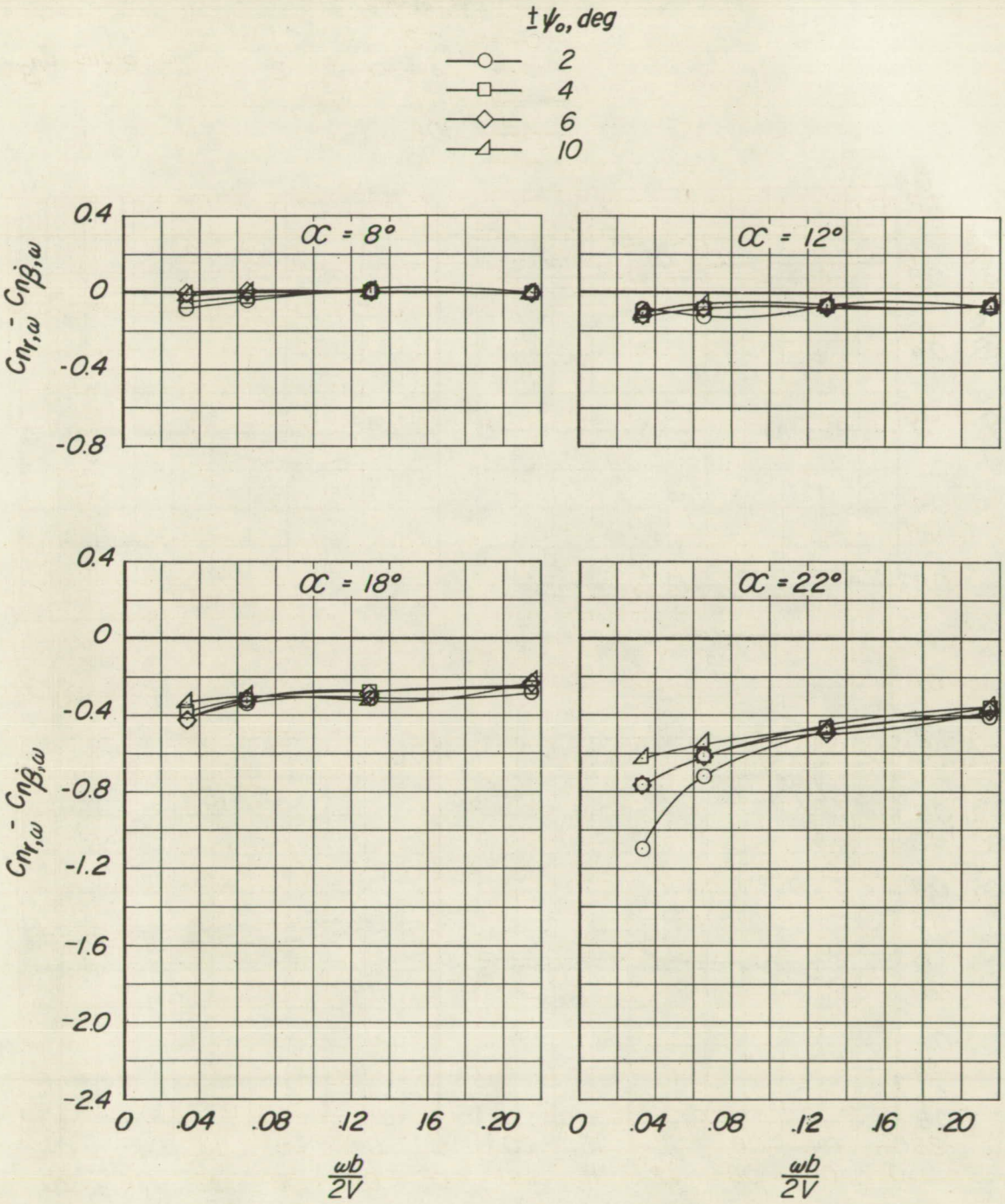

(b) Swept wing.

Figure 11.- Continued.

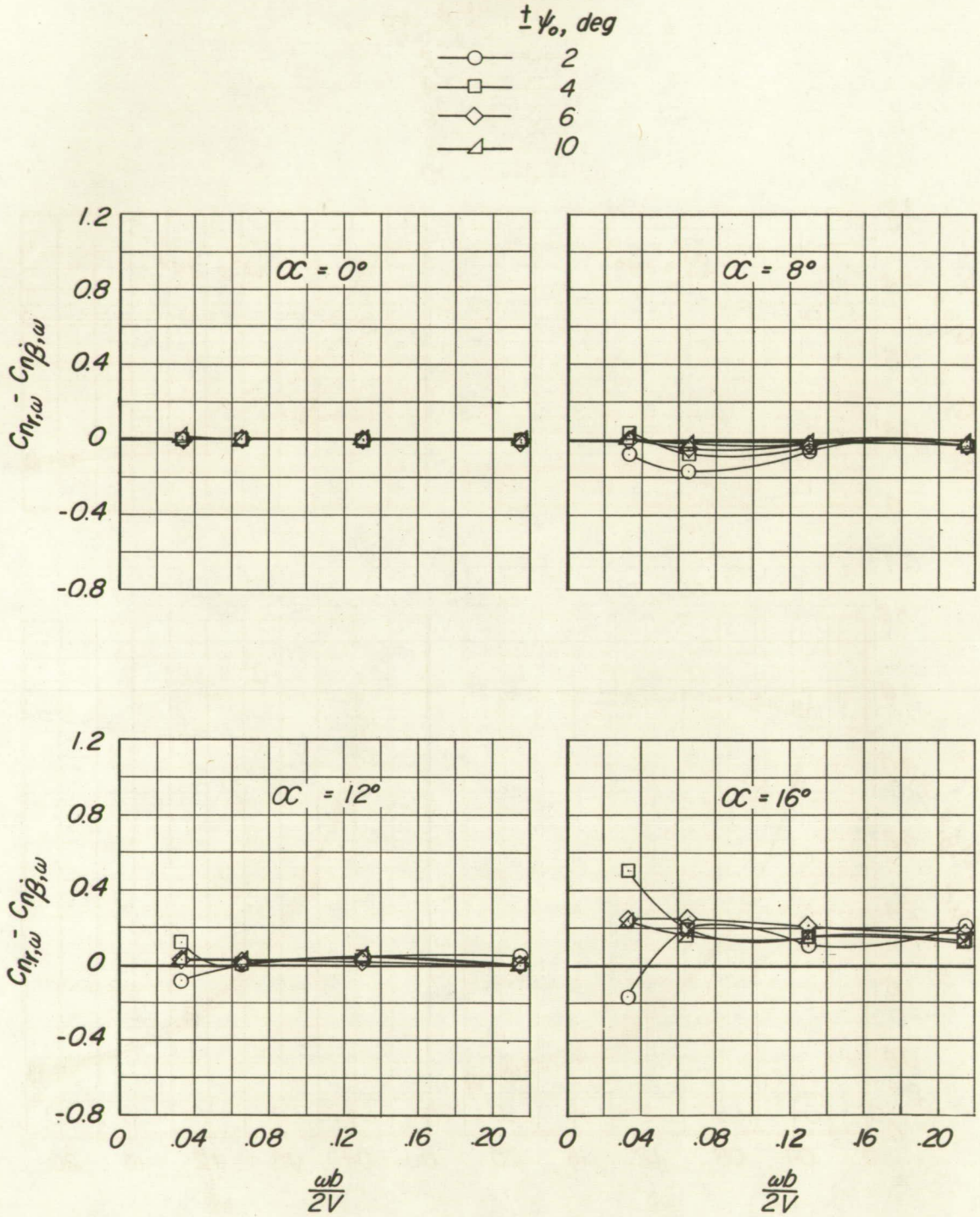

(c) Unswept wing.

Figure 11.- Concluded.

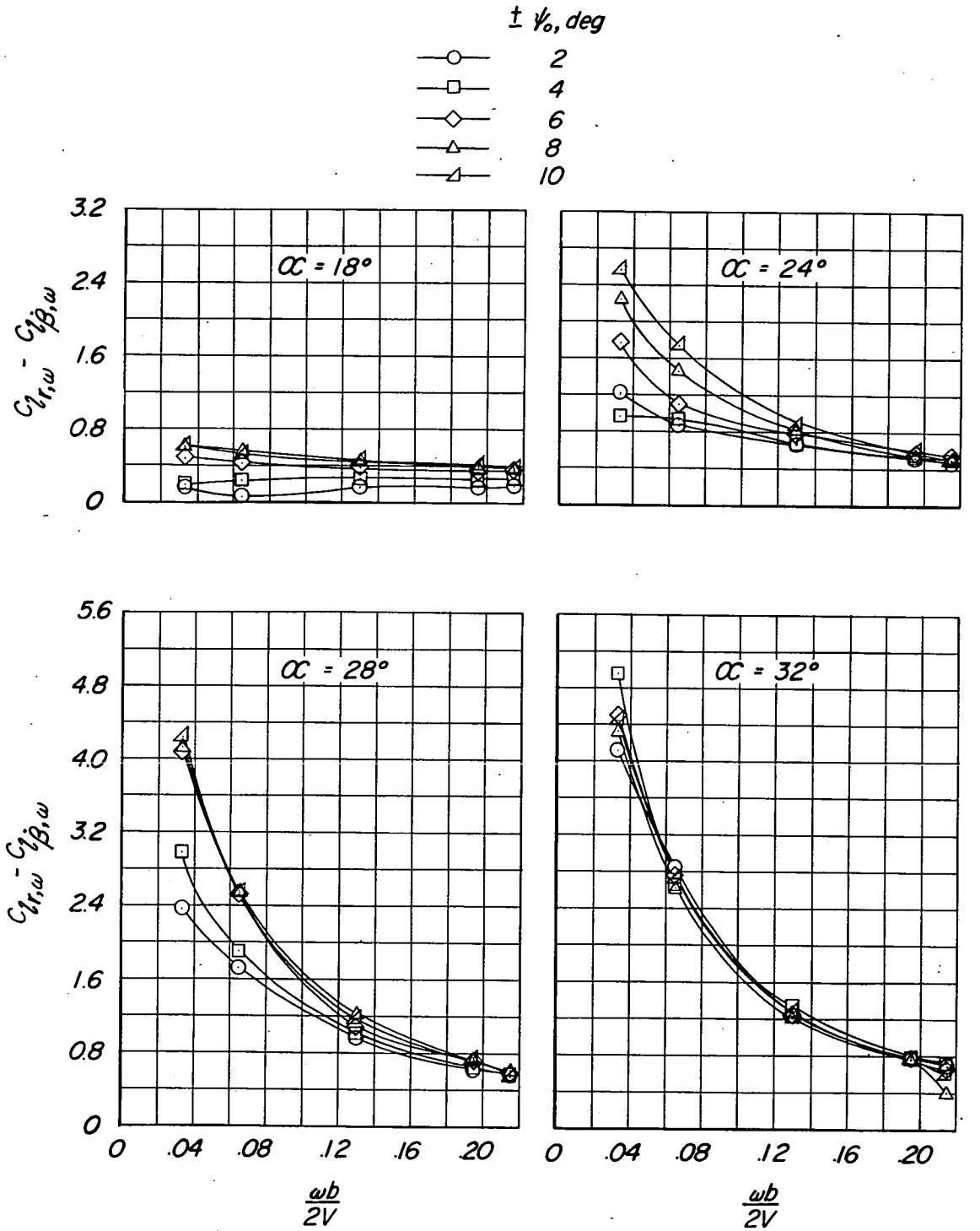

(a) Delta wing.

Figure 12.- The effect of frequency parameter on the rolling moment due to yawing.

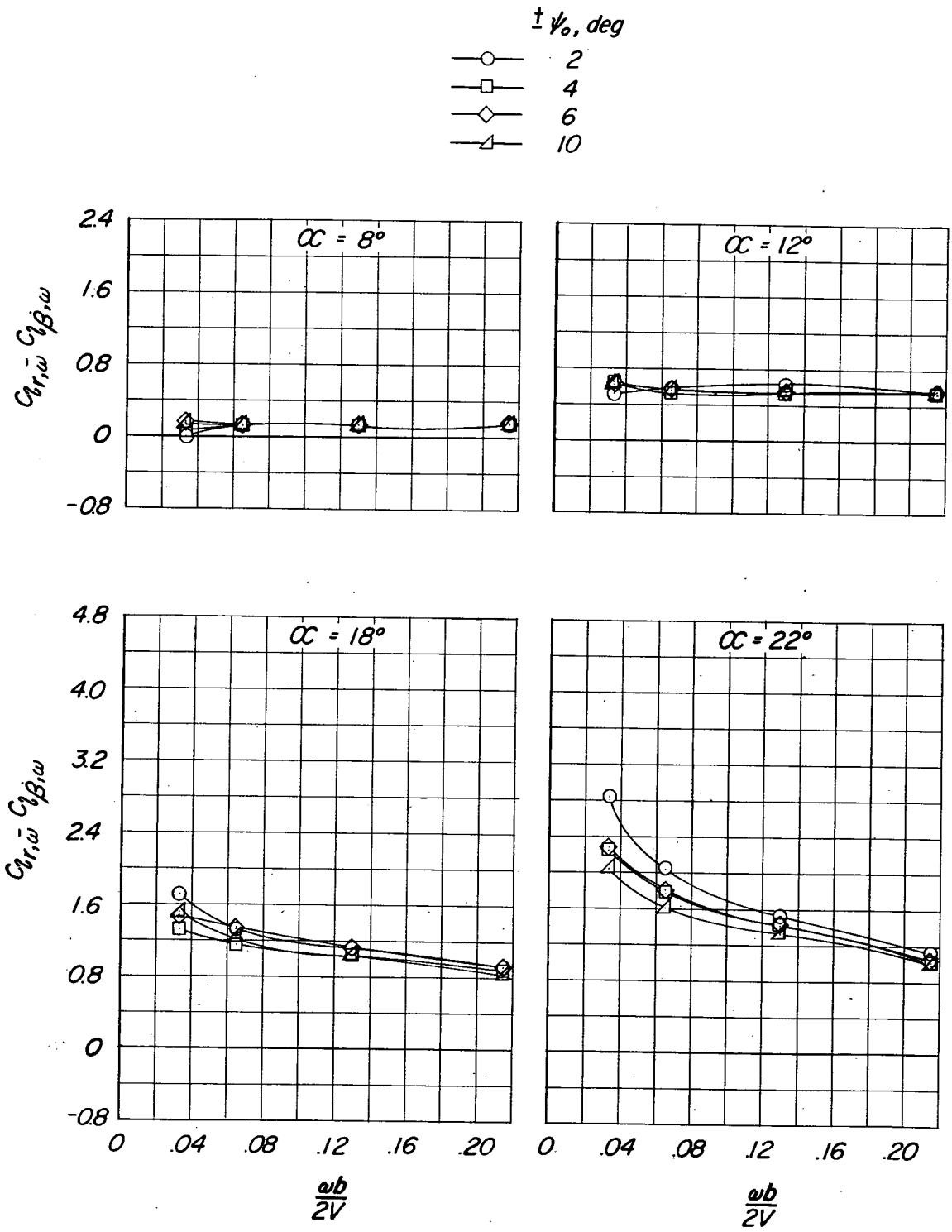

(b) Swept wing.

Figure 12.- Continued.

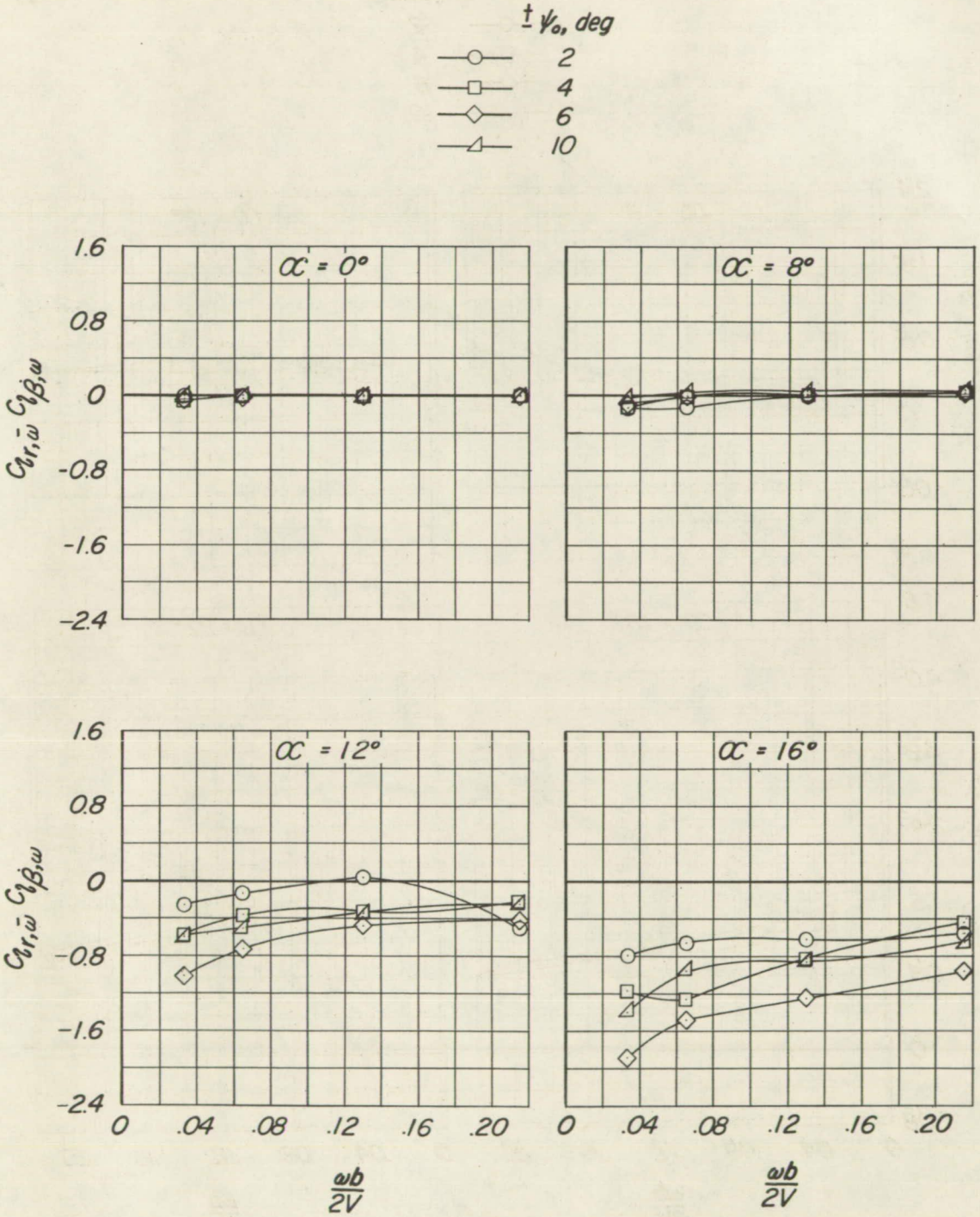

(c) Unswept wing.

Figure 12.- Concluded.

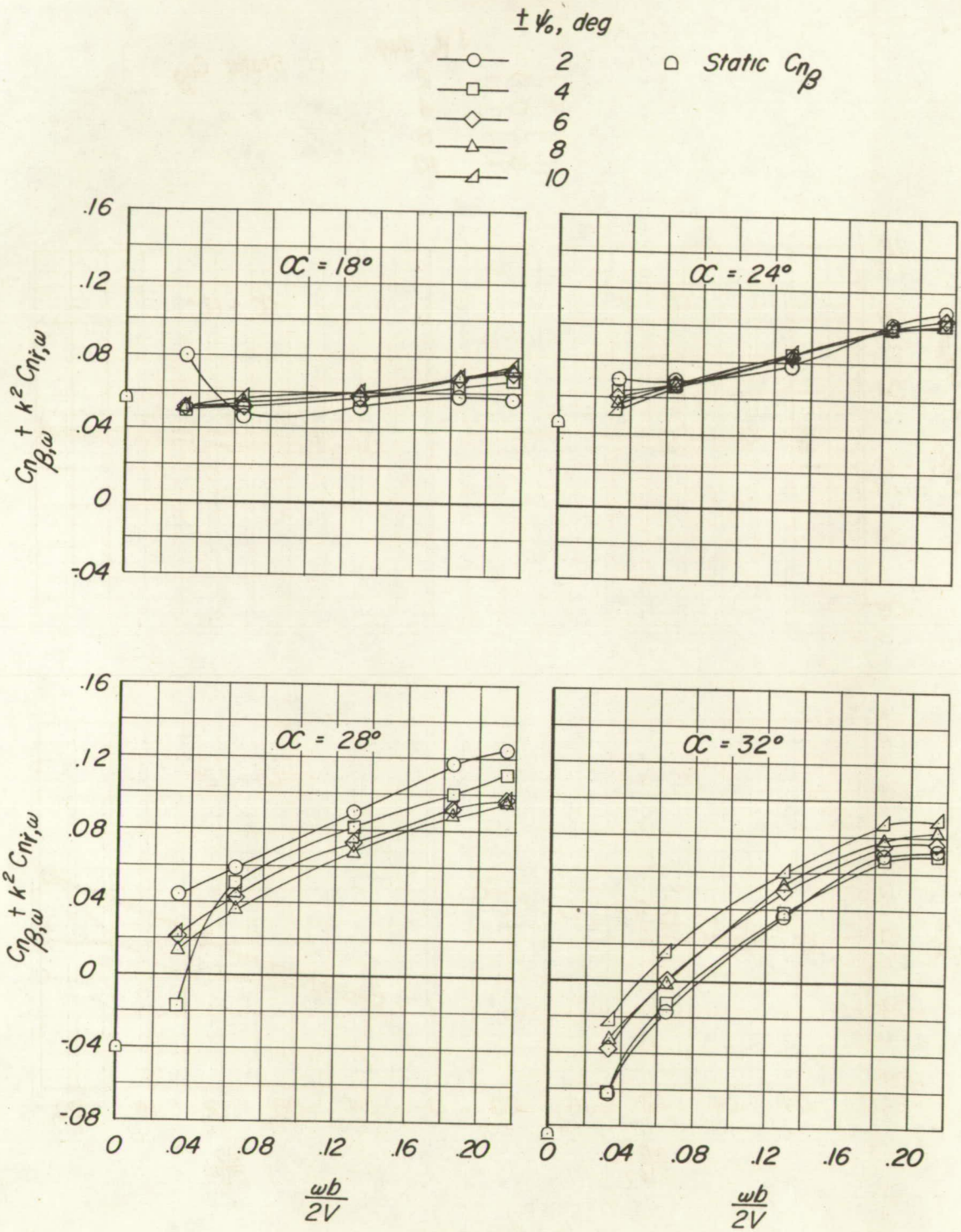

(a) Delta wing.

Figure 13.- The effect of frequency parameter on the directional-stability derivative.

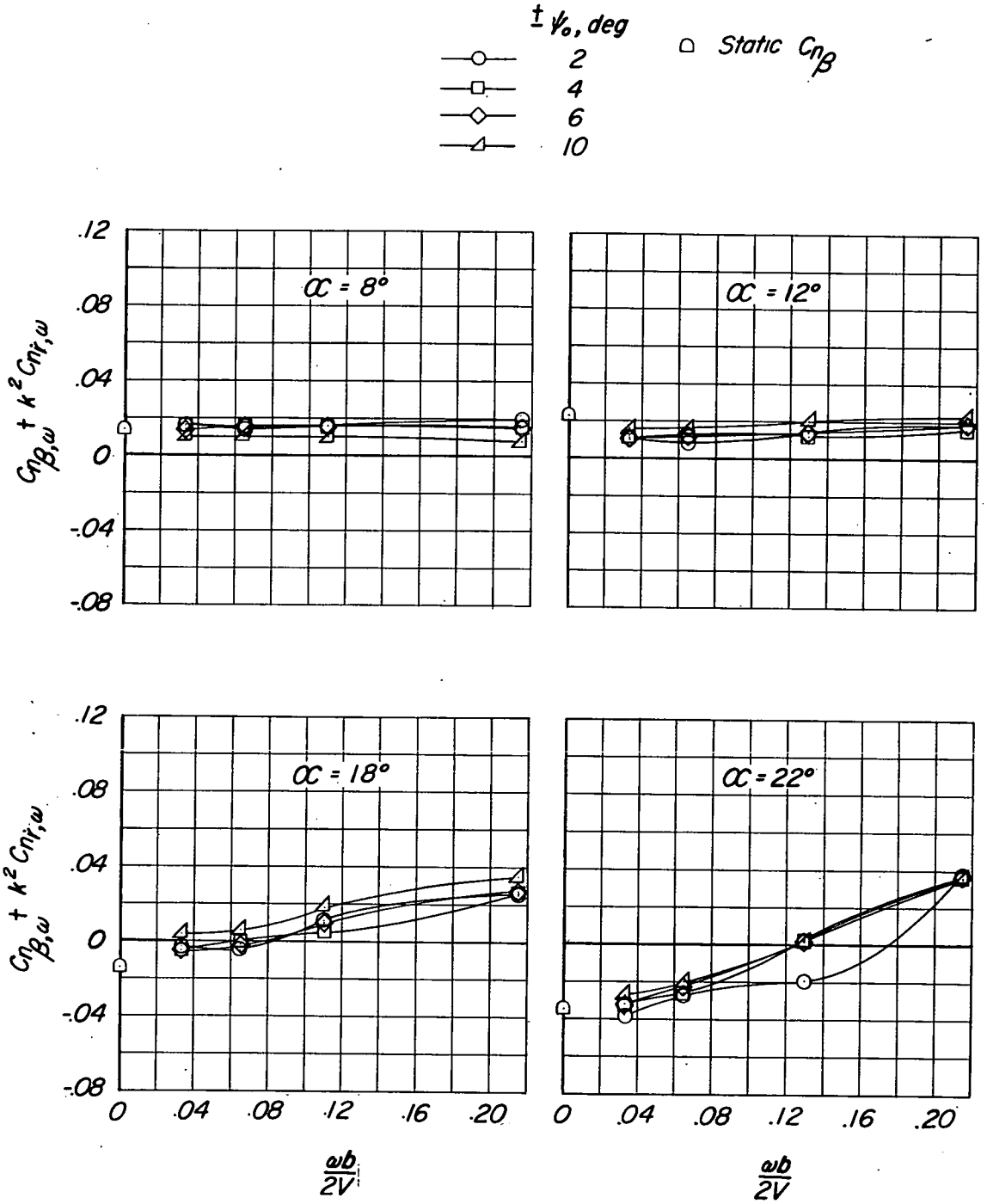

(b) Swept wing.

Figure 13.- Continued.

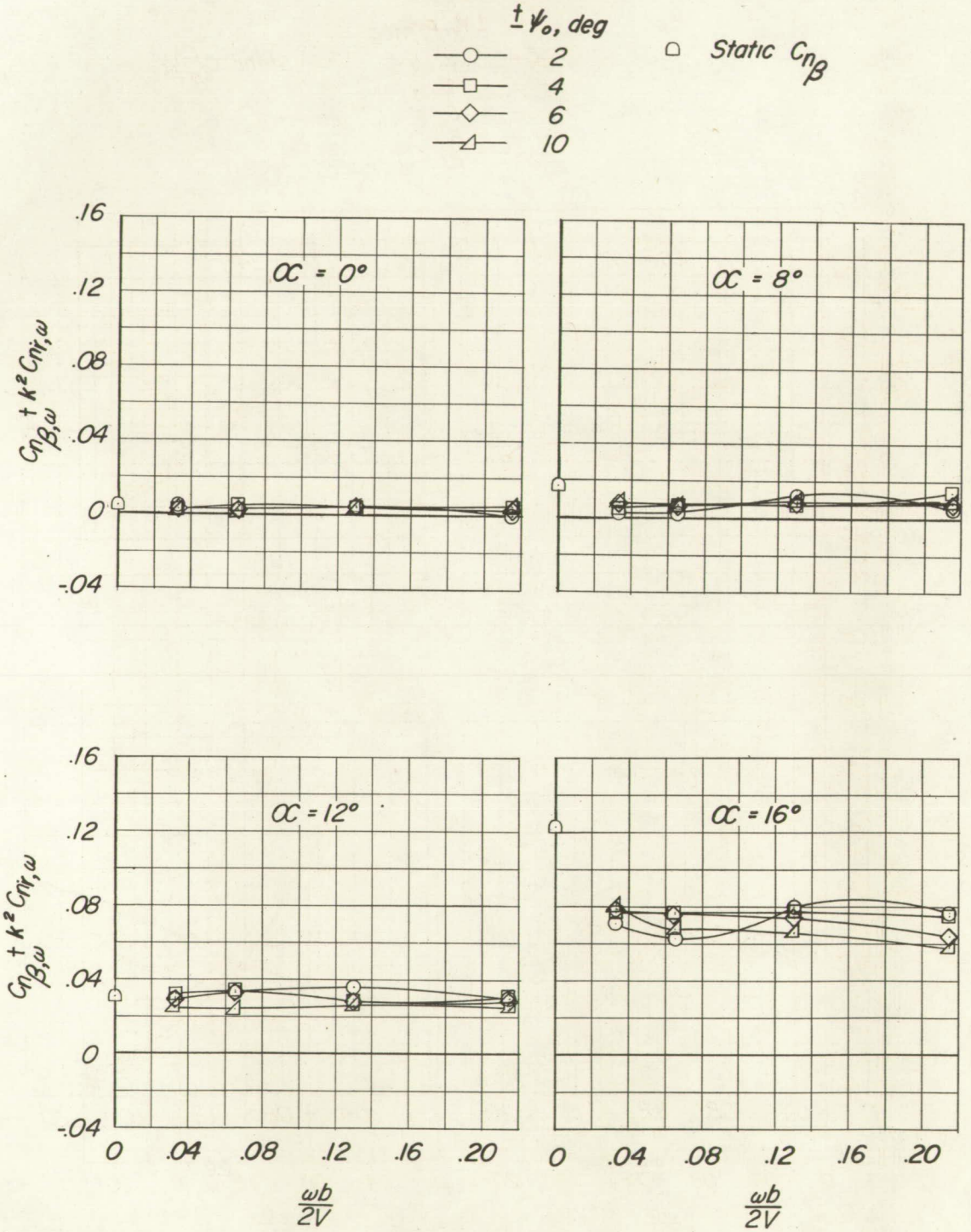

(c) Unswept wing.

Figure 13.- Concluded.

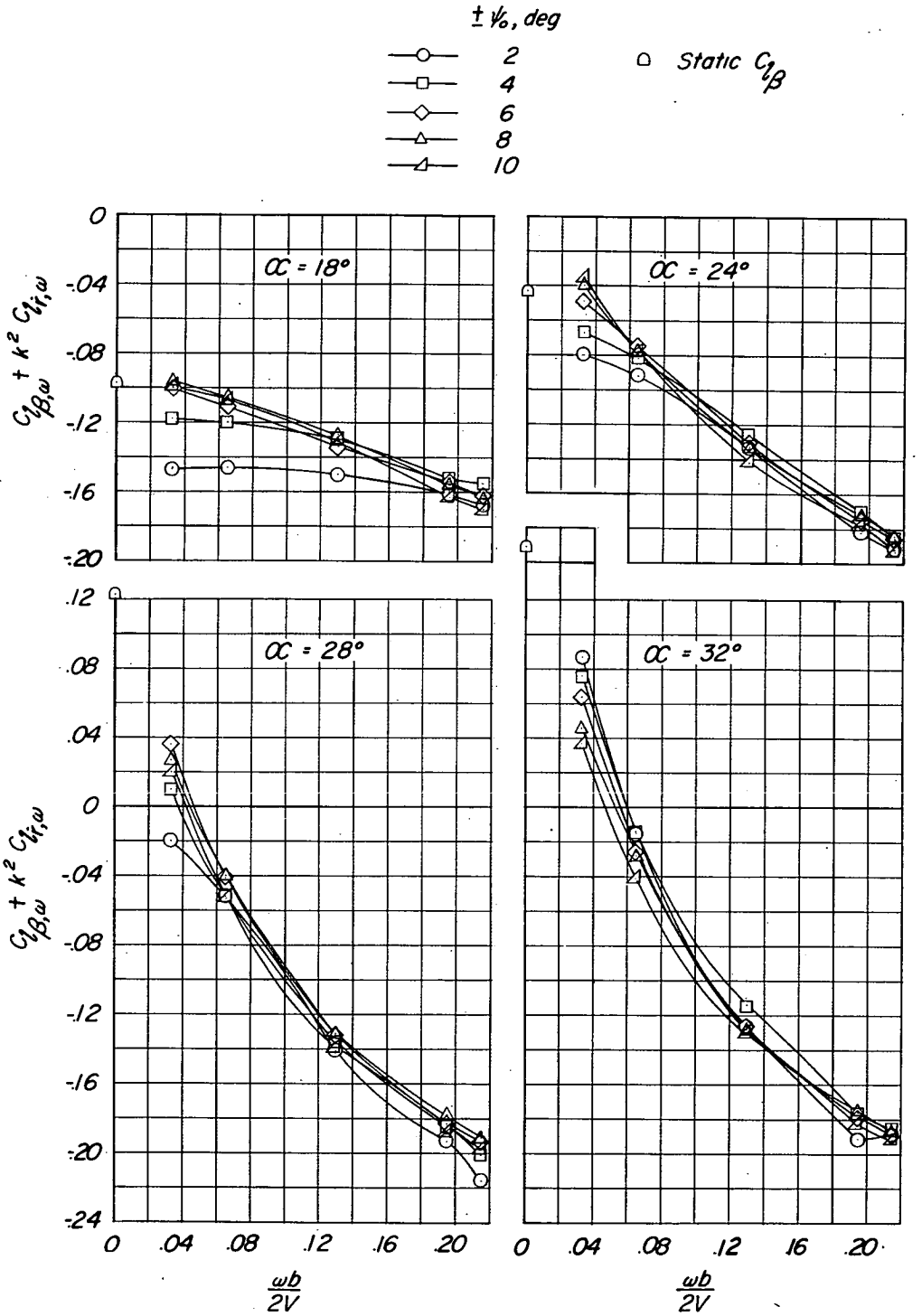

(a) Delta wing.

Figure 14.- The effect of frequency parameter on the effective-dihedral derivative.

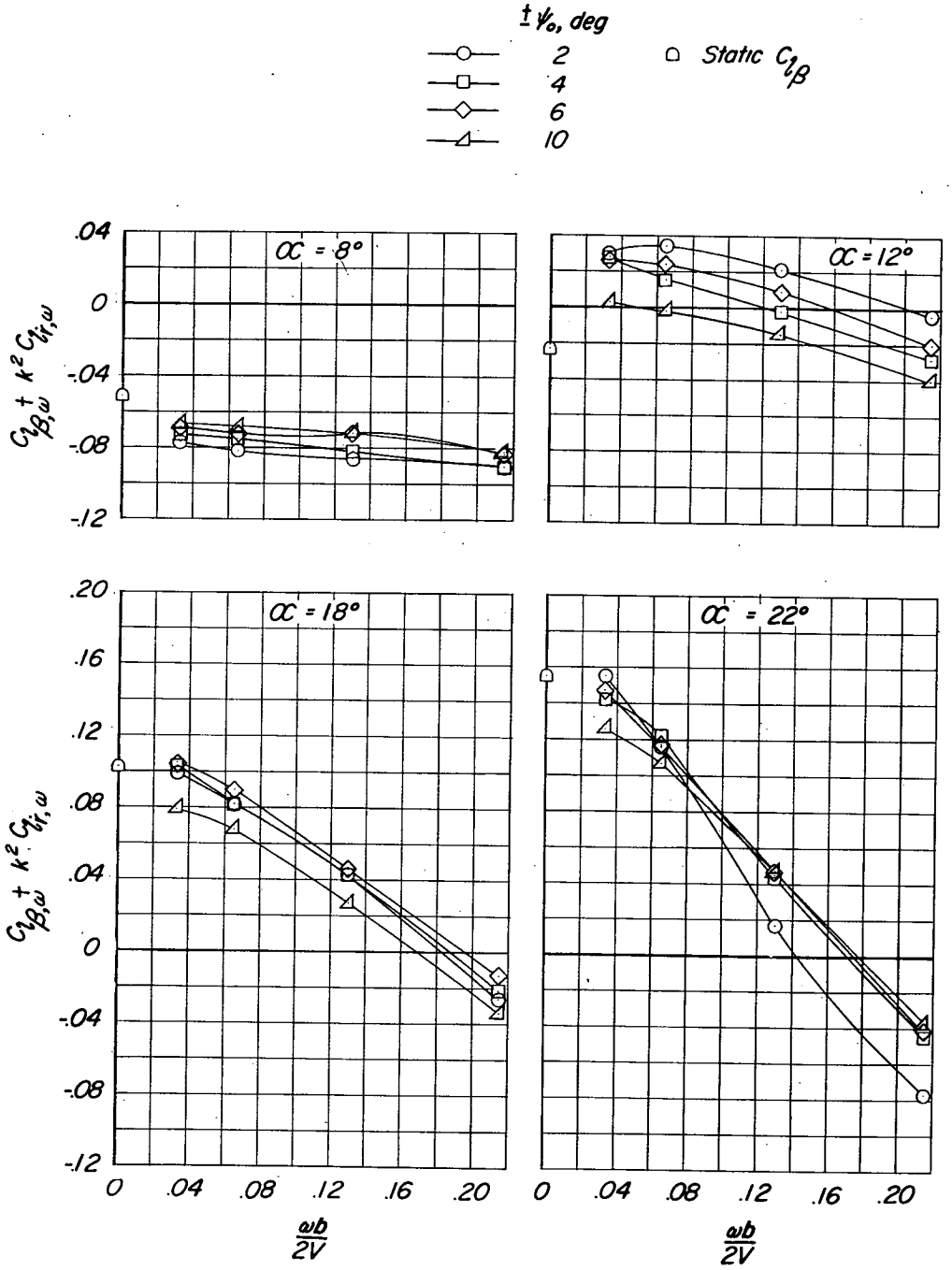

(b) Swept wing.

Figure 14.- Continued.

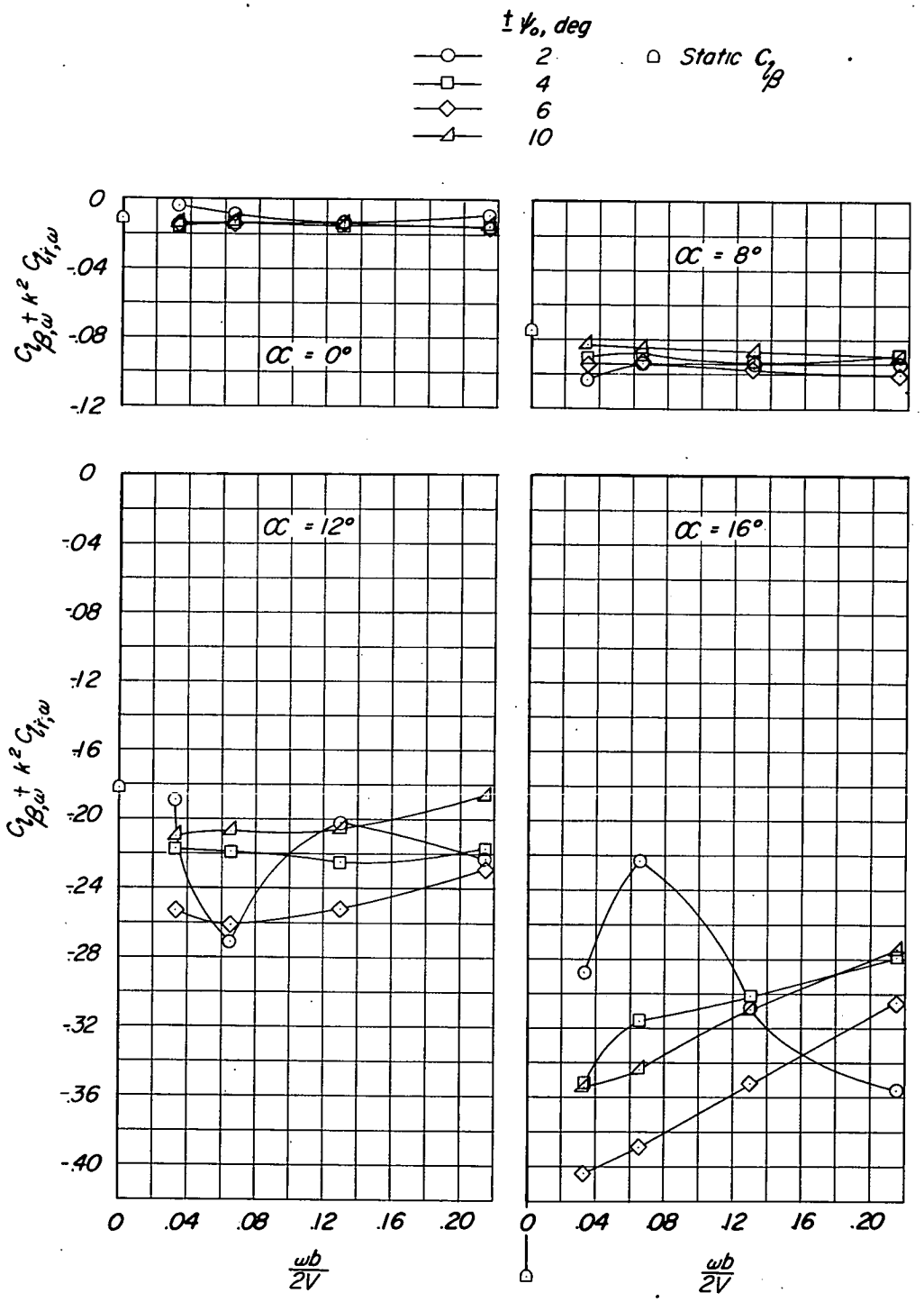

(c) Unswept wing.

Figure 14.- Concluded.

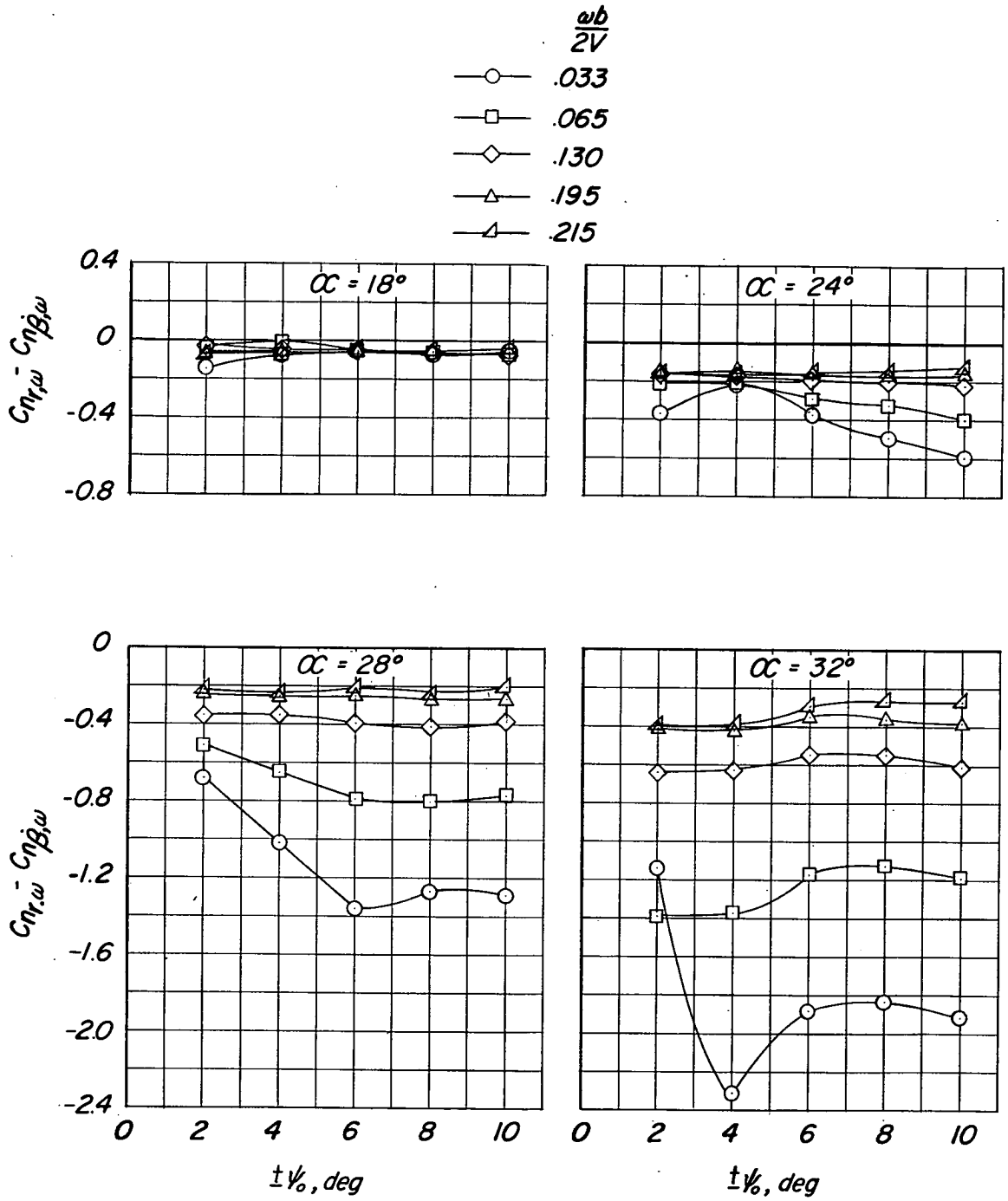

(a) Delta wing.

Figure 15.- The effect of amplitude on the damping-in-yaw derivative.

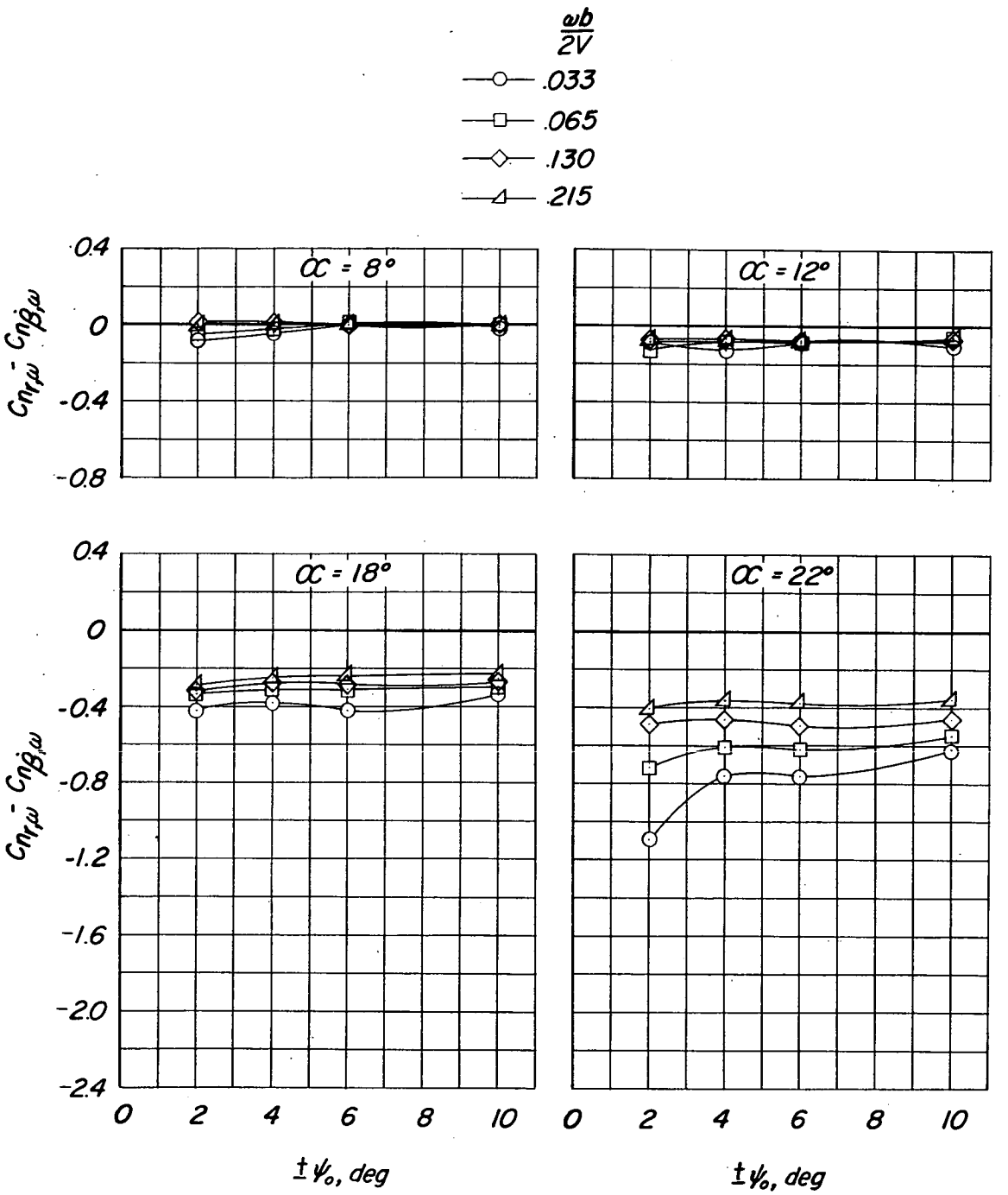

(b) Swept wing.

Figure 15.- Continued.

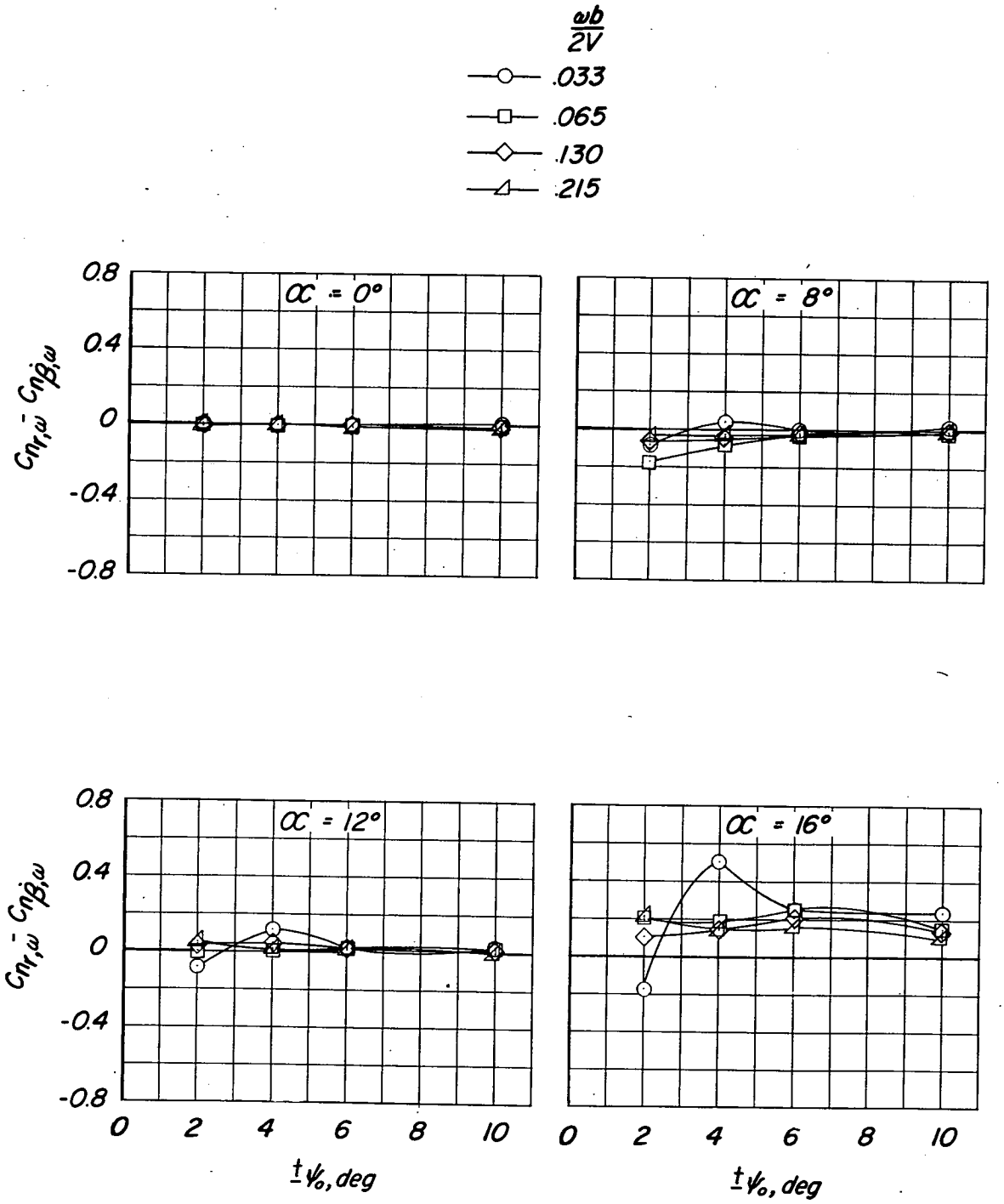

(c) Unswept wing.

Figure 15.- Concluded.

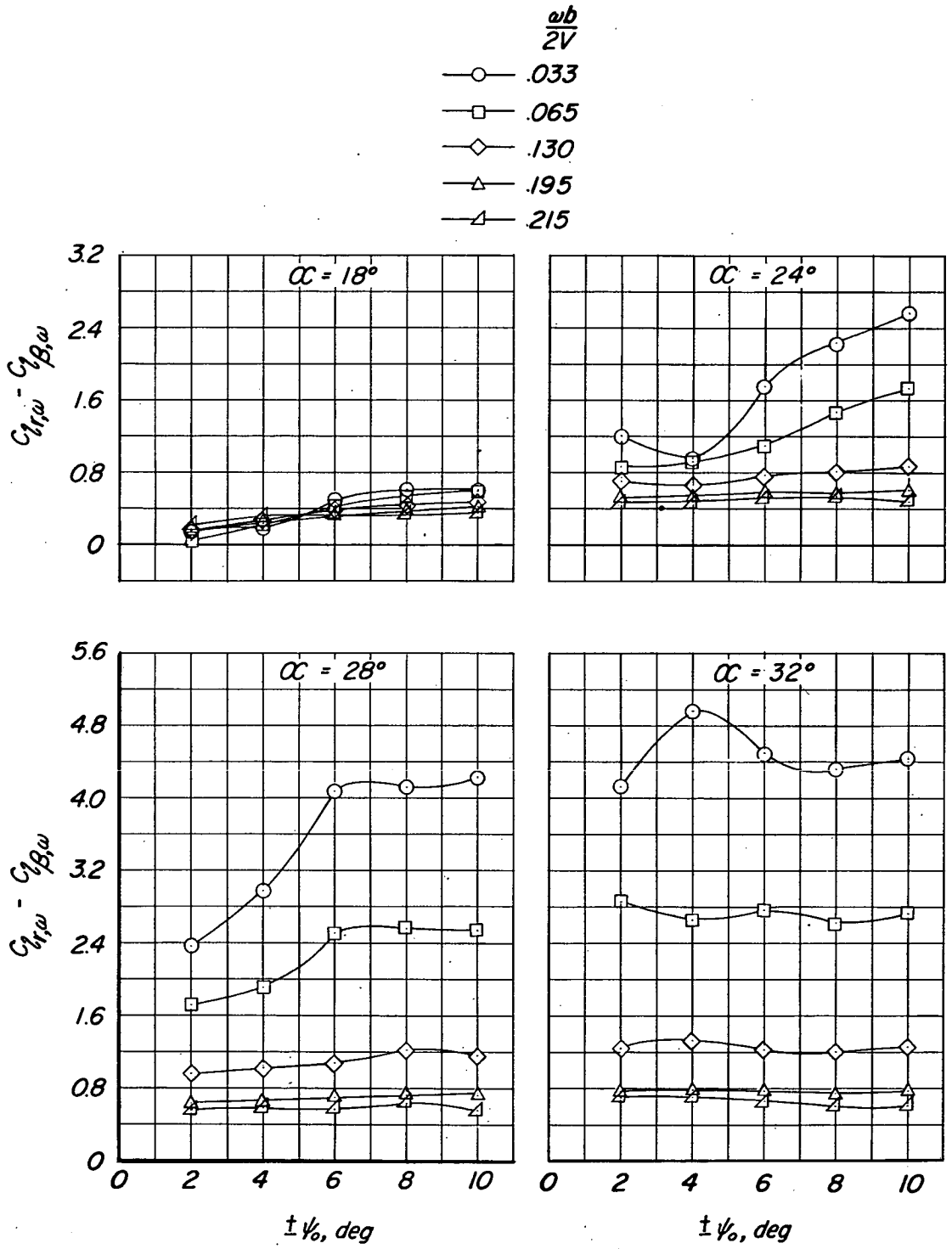

(a) Delta wing.

Figure 16.- The effect of amplitude on the rolling-moment-due-to-yawing derivative.

[redacted]

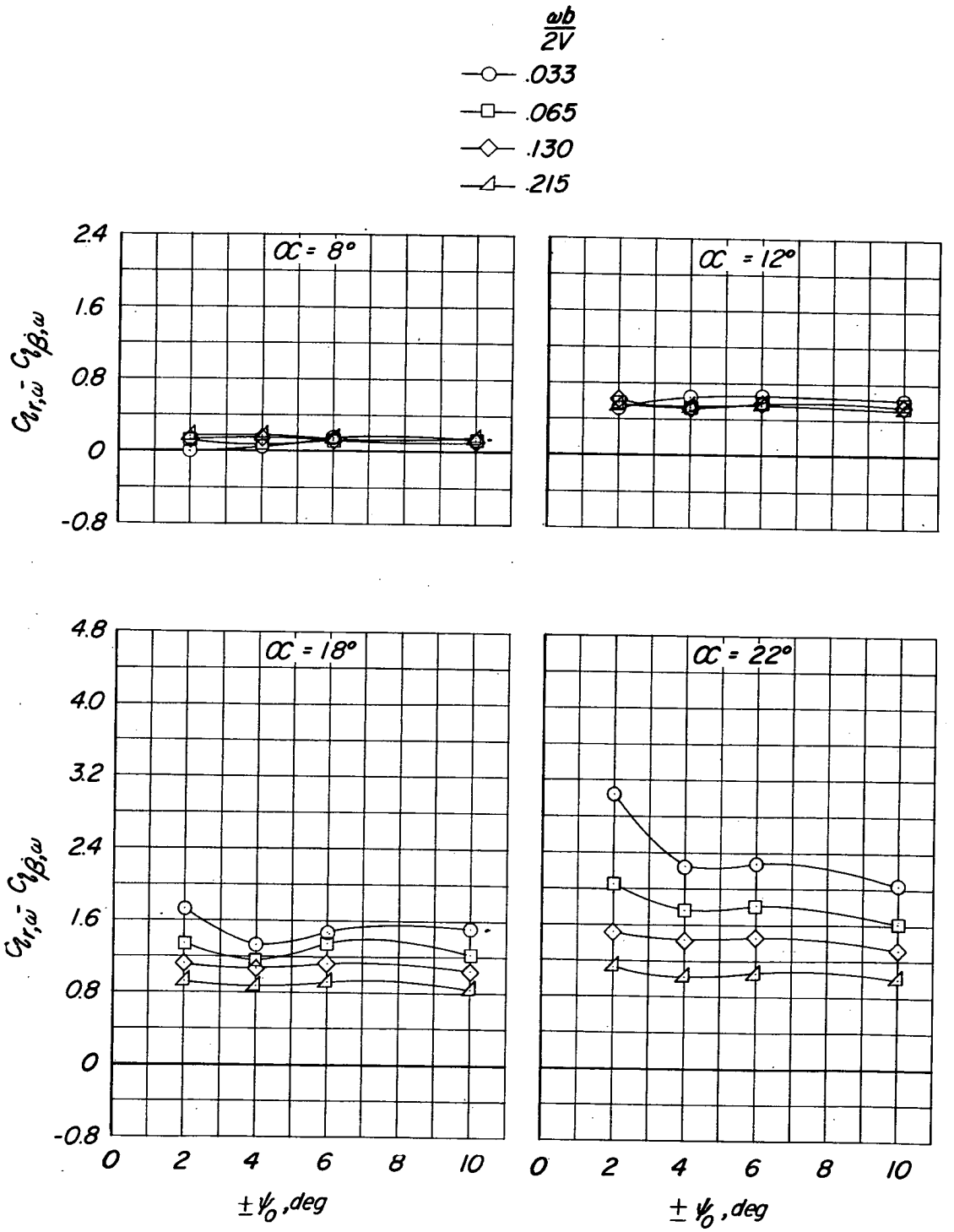

(b) Swept wing.

Figure 16.- Continued.

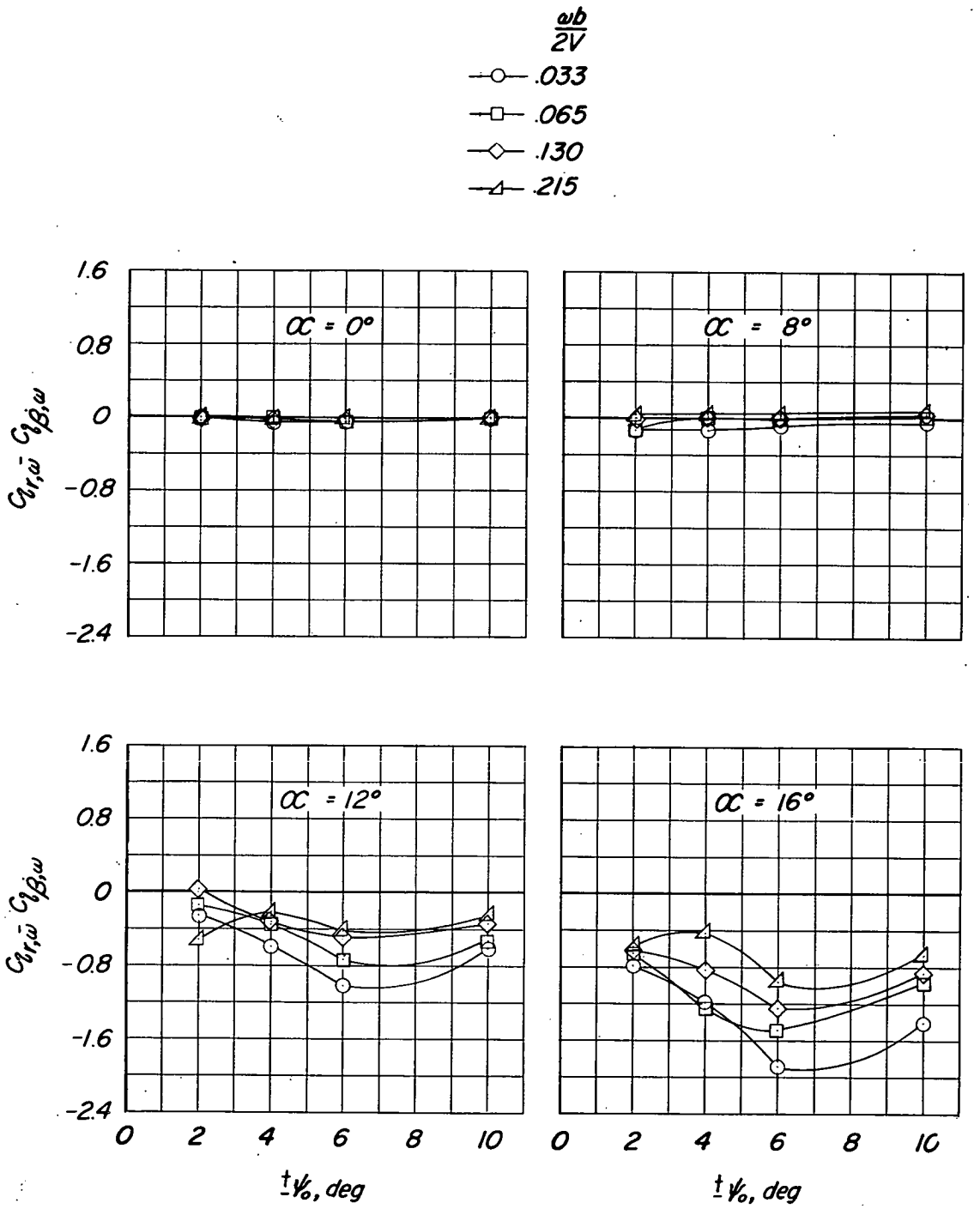

(c) Unswept wing.

Figure 16.- Concluded.

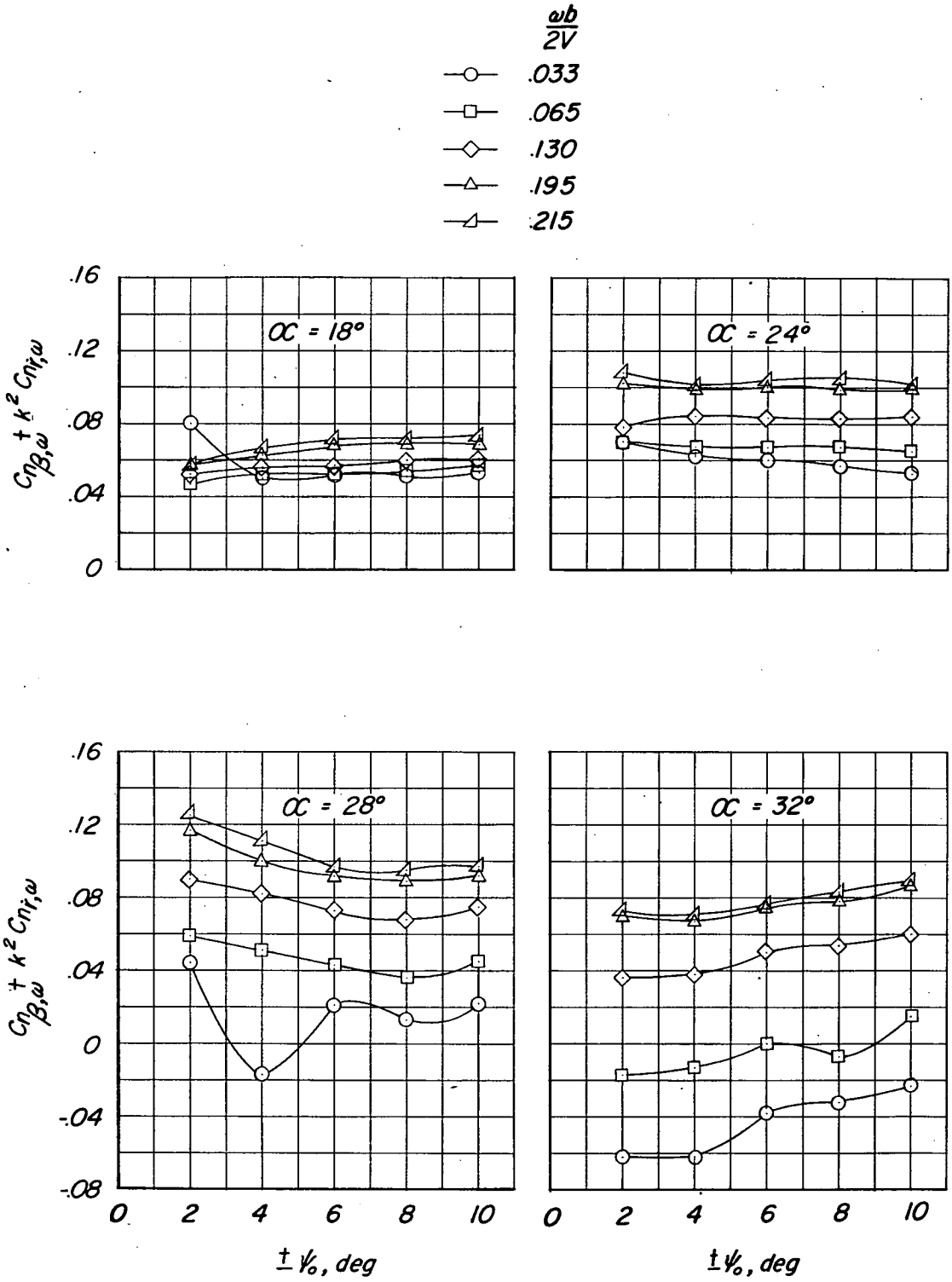

(a) Delta wing.

Figure 17.- The effect of amplitude on the directional-stability derivative.

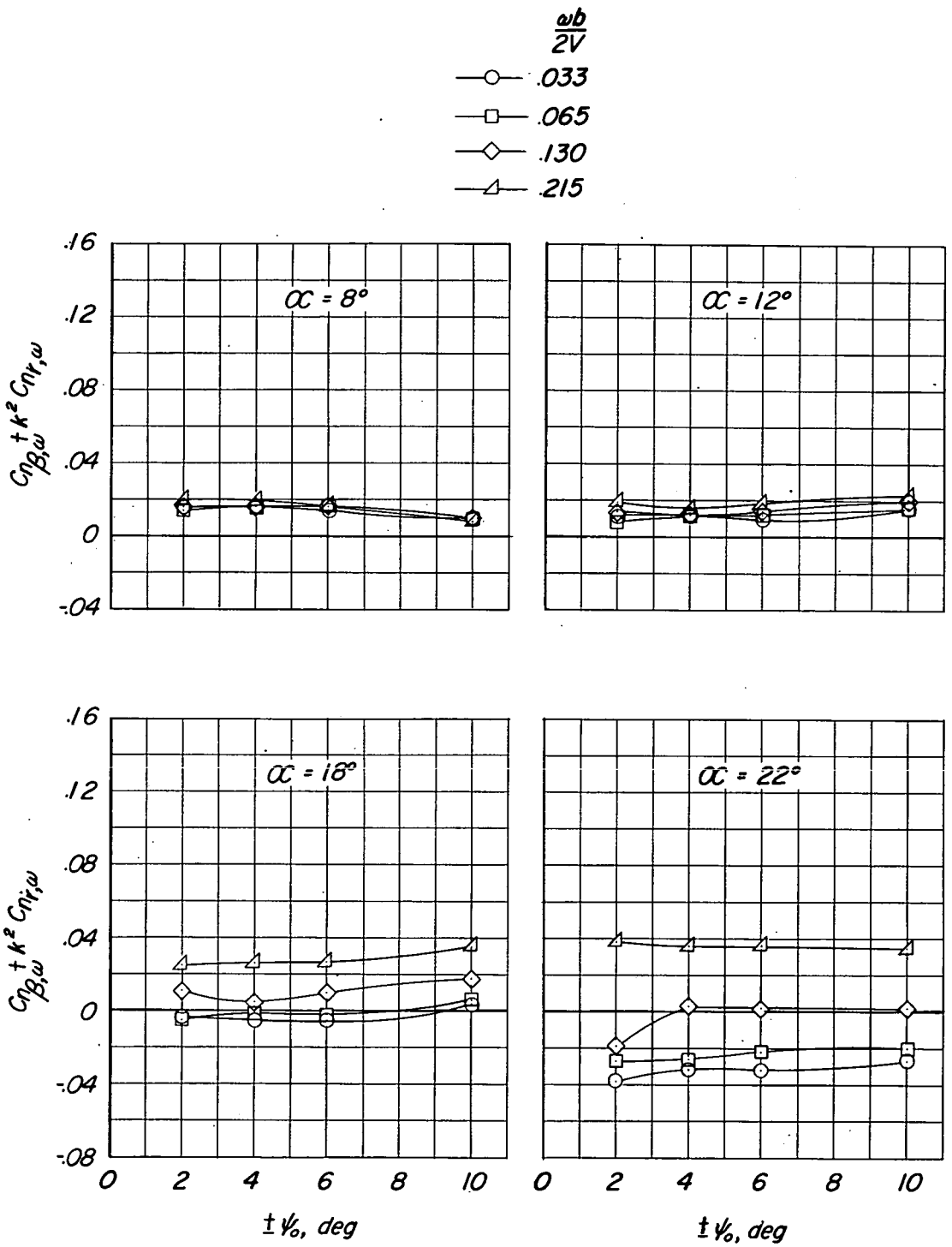

(b) Swept wing.

Figure 17.- Continued.

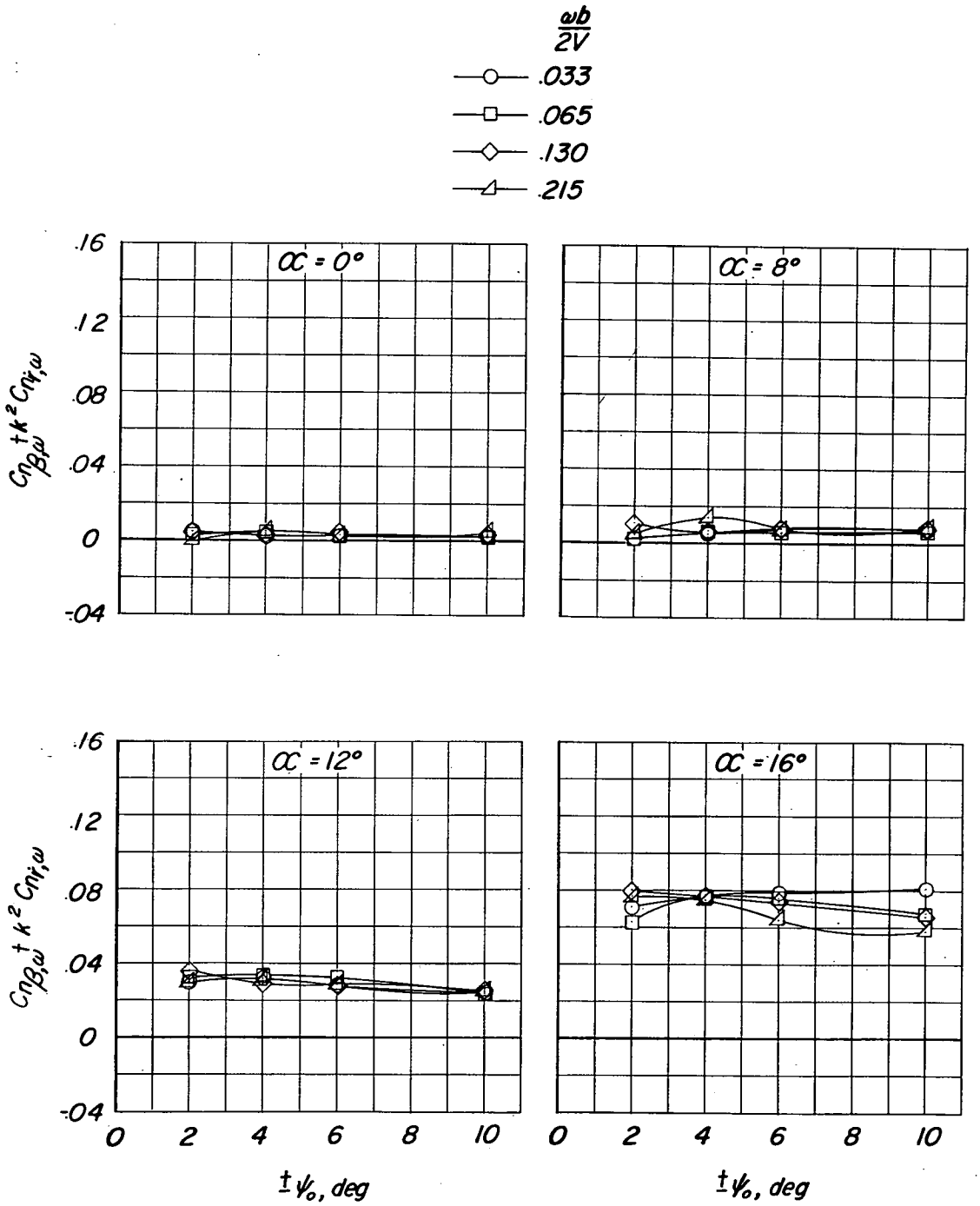

(c) Unswept wing.

Figure 17.- Concluded.

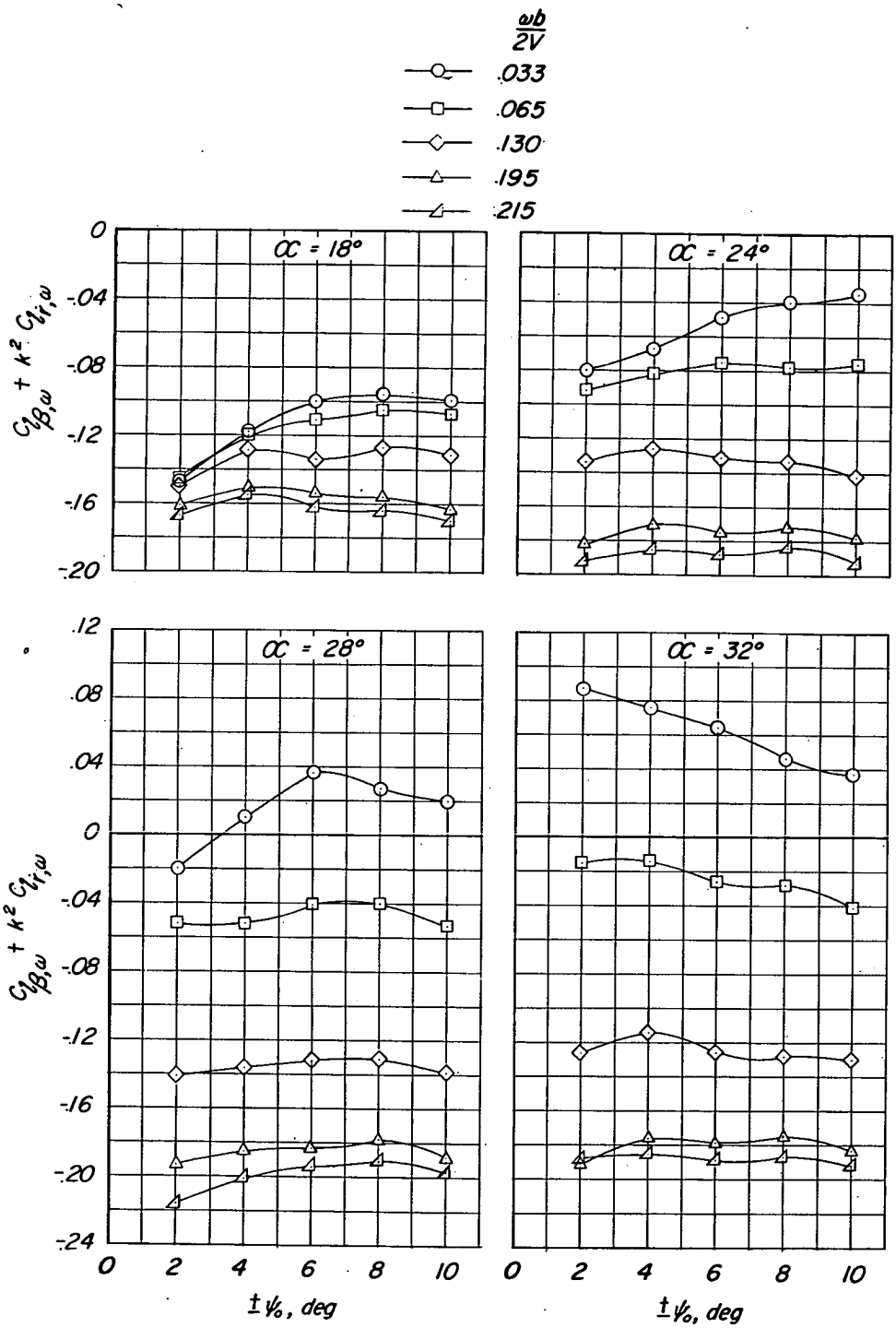

(a) Delta wing.

Figure 18.- The effect of amplitude on the effective-dihedral derivative.

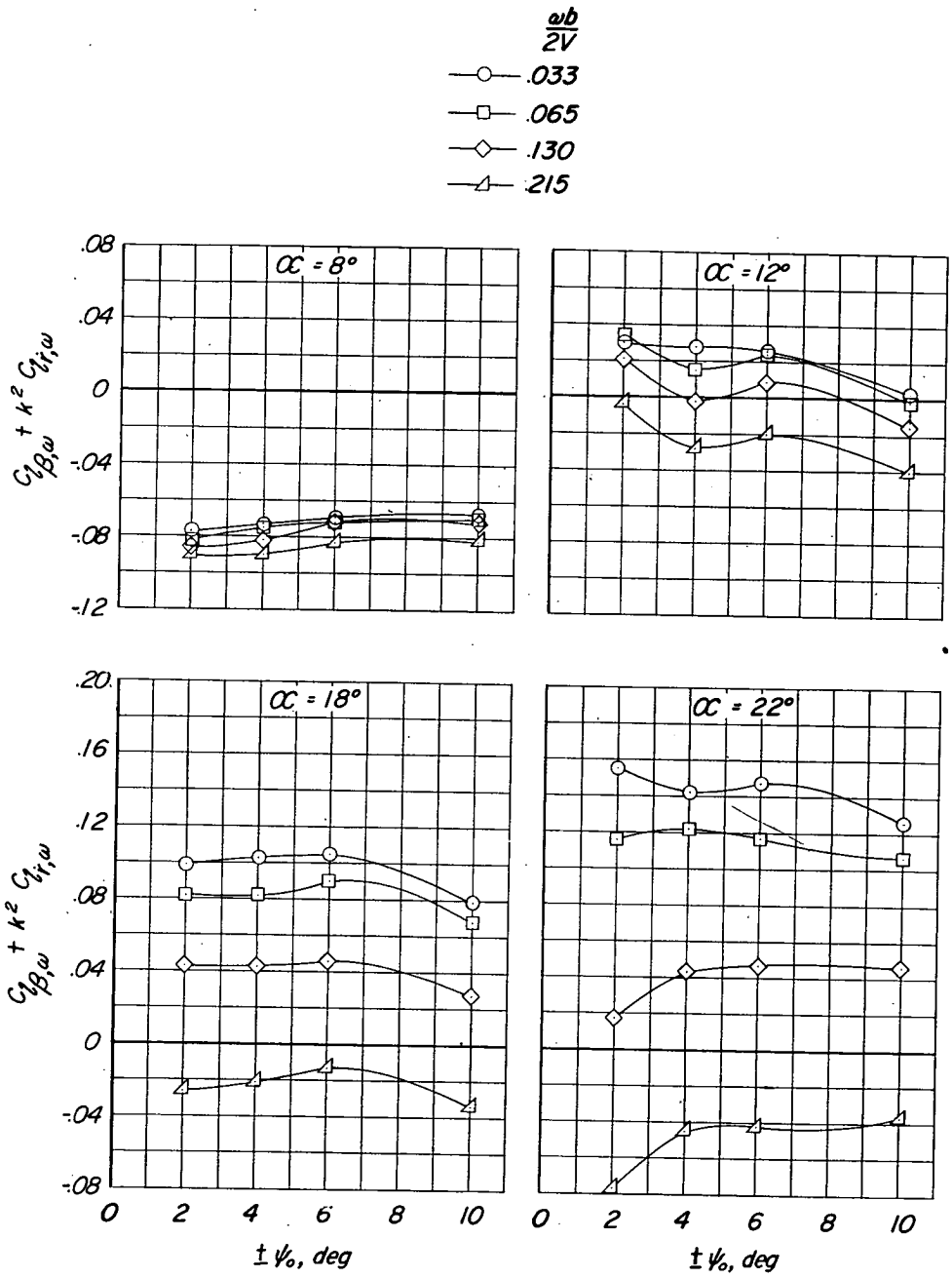

(b) Swept wing.

Figure 18.- Continued.

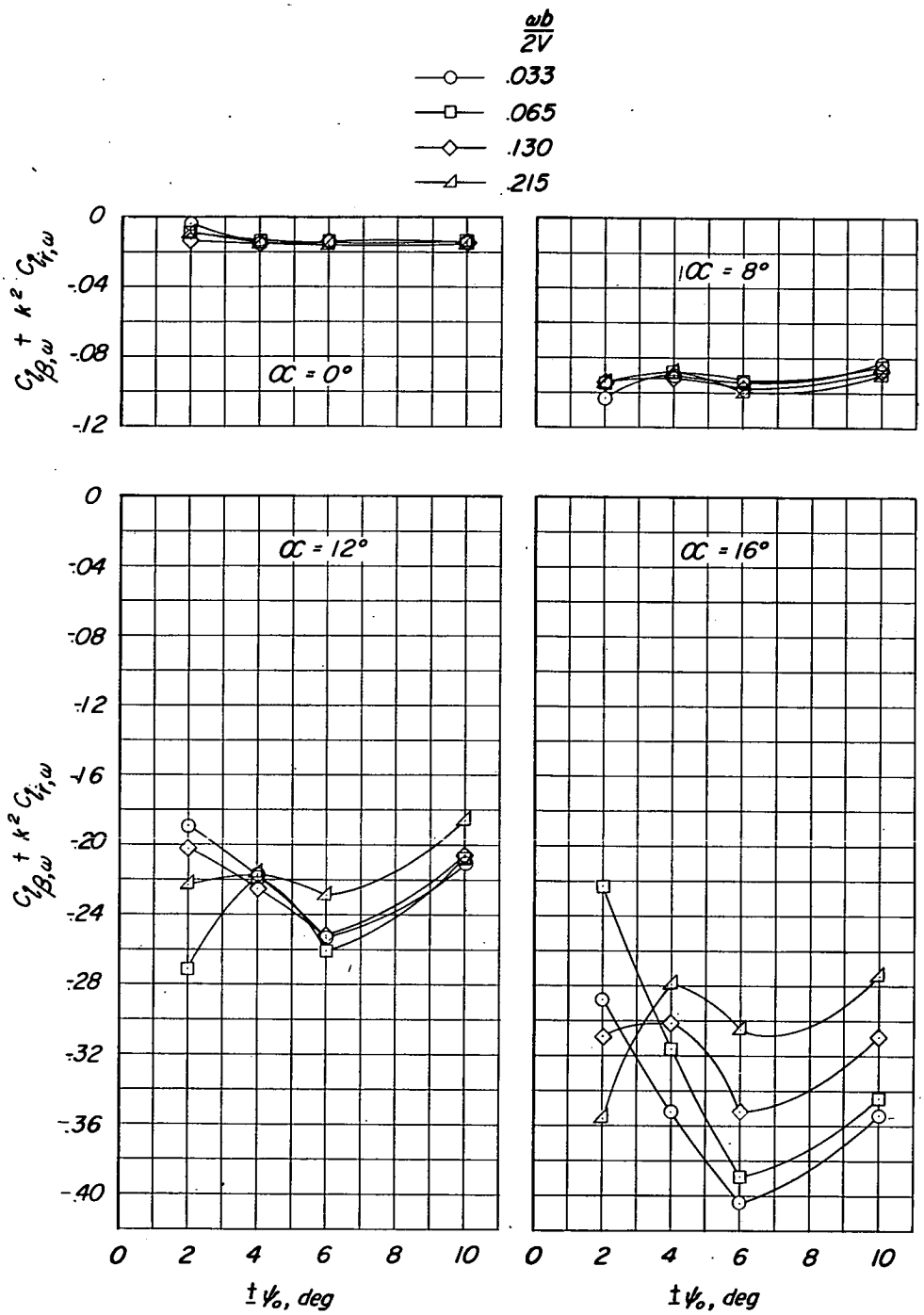

(c) Unswept wing.

Figure 18.- Concluded.

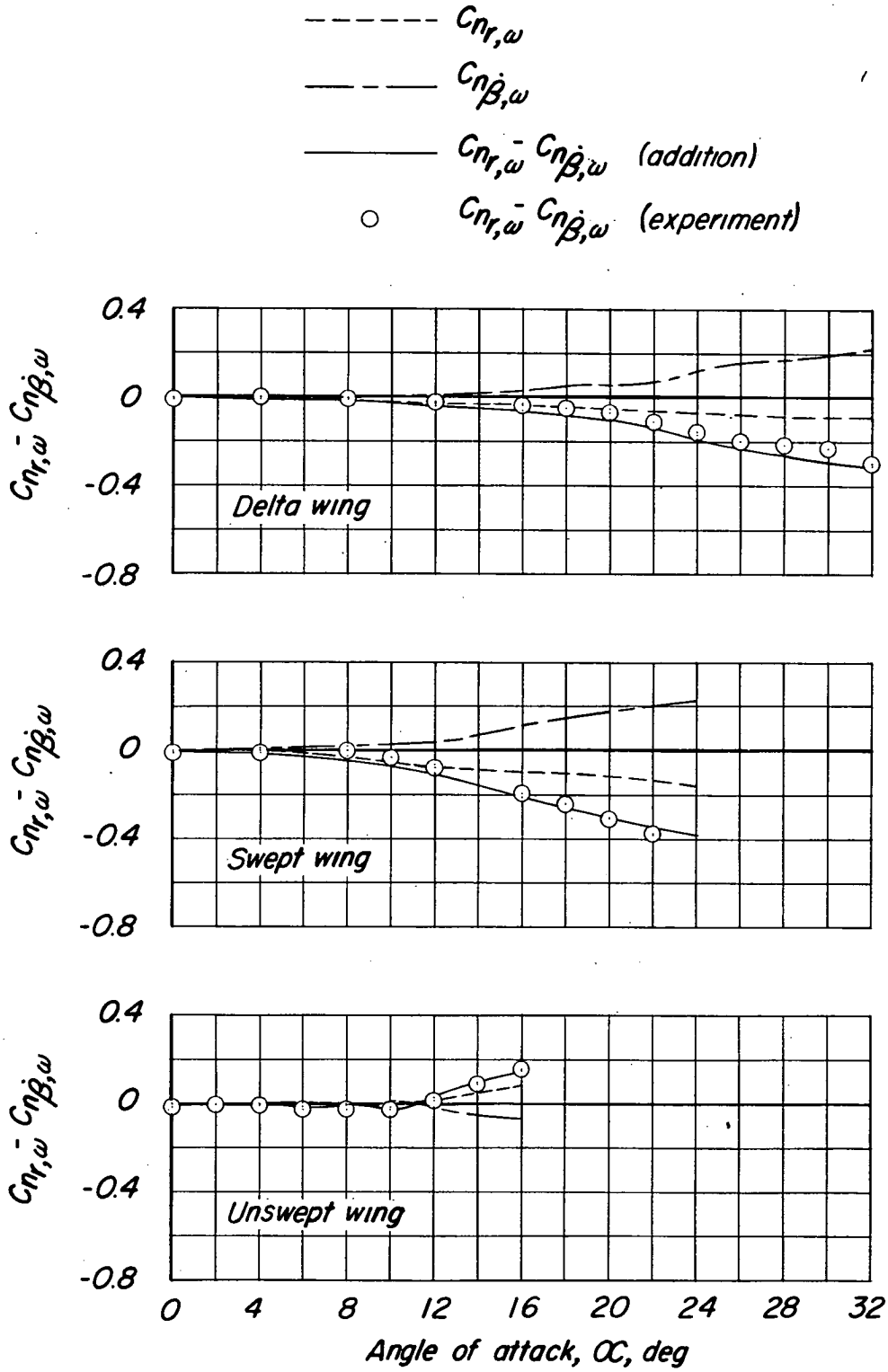

Figure 19.- Comparison of the component and the combination derivatives making up the damping in yaw. $\omega b/2V = 0.22$; $\psi_o = 6^\circ$ or 8°.

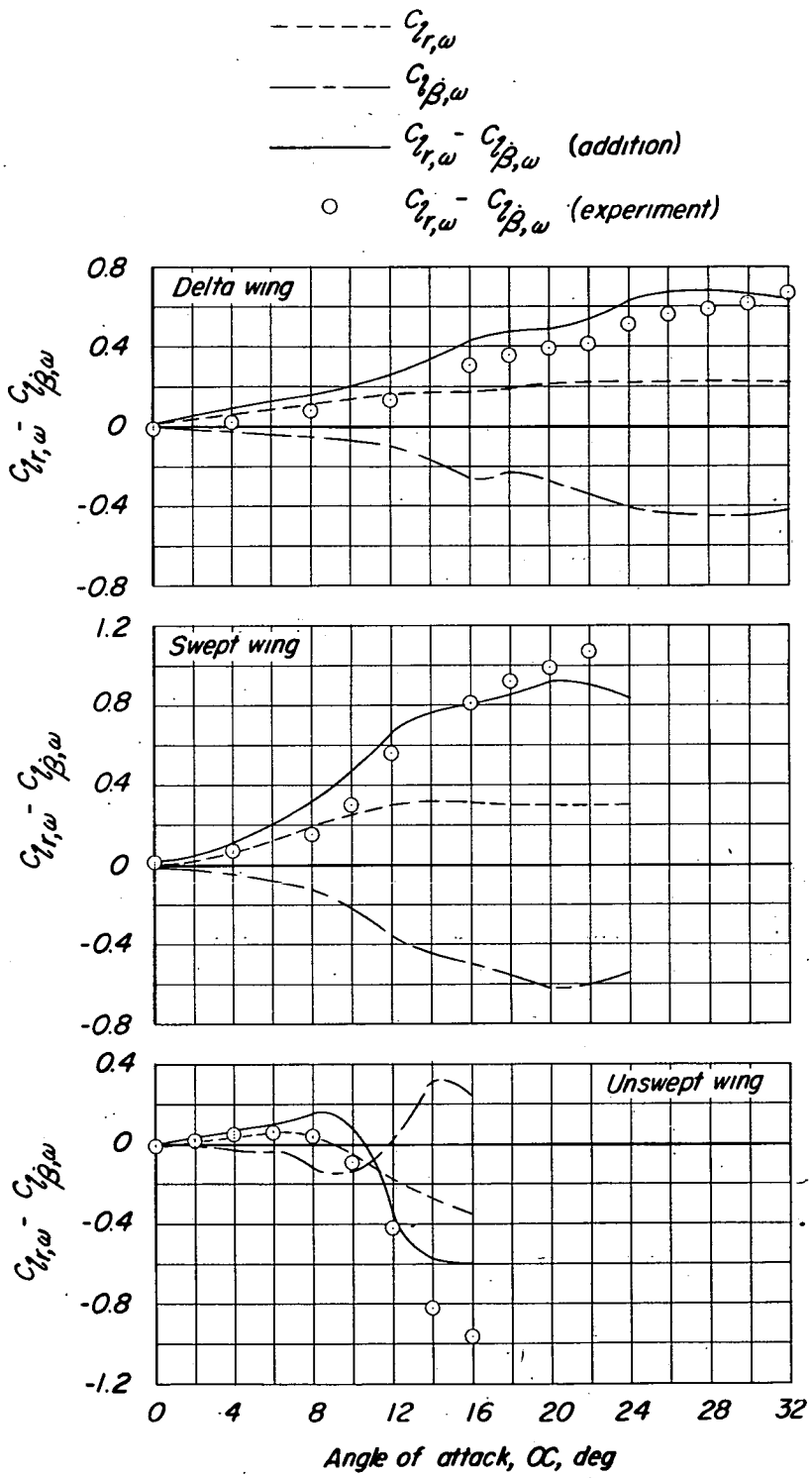

Figure 20.- Comparison of the component and the combination derivatives making up the rolling moment due to yawing. $\omega b/2V = 0.22$; $\psi_o = 6^o$ or 8°.

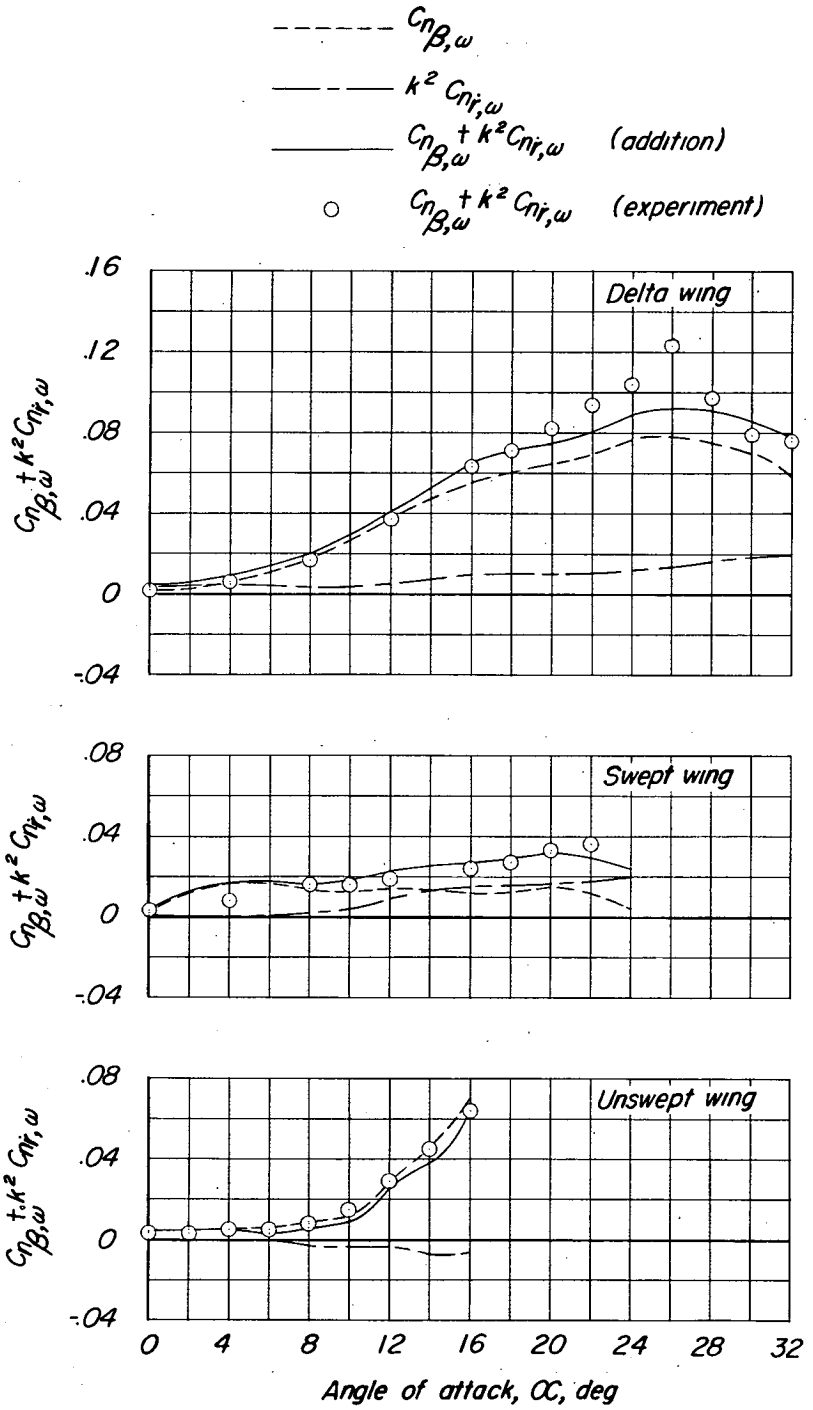

Figure 21.- Comparison of the component and the combination derivatives making up the directional stability $\omega b/2V = 0.22$; $\psi_o = 6^\circ$ or 8°.

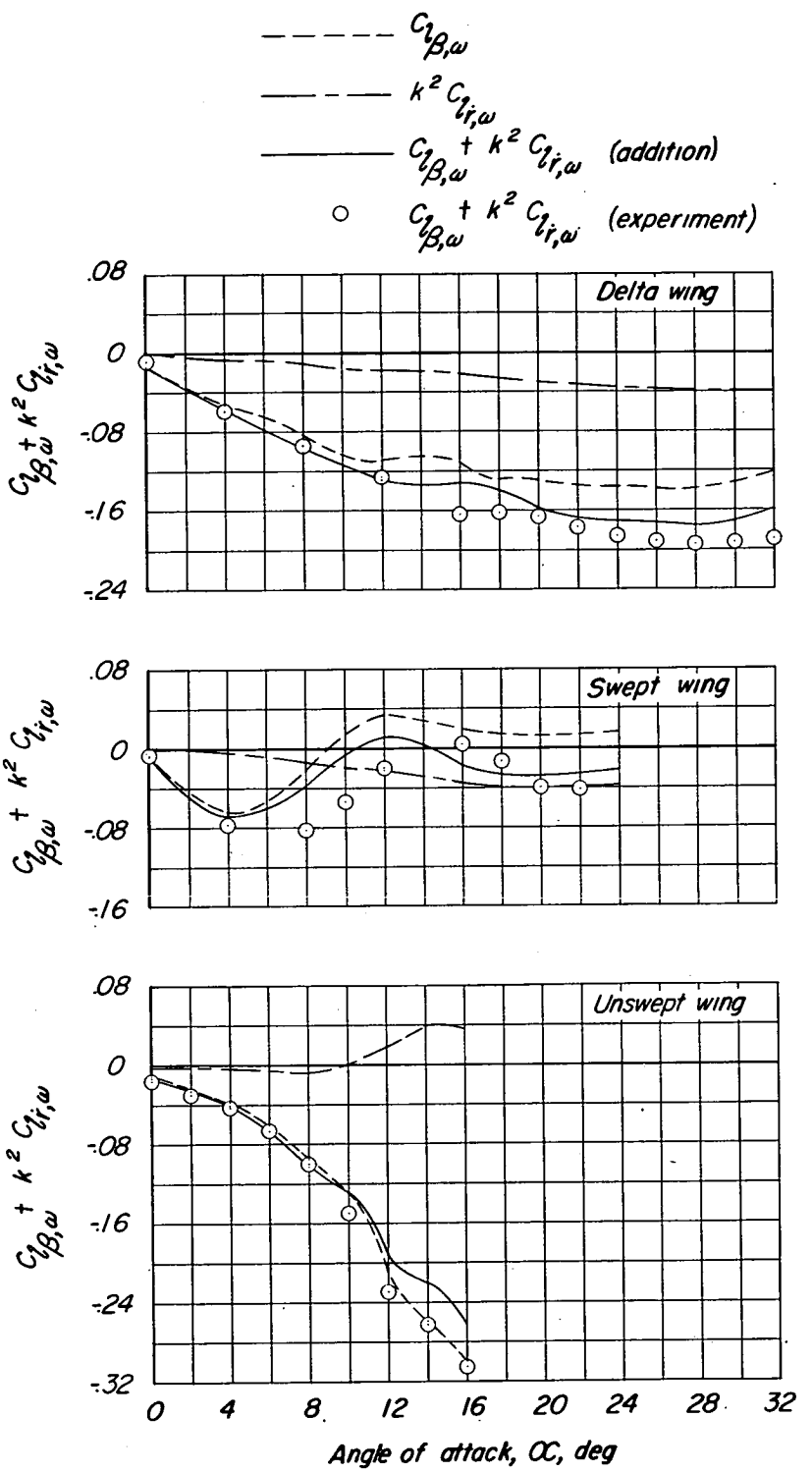

Figure 22.- Comparison of the component and the combination derivatives making up the effective dihedral. $\omega b/2V = 0.22$; $\psi_o = 6^o$ or 8°.

NACA - Langley Field, Va.